Adaptive High Throughput CDMA-based Wideband Waveform with Robust Timing and Frequency Synchronization for SDR-based Tactical Networks

by

Muhammad Zeeshan

Supervised by

Dr. Shoab A. Khan

THESIS

submitted in partial fulfillment of the

requirements for the degree of

DOCTOR OF PHILOSOPHY

in

ELECTRICAL ENGINEERING

Department of Electrical Engineering

COLLEGE OF ELECTRICAL & MECHANICAL ENGINEERING

NATIONAL UNIVERSITY OF SCIENCES & TECHNOLOGY

2015

Acknowledgements

I would like to express my gratitude to my advisor Dr. Shoab A. Khan, Head of the Department of Computer Engineering, for his support, encouragement, guidance and enduring patience. It has been a great experience and true privilege in working with him. His support, advice and guidance has been a great source of encouragement for me.

I gratefully acknowledge Dr. Tahir Zaidi, from College of EME, whose guidance and support helped me in refining and improving my research work. I would never forget the sincere and selfless help of Dr. Muhammad Salman. Throughout my coursework and thesis, he has been a source of great inspiration for me. I am highly indebted to Dr. Shahzad Amin Sheikh, Head of the Department of Electrical Engineering, who helped me a lot during the course of my MS and PhD. I greatly appreciate all my instructors, friends and colleagues especially Dr. Mohammad Bilal Malik, Dr. Fahad Mumtaz Malik, Mr. Nauman Anwar Baig, Mr. Rahat Ali and Mr. Nauman Razzaq.

I am also grateful to my dearest friend Muhammad Waqas Khan, Senior Engineer at Kahuta Research Laboratories (KRL), for the matchless friendly support and encouragement. I also thank Mr. Sabahat Aleem Malik, from Huawei, Qatar, Dr. Nabeel Khan, from Federal Urdu University, Islamabad, Mr. Muhammad Hanif, from University of Victoria, Canada, Mr. Zain Mehtab, from RWTH Aachen University, Germany, and Mr. Ibtisam Haq, from Technical University of Munich (TUM), Germany, Mr. Atif Shabbir, Mr. Sulaiman Sadiq, Mr. Syed Ali Jabir, Mr. Umer Farooq, Mr. Waqar Ahmed, Mr. Haseeb-ur-Rehman and Mr. Naeem Amjad, all from Center for Advanced Research in Engineering (CARE), for their help and support.

My sincere thanks go to my parents, brother and sisters for their never-fading love, care, understanding and encouragement. The prayers of my loving mother and father have made me reach this milestone.

Dedication

I would like to dedicate this thesis to my loving parents ...

Abstract

The future tactical systems require network based seamless communication with precise, accurate and reliable information. To achieve this end, a multi-mode high throughput CDMA-based wideband networking waveform for software defined radio is proposed. The proposed waveform has several different modes of operation and the maximum achievable throughput of 17.2 Mbps. Novel algorithms for the waveform's physical layer transmitter and receiver including sampling clock recovery, burst detection, and carrier frequency offset estimation and compensation are proposed. For Sampling clock recovery, a novel three stage Modified Square Timing Recovery (MSTR) algorithm is proposed. For burst detection, two novel algorithms based on Time Domain Repetitive (TDR) and Differentially Modulated (DM) training sequences are proposed. For carrier frequency offset estimation, a novel algorithm based on modified FFT and quadratic interpolation is proposed. A novel two stage carrier frequency offset estimator with improved performance is also proposed which consists of Maximum Likelihood Data Aided (MLDA) estimation and Sample-by-Sample Residual Offset (S2RO) estimation stages. To reduce the packet re-transmissions overhead and achieve better throughput, a novel link adaptation technique is proposed, which is based on fuzzy inference system by considering Quality of Service and throughput requirement of user/application. The throughput adaptation is achieved by changing the modulation technique and the number of multicodes assigned to each user. The novelty of the proposed algorithms is selected by considering the implementation affinity. The performance improvement of the proposed algorithms is demonstrated by comparing them with a set of known existing methods. It is shown through simulation results that the proposed algorithms are superior in terms of performance, throughput and computational complexity. The proposed algorithms are implemented using Field Programmable Gate Array and Digital Signal Processor on SDR platform. Actual results from hardware are compared and verified with the simulation results to demonstrate the effectiveness of the proposed techniques. This

wideband SDR waveform based on the proposed algorithms finds many real world applications in both the tactical and commercial scenarios. Some examples include biometrics, video conferencing, IP data, file transfer, situational awareness, messaging, voice push to talk, simultaneous voice and data transfer.

Table of Contents

List of Tables

List of Figures

List of Abbreviations

3GPP	3rd Generation Partnership Project
ADC	Analog-to-Digital Converter
AMC	Adaptive Modulation & Coding
ANW2	Adaptive Networking Wideband Waveform
ATDMA	Adaptive Time Division Multiple Access
AWGN	Additive White Gaussian Noise
BER	Bit Error Rate
CDMA	Code Division Multiple Access
CFO	Carrier Frequency Offset
COA	Centroid of Area
CP	Cyclic Prefix
CQI	Channel Quality Indicator
CRB	Cramer-Rao Bound
CSMA	Carrier Sense Multiple Access
DDC	Digital Down Converter
DM	Differentially Modulated
DSP	Digital Signal Processor

DSSS	Direct Sequence Spread Spectrum
ESCA	Extended Schmidl and Cox Algorithm
FEC	Forward Error Correction
FFT	Fast Fourier Transform
FIS	Fuzzy Inference System
FPGA	Field Programmable Gate Array
FRBS	Fuzzy Rule Based System
FRM	Fuzzy Rule Matrix
GPP	General Purpose Processor
HDR	Hardware Defined Radio
HSDPA	High Speed Packet Data Access
HWT	Haar Wavelet Transform
ISI	Intersymbol Interference
JTRS	Joint Tactical Radio System
LOS	Line of Sight
LTE	Long Term Evolution
MAC	Medium Access Control
MAI	Multiple Access Interference
MANET	Mobile Ad hoc Networking
MF	Membership Function

ML	Maximum Likelihood
MMI	Modulation & Multicode Index
MMLDA	Modified Maximum Likelihood Data Aided
MMSE	Minimum Mean Square Error
MRC	Maximal Ratio Combining
MST	Modified Square Timing
MSTR	Modified Square Timing Recovery
NDA	Non-Data Aided
NLOS	Non Line of Sight
OFDM	Orthogonal Frequency Division Multiplexing
PN	Pseudo-noise
PSD	Power Spectral Density
PSK	Phase Shift Keying
PTT	Push To Talk
QAM	Quadrature Amplitude Modulation
QoS	Quality of Service
RF	Radio Frequency
RRC	Root Raised Cosine
S2RO	Sample-by-Sample Residual Offset
S4RLSWAM	Steady-State State-Space Recursive Least Squares with Adaptive Memory

SCO	Sampling Clock Offset
SDNR	Software Defined Networking Radios
SDR	Software Defined Radio
SNR	Signal-to-Noise Ratio
SPR	Sample Point Reordering
STFT	Short Time Fourier Transform
STR	Square Timing Recovery
SUI	Stanford University Interim
TDMA	Time Division Multiple Access
TDR	Time Domain Repetitive
TWWiN	Tactical Wideband Wireless Network
WBNR	Wideband Networking Waveform
WNW	Wideband Networking Waveform

List of Symbols

T	Symbol duration	12
T_c	Chip duration	12
G	Spreading gain	12
K	No. of users	25
c_k	Spreading code of the k^{th} user	25
$g(t)$	Chip pulse shaping function	25
$s_k(t)$	Trasnmitted signal of k^{th} user	25
d_k	Transmitted data of k^{th} user	26
$\alpha_{kl}(t)$	Time varying path gain for l^{th} path and k^{th} user	26
$f_{D,kl}$	Doppler spread for l^{th} path and k^{th} user	26
τ_{kl}	Delay spread for l^{th} path and k^{th} user	26
γ_k	Number of multipath for k^{th} user	26
B	No. of total symbols/burst	26
N_s	Upsampling factor (No. of samples/symbol)	27
$\epsilon_k(nT_s)$	n^{th} sample of the time varying delay for k^{th} user caused due to SCO	27
$\tilde{\epsilon}$	Post-filtered SCO estimate corresponding to n^{th} sample	30
$\hat{\epsilon}$	SCO estimate before filtering corresponding to n^{th} symbol	30
α	Integer part of the SCO estimate	33
δ	Fractional part of the SCO estimate	33
f_k	Decouped/correlated data of k^{th} user	36
N_d	No. of data symbols/burst	37
R	Roll-off factor for RRC filter	37
K'	No. of symbols used for SCO estimation	37
λ_{init}	Initial value of forgetting factor	37
N	No. of spread samples in training sequence	46

Chapter 1

Introduction

The full range capability of the traditional radio systems was provided by hardware elements. Due to this reason, those radios could be termed Hardware Defined Radios (HDR). With the evolution of software engineering, the concept of Software Controlled Radios was presented. Nowadays, the true Software Defined Radios (SDR), in which a wide range of capabilities is implemented through the software configurable components, are being fielded [1]. Specifically, SDR is a radio transceiver in which a software defines the key radio parameters and the fundamental aspects of the radio's operation can be changed by reconfiguring that software [2].

In these days, SDR has become an enabling technology in many signal processing and communication applications because a single platform can be used to provide multiple functionalities through various software configurations. SDR supports broad range of frequencies and its initial configurations can be modified for user requirements. It can be termed as a flexible radio that is able to accommodate various protocols and formats [3]. Most SDRs utilize a Field Programmable Gate Array (FPGA), Digital Signal Processor (DSP) and General Purpose Processor (GPP) in their architectures. The intelligent part of systems use processors (GPP or DSP) and computationally extensive part normally goes on FPGA [4].

A substantial research effort has been made for several years to investigate the potential of applying the Software Defined Radio (SDR) approach to a wide range of wireless communications applications. However, present wireless communication transceivers based on SDR technology are used primarily in high-end applications [5]. Examples are wireless military communication equipment and base station equipment. The future SDR-based

networks will have to support a wide variety of data-intensive applications such as streaming video, biometrics, IP data while offering a high degree of survivability, mobility and security. Due to these requirements, the developments for the future networks are moving toward wideband and digital signal based networking [6]. Wideband networking radio waveform can overcome the insufficient capacities of the conventional narrowband wireless channel, so that it provides higher data transmission rate to support multimedia and bulky data traffic.

Direct Sequence Spread Spectrum (DSSS) is conventionally used in the physical layer of wideband waveforms. The purpose of DSSS scheme is to make the networking radios work under noise floor without affecting primary license users in the used spectrum. DSSS is well suited for the SDR networks due to anti-jamming, anti-interference, high frequency efficiency and robustness against multipath fading effects [7]. Multiple access in DSSS/SDR-based wideband networks is provided by Carrier Sense Multiple Access (CSMA), Time Division Multiple Access (TDMA) etc. Despite the advantages of DSSS, timing synchronization is one of the major concerns. The problem of timing synchronization includes; (1) Estimation and Compensation of time varying Sampling Clock Offset (SCO) caused due to sampling clock inaccuracies and (2) Detection of the Start of burst for burst mode of transmission. Estimation and compensation of Carrier Frequency Offset (CFO) and equalization are also needed. Moreover, the problem of timing synchronization becomes more complicated in multiuser Code Division Multiple Access (CDMA) networks because all the users simultaneously share time and frequency, and burst transmissions from all the users are mostly asynchronous.

To optimize the use of scarce SDR resources, efficient algorithms for resource allocation/utilization are required. Different applications (e.g. Push To Talk (PTT), position tracking, point-to-point calls, messages, file transfer, video communication etc) have different Quality of Service (QoS) requirements. This involves adapting the parameters of the SDR waveform to changing conditions/requirements. This process is called Link Adaptation [8]. It usually comprises of two parts; (1) Varying the waveform parameters at the

physical layer, and 2) Use of Adaptive TDMA.

In this thesis, we propose a multi-mode high throughput wideband networking waveform for software defined radio with a maximum achievable throughput of 17.2 Mbps. Single code/multicode Code Division Multiple Access (CDMA) and Time Division Multiple Access (TDMA) are used as multiple access schemes. Novel algorithms for the training sequence design, sampling clock offset estimation and compensation, burst detection, and carrier frequency offset estimation and compensation are proposed. For Sampling clock recovery, a novel three stage Modified Square Timing Recovery algorithm is proposed. For burst detection, two novel algorithms based on Time Domain Repetitive and Differentially Modulated training sequences are proposed. For carrier frequency offset estimation, a novel algorithm based on modified FFT and quadratic interpolation is proposed. A novel two stage carrier frequency offset estimator with improved performance is also proposed which consists of Maximum Likelihood Data Aided estimation and Sample-by-Sample Residual Offset estimation stages. To reduce the packet re-transmissions overhead and achieve better throughput, a novel link adaptation technique is proposed, which is based on fuzzy inference system by considering Quality of Service and throughput requirement of user/application. Figure 1.1 shows the overview of the physical layer of the proposed waveform.

1.1 Existing Wideband Waveforms

Software defined radio provides a platform capable of supporting different waveforms. In other words, the SDR platform consists of the basic configurable hardware components and the necessary software required to host a waveform. An SDR waveform is defined as a program through which the ultimate Radio Frequency (RF) signal, modulation technique, frequency, protocols, performance and security features are defined [9]. Due to the high data rate network-based requirements of the future tactical and strategic applications, the developments for the future SDR waveforms are moving toward wideband networking waveforms. In this section, we describe some well-known SDR wideband networking waveforms

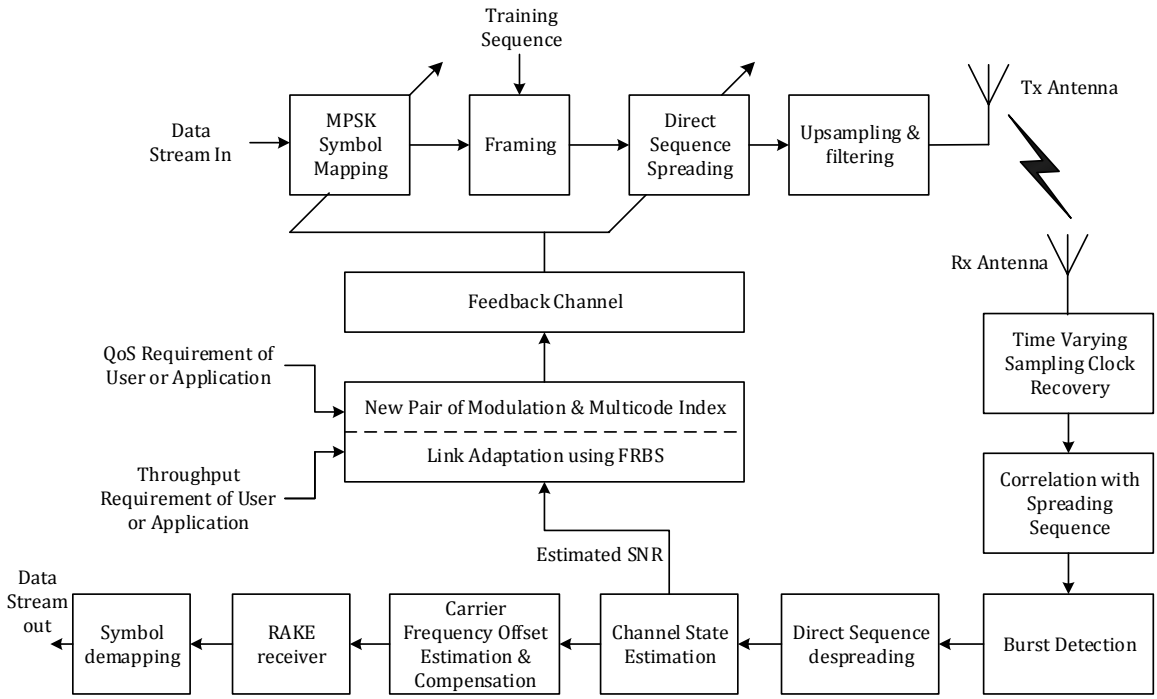

Figure 1.1: Overview of the physical layer of the proposed waveform

with their capabilities as well as limitations.

1.1.1 Tactical Wideband Wireless Network Waveform

The Tactical Wideband Wireless Network (TWWiN) waveform [10] is developed primarily for maritime communications. This waveform is based on frequency hopped Orthogonal Frequency Division Multiplexing (OFDM) which is a well-known scheme with high spectral efficiency and provides high data rates for wireless applications. Synchronization algorithms presented in [11] and [12] are used to provide the timing and carrier estimation performance for frequency hopped OFDM waveform. The spectral efficiency of the TWWiN waveform is increased by using OFDM with frequency hopping [13]. Some important features of TWWiN waveform are:

- Anti-jam operation

- Data rates up to 2 Mbps
- Adaptive modulation
- High spectral efficiency

The disadvantages/limitations of the TWWiN waveform are

- Highly sensitive to synchronization errors
- Data rate scalability is low

1.1.2 ASELSAN's Wide Band Networking Radio Waveform

Wide Band Networking Radio (WBNR) waveform is developed by ASELSAN, a Turkish company [14]. This waveform is one of the several other supported by the Software Defined Networking Radios (SDNR) developed by ASELSAN. This waveform uses Direct Sequence Spread Spectrum (DSSS) to provide high anti-jamming capability. The WBNR waveform mode of the ASELSAN SDNR operates in Time Division Multiple Access (TDMA) networking which is configured through a central radio working as base station [15]. Some important features of WBNR waveform are:

- High Anti-jamming capability
- User data throughput up to 112 kbps
- TDMA channel access
- Full duplex communication

The disadvantages/limitations of the WBNR waveform are

- No link adaptation mechanism
- Limited network capacity

- Low data throughput
- A central control station is needed for network establishment

1.1.3 Harris' Adaptive Networking Wideband Waveform

Adaptive Networking Wideband Waveform (ANW2) [16] is developed by Harris, a well-known US company. This waveform is featured by Falcon III Harris' radio family. It is an ad hoc, self-healing and self-forming waveform supporting high speed and adaptive networking capabilities. ANW2 doesn't need any central base station radio for network establishment because of its intelligent protocols through which every radio automatically discovers and joins the established network [17]. The modulation scheme used in ANW2 is not disclosed by Harris corporation. Some important features of ANW2 are:

- Self-healing and self-forming capabilities
- User data throughput up to 2 Mbps
- No central infrastructure
- Full duplex voice and IP data communication
- Modulation switching according to channel conditions
- Supports up to 30 radios in a sub-network

1.1.4 Thales' TrellisWare TopX-II Waveform

TrellisWare TopX-II Waveform [18] is developed by Thales, a well-known French company. This waveform is featured by Thales' Wideband Networking Radio (WNR). The waveform uses Continuous Phase Modulation (CPM) with cooperative diversity to achieve high throughput. The waveform also supports Mobile Ad hoc Networking (MANET) and multi-hop network coverage. Some important features of TrellisWare TopX-II Waveform are:

- Self-healing and self-forming capabilities
- Data throughput up to 2 Mbps
- Simultaneous voice and data communication
- Multi-hop network coverage

The disadvantages/limitations of the WBNR waveform are

- No link adaptation mechanism

1.1.5 JTRS Wideband Networking Waveform

Joint Tactical Radio System (JTRS) Wideband Networking Waveform (WNW) is a multi-mode waveform based on Orthogonal Frequency Division Multiplexing (OFDM) at the physical layer [19]. It offers multiple modes of operation by varying the modulation scheme, Forward Error Correction (FEC) and diversity factor. The waveform is also data rate adaptable in that it maximizes the data rate in almost every channel condition. Time Division Multiple Access (TDMA) and Carrier Sense Multiple Access (CSMA) are used as channel access schemes. Some important features of JTRS WNW are:

- Mobile ad hoc networking capability
- Data throughput up to 11.5 Mbps
- Simultaneous voice and data communication
- Data rate adaptation
- Multiple modes of operation

1.2 Objectives and Problem Statement

The future strategic and tactical systems require high throughput, network based seamless communication with precise, accurate and reliable information. The importance of interoperability among various defense counterparts and seamless voice and data communication among the users of tactical and strategic networks is gradually increasing. Due to these requirements, the future SDR waveform developments require the following objectives to be met.

- High anti-jamming and anti-interference capabilities
- High user throughput to support variety of high data rate applications
- Robustness to multipath fading effects and harsh channel conditions
- Efficient algorithms to estimate and compensate time-frequency offsets between the transmit and receive radios
- Simultaneous voice and IP data communication
- Self-healing and self-forming capabilities without needing any central infrastructure
- High network capacity
- Precise and reliable information requiring better synchronization algorithms
- Multiple modes of operation for all channel conditions
- Link adaptation to provide maximum possible data rates
- Effective adaptation of system parameters and protocols to reduce packet re-transmissions overhead

Keeping in view the objectives mentioned above, the aim of this thesis is to design a multi-mode high throughput wideband networking waveform physical layer for software

defined radio with efficient time-frequency synchronization and link adaptation algorithms to provide precise and reliable information with maximum possible throughput, reduced packet re-transmissions penalties and ease of real-time implementation.

1.3 Overview of the Proposed Waveform

The overview of the physical layer of the proposed wideband networking waveform is shown in figure 1.1. Multicode CDMA is used to increase anti-jamming ability as well as the network capacity of the system by using it in conjunction with adaptive TDMA at the Medium Access Control (MAC) layer. At the transmitter side, within each allocated time slot, the data stream is first mapped using M-PSK symbol mapping, where M is the modulation index. Bursts of the symbols are formed in which specific training sequence is inserted prior to each data burst. After multicode direct sequence spreading, upsampling and Root Raised Cosine (RRC) filtering, the data is modulated with the carrier generated from the reference oscillator. After passing through channel, the data is received at the receivers front-end. The crystal oscillator of the receiving device generates Sampling Clock Offset (SCO) and Carrier Frequency Offset (CFO). At the digital front end, firstly, SCO is estimated and compensated. The next blocks are correlation and Burst detection. The output data from previous stage including training sequence is correlated with the spreading sequence at chip rate and fed to the burst detection block which detects the valid bursts. After the detection of each valid burst, data at chip rate is converted to symbols through despreading (down-conversion) by spreading gain. Then channel estimation block includes both the estimation of Signal-to-Noise Ratio (SNR) and channel state. The link adaptation algorithm based on fuzzy inference system generates a new pair of modulation and multicode indices for the next transmission based on the estimated received SNR, Quality of Service (QoS) and throughput requirements. The next blocks include Carrier Frequency Offset (CFO) recovery, RAKE receiver and symbol de-mapping. The main focus of this thesis was to propose efficient time-frequency synchronization and link adaptation algo-

rithms to provide reliable information with maximum possible throughput and reduced packet re-transmissions penalties. More specifically, novel and efficient algorithms for the following are proposed.

1.3.1 Sampling Clock Recovery

The Sampling Clock Offset (SCO) arises due to the inherent mismatch between the crystal oscillators of transmit and receive radios [20]. This offset degrades the performance heavily, if not estimated and compensated properly. For multiuser CDMA system, it becomes more difficult to estimate the offset because each radio receives the composite signal from all the transmit radios. Moreover, this offset varies slowly with time due to thermal drift [21]. We propose Modified Square Timing Recovery (MSTR) algorithm consisting of three stages for both the single and multiuser cases.

1.3.2 Training Sequence Design and Burst Detection

The proposed wideband waveform operates in burst mode where the size of each burst is chosen so that the channel behaves time invariant to each burst. The start of each burst needs to be detected to further process the data. Moreover, the correct detection of start of burst is very important as it directly affects the adaptive time slot allocation algorithm. Two novel algorithms for burst detection are proposed which are based on two different specifically designed training sequences. The first is Time Domain Repetitive (TDR) training sequence and the other is Differentially Modulated (DM) training sequence. Both the single and multiuser cases are investigated.

1.3.3 Carrier Frequency Offset Estimation and Compensation

The problem of Carrier Frequency Offset (CFO) arises due to the inherent inaccuracy of the local oscillators at the transmit and receive radios. Two novel algorithms for the estimation and compensation of CFO are proposed. The first algorithm is based on Fast Fourier Trans-

form (FFT) and interpolation [22] and the other algorithm consists of two stages namely Maximum Likelihood Data Aided (MLDA) estimation and Sample-by-Sample Residual Offset (S2RO) estimation [23].

1.3.4 Link Adaptation

The process of changing the system parameters and/or protocols according to the varying channel conditions and user requirements is termed as link adaptation. In packet-based communication, effective link adaptation becomes more important because a small value of bit error rate can result in a high packet error rate, thereby increasing the packet retransmission penalty. In this thesis, we propose a novel link adaptation scheme based on fuzzy inference system (FIS) that selects the most suitable value of modulation and multicode indices based on channel conditions, QoS and user/application throughput requirements.

1.4 Fundamental Concepts

The proposed wideband waveform uses both the single code and multicode CDMA as well as adaptive TDMA as multiple access schemes. Therefore, we briefly explain these technologies.

1.4.1 Adaptive Time Division Multiple Access

In TDMA, the available spectrum is accessed by each radio at specific time slots. Medium Access Control (MAC) layer monitors these assigned time slots. Figure 1.2 shows the TDMA scheme. The Adaptive TDMA (ATDMA) Protocol is provides real-time voice and data communication in a tactical warfare environment. The real-time requirement is met in ATDMA based MAC protocol by guaranteeing the allocation of slots within the delay bound, while reliability is ensured by allocating conflict free time slots.

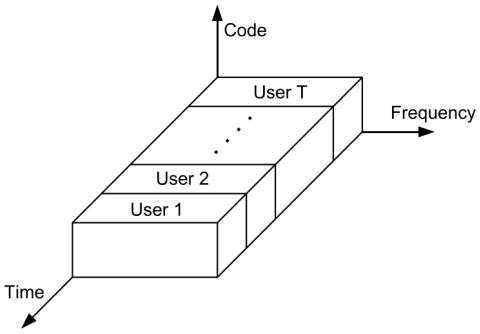

Figure 1.2: Time Division Multiple Access

1.4.2 Code Division Multiple Access

In CDMA, each radio can access the complete available spectrum at any time. Figure 1.3 shows the CDMA scheme. All the users/radios are separated by using user specific spreading sequences. These spreading sequences (also called spreading codes) are used to spread the data at chip rate which is higher than the symbol rate by an amount equal to spreading gain. Let T be the symbol duration and T_c be the chip duration, then the spreading gain G is defined as

$$G = T/T_c \tag{1.1}$$

Figure 1.4 shows the working principle of a simple CDMA system.

1.4.3 Multicode CDMA

Multicode CDMA is a technique to provide variable throughput depending upon the QoS requirements [24]. The idea is to assign more than one spreading codes to a user requiring high data rate if the other users are idle or require low data rates. This multicode system retains the benefits of CDMA system e.g. anti-jamming ability, robustness against multipath effects etc. Figure 1.5 shows the block diagram of a typical multicode CDMA system.

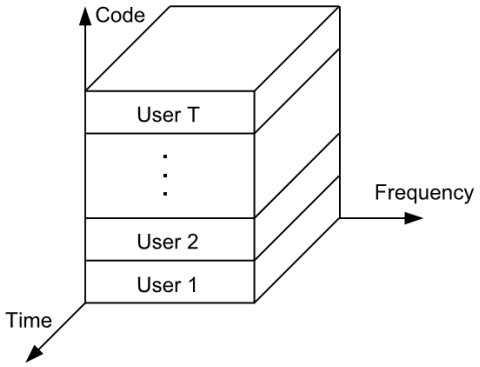

Figure 1.3: Code Division Multiple Access

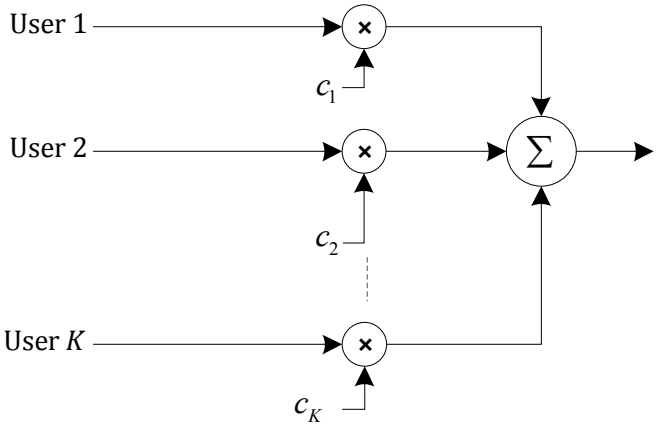

Figure 1.4: CDMA block diagram

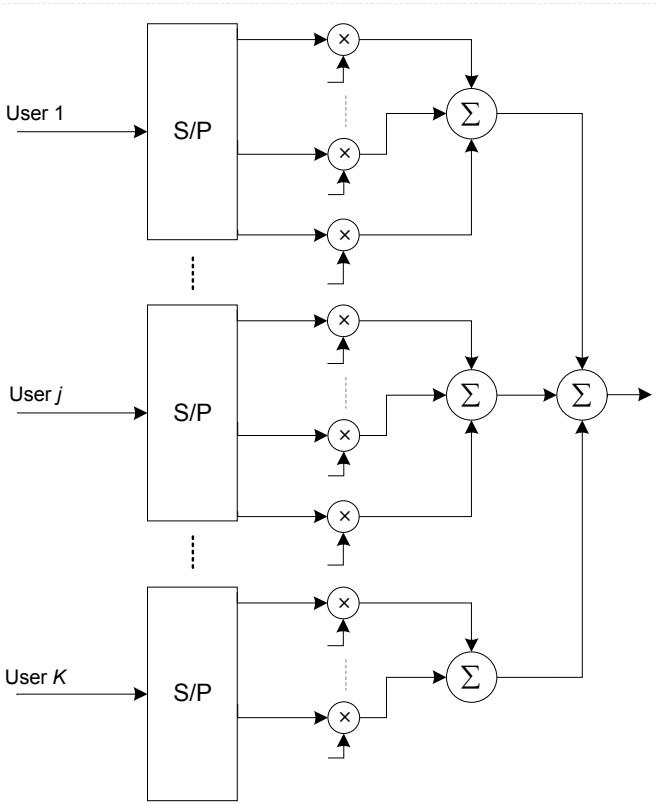

Figure 1.5: Multicode CDMA block diagram

1.5 Structure of Thesis

Rest of the thesis is organized as follows.

Chapter 2 gives a detailed review of the existing algorithms and techniques for time-frequency synchronization and link adaptation at the physical layer of CDMA-based wide-band waveforms or other infrastructureless CDMA systems.

Chapter 3 presents the proposed Modified Square Timing Recovery (MSTR) algorithm for SCO estimation and compensation. All the three stages including SCO estimation, post-filtering and compensation are described. Both the single and multiuser cases are investigated and simulation results are presented in this chapter.

The proposed burst detection algorithms are given in chapter 4. It also includes the

proposed specifically designed training sequences. Simulation results for both the single and multiuser CDMA scenarios are also part of this chapter.

The proposed FFT and interpolation based CFO estimation algorithm is presented in chapter 5. It also includes the novel two stage algorithm for CFO recovery. Computational complexity comparison and simulation results are also included. It also contains the channel estimation algorithm.

Chapter 6 presents the proposed novel link adaptation algorithm. It starts with the system model, followed by the optimization problem and the proposed fuzzy inference system based link adaptation scheme.

Chapter 7 gives the brief overview of the physical layer implementation including the design partitioning, FPGA and DSP implementations and comparison of results from hardware and simulation.

Finally, chapter 8 concludes the thesis and gives some future recommendations for researchers in this field.

Chapter 2

Literature Review

Software defined radio waveform design has been an active area of research since last two decades. More specifically, to support data intensive applications and bulky data traffic in tactical and strategic battlefields, the waveform developers are moving towards high throughput network-based digital wideband waveform design. The goal of this thesis is also to design a high throughput CDMA based wideband networking waveform for which efficient time/frequency synchronization and data rate adaptation algorithms are required. Several algorithms and techniques have been proposed by researchers in this field in recent years as well as many years ago. In this chapter, some of the prominent and recent developments are summarized. To provide a better insight to the reader, the literature review is divided into sections such as sampling clock recovery, burst detection, carrier frequency offset estimation and link adaptation. A detailed review of the existing wideband networking waveforms has already been presented in section 1.1 of chapter 1.

2.1 Sampling Clock Recovery

The timing synchronization at the physical layer of the proposed wideband waveform consists of two parts; (1) Sampling clock recovery, and (2) Burst detection. The Sampling Clock Offset (SCO) is present due to the inherent mismatch between the transmit and receive crystal oscillators. Due to thermal drift, this sampling clock frequency offset will also change slowly in time [21]. A time domain-based sampling clock offset estimation and correction algorithm is presented in [25]. In this paper, authors explain the cause of sampling clock offset and analyze the effect of this offset on the communication system's performance.

This algorithm is more specific to Orthogonal Frequency Division Multiplexing (OFDM) waveforms. A more generic low complexity algorithm for sampling clock offset estimation is proposed in [26]. This algorithm is non-data-aided and is based on feed-forward timing estimation. The computational complexity of this algorithm is almost equal to that of standard Square Timing Recovery (STR) algorithm proposed by Oerder and Meyr [27] and higher than the well-known Phase Locked Loop (PLL) method. However, it is superior in terms of Minimum Mean Square Error (MMSE) and jitter performances. Authors have also presented the FPGA implementation method on SDR platform. One major drawback of this algorithm is that it is only applicable to constant offsets and cannot be applied directly to the systems where time varying sampling clock offsets are present.

Another algorithm for fractional timing estimation using two samples per symbol along with the interpolation-based compensation is proposed in [28]. An important contribution of this scheme is that the baseband signal is complex modulated with a complex exponential at one half of the symbol rate. This is followed by lowpass filtering which results in a signal containing the information of symbol timing offset. Both the algorithms [26] and [28] have two major limitations. Firstly, they are only valid for constant drift between the transmitter and receiver sampling clocks and secondly, they do not incorporate the multipath channel effects while evaluating the estimator's performance. An algorithm based on Sample Point Reordering (SPR) is proposed in [29] but it assumes sampling clock inaccuracies of up to only 12 ppm which is totally impractical in case of software defined radios. Moreover, the performance of this estimator is affected by the amount of frequency offset present in the received signal.

Algorithm for joint estimation of SCO and CFO is proposed in [30–32]. The authors of [30,31] have targeted OFDM systems but the presented algorithm use predefined preambles for the estimation and doesn't require cyclic prefix (CP). The algorithm is computationally less extensive as compared to the Maximum Likelihood scheme [33]. However, the frequency domain processing time is increased by the use of preamble. A two dimensional linear least square (LS) estimation of SCO is proposed in [32]. However, this algorithm is not suitable

for SDR based burst mode networks because of its high computational complexity.

2.2 Burst Detection

The conventional approach for burst detection is based on calculating the energy of the received signal and comparing it to a threshold. An example of such kind of algorithm is given in [34]. The authors have developed the closed form expressions for the probability of false alarm and probability of detection in Additive White Gaussian Noise (AWGN), flat and multipath fading channels. Although energy based burst detectors are very simple and do not require preamble but they are unable to adapt to various mobile communication channels. The reason is that the received signal energy varies with the changing noise level and channel conditions. Hence, a fixed threshold results in either high false alarm probability or low detection probability.

A burst detection technique based on on-off keying during the preamble duration followed by Markov chain search is given in [35]. Another preamble based synchronization algorithm is given in [36] which is based on using Barker sequence of length 7 as a preamble. A two step algorithm with windowing method is introduced. The preamble is modulated prior to spreading by differential phase shift keying. The correct detection is declared upon locating the Barker sequence based preamble. The performance of the algorithm is analyzed in AWGN and frequency selective fading channels through simulation. A hybrid correlator architecture based burst detection algorithm is proposed in [37]. The parallel structure of matched filter and serial structure of correlator are combined to form a hybrid correlator architecture. The detection performance of the hybrid correlator and serial/parallel structures is analyzed by setting a detection threshold that obtains a constant false alarm rate.

A periodic variance threshold searching method for burst detection in Direct Sequence Spread Spectrum systems is given in [38] which is based on Short Time Fourier Transform (STFT). The periodicity of the STFT of DSSS signal is exploited to detect the signal by

setting a threshold on the signal variance. The method is simple and easy to implement but the authors have analyzed the performance of the algorithm in AWGN only. In fading channels, the performance is degraded to a large extent. Another algorithm for the detection of DSSS signals using Haar Wavelet Transform (HWT) is given in [39]. The detection algorithm uses the second order moments of the autocorrelation of the DSSS signal after taking HWT. This method is computationally extensive but shows better performance at low SNRs in AWGN. The algorithm is also capable of estimating the symbol period using the same HWT technique.

An autocorrelation based detection algorithm for DSSS signals in cognitive radios is proposed in [40]. In the first stage, this algorithm finds the peaks of the spreading sequence autocorrelation. In the second stage, the decision of burst detection is made through cumulative peak-to-average calculation. The algorithm is based only on pseudo-noise (PN) sequence autocorrelation peaks and there is no decision metric for signal detection. Another drawback is that if the number of sampling points are decreased, the probability of detection decreases very rapidly. Another correlation-based algorithm for the detection of DSSS packet through a specifically designed preamble is proposed in [41]. The proposed preamble consists of a number of blocks, spread through the corresponding spreading sequence. The performance of this algorithm is degraded if the carrier frequency offset is not compensated earlier properly.

One possible approach for increasing the detection probability without much increasing the probability of false alarm is to use adaptively varying threshold. One such scheme is proposed in [42] using Constant False Alarm Rate (CFAR). This adaptively varying threshold scheme is only applicable to single user CDMA systems. Another adaptively varying threshold scheme for burst detection is proposed in [43] which gives improved detection performance as compared to the one in [42]. This algorithm adjusts the detection threshold using the pre-estimated correlation energy. This is done in the threshold generation mode prior to the search mode.

2.3 Carrier Frequency Offset Estimation

Several algorithms for Carrier Frequency Offset (CFO) estimation have been proposed by many researchers. Some of these algorithms estimate CFO jointly with the channel and/or timing estimation. An algorithm for joint estimation of channel and frequency offset is given in [44], which provides the estimates of frequency offset and channel in closed form. Firstly, the multiuser estimation problem is conerted into single user estimation problems and secondly, the obtained nonlinear multivariate problem is solved. This algorithm is computationally extensive and the estimation accuracy decreases for large amount of CFO. A suboptimal ESPIRIT based algorithm is given in [45], which is less computationally extensive but its performance in multipath fading channels is not satisfactory. A blind CFO estimation method is proposed in [46] which is applicable only to the estimation of small residual offsets. This algorithm is based on generalized eigenvalue problem and estimates the residual frequency offsets and channel state efficiently.

An efficient algorithm for the joint estimation of frequency offset and propagation delay is given in [47], but it is computationally very complex. In the same paper, another suboptimal algorithm has been proposed which has lesser complexity but its variance is high as compared to Cramer-Rao Bound (CRB). A Non-Data Aided (NDA) estimation algorithm based on determinant minimization is given in [48]. The authors of [48] also compare the performance of their proposed estimator with the Generalized Eigenvalue Problem (GEVPM) and Modified GEVPM based algorithm. The problem with this estimator is that its accuracy is decreased at low SNRs. Two generalized CFO estimation algorithms are given in [49, 50]. Both these algorithms show large Mean Square Error (MSE) at low SNRs. Also, both these algorithms do not consider multipath fading channel effects.

Several two stage algorithms for Carrier Frequency Offset (CFO) estimation have also been proposed by many researchers. A two stage frequency synchronization algorithm is proposed in [51]. In the first stage, this algorithm finds a coarse estimate of the frequency offset by minimizing the determinant of a CFO-dependent matrix and iteratively finds a fine

estimate using adaptive Least Mean Square (LMS) algorithm in the second stage. This algorithm is more suited for joint CFO and channel estimation and pose extra computational burden for frequency offset estimation only. Another two stage CFO estimation algorithm is proposed in [52] which is more specific to Orthogonal Frequency Division Multiple Access (OFDMA) system but can be applied to other systems by minor changes. This algorithm is based on subspace processing so as to estimate the CFOs of all the users simultaneously. In [53], an algorithm is proposed for estimating large frequency offsets by using the autocorrelation and half periodic approach. This algorithm solves the contradiction between the frequency offset estimation range and estimation accuracy. The algorithm is simple and easy to implement but its performance is very poor at low SNRs.

Another two stage carrier frequency offset algorithm is proposed in [54]. The coarse estimation stage of this algorithm exploits the autocorrelation of the known preamble sequences [55], whereas the fine estimation stage uses a suboptimal estimator with performance close to Cramer-Rao Lower Bound (CRLB) for high values of SNR [56]. Moreover, the closed form expressions for the fine estimation of CFO are also derived, assuming high SNR and low frequency deviations. Both these assumptions are not practical in SDR networks. Another drawback of this algorithm is its high computational complexity due to the accumulation of preambles of consecutive bursts needed to reduce the estimator variance so as to approach the CRLB.

To reduce the computational complexity and provide the same Bit Error Rate (BER) performance as that of the conventional two stage algorithm given in [54], another two stage algorithm is proposed in [57]. It offers reduced computational complexity by modifying the Extended Schmidl and Cox Algorithm (ESCA) [58–60] in the coarse CFO estimation stage. The fine estimation stage correlates the preambles of the consecutive bursts [61]. A high performance frequency estimation algorithm is given in [62] which consists of three stages. The first two stages consist of coarse CFO estimation and third stage finds fine frequency estimate by eliminating the influence of modulation on the data.

2.4 Link Adaptation

Efficient algorithms for resource allocation/utilization are required to optimize the use of scarce SDR resources. This involves adapting the transmission parameters of the SDR waveform to changing channel conditions, QoS and data rate requirements. This process is called link adaptation. A simple example is the transmit power control algorithm, in which the transmission power is altered based on channel variations and fading because a low transmit power is sufficient under good channel conditions. A well-known link adaptation strategy is adaptive modulation and coding (AMC) [63, 64]. In AMC, the channel coding rate and modulation technique are changed according to the varying channel behavior.

Many varieties of AMC strategies are proposed by many researchers in recent years. One such technique is proposed in [65] for mobile-WiMax technology using software defined radio to achieve maximum throughput by retaining a threshold bit error rate. Another paper [66] proposes a channel quality indicator (CQI) mechanism for cooperative MIMO systems over frequency selective fading channels. The corresponding throughput performance in fading channels is analyzed. A protocol for adaptive modulation and coding is developed in [67] for a typical wireless communication system. The limitation of this paper is the assumption that the channel is a slow Nakagami-m. The performance of the proposed algorithm in achieving a target packet error rate is analyzed. An algorithm for achieving interference alignment through adaptive modulation and coding is proposed in [68] based on channel state information. Interference alignment is a technique that tries to align all the interfering signals frequency, time or space domain. It requires accurate channel state information which is not available in practical systems. An adaptive scheme is proposed which tries to obtain perfect channel state information from the imperfect channel state information.

An efficient scheduling algorithm for adaptive modulation and coding that guarantees the QoS requirements of individual users is proposed in [69]. The Information from both the data link and physical layers are used to schedule the system parameters and protocols to achieve maximum throughput. This is why the proposed algorithm is called QoS-based

cross layer scheduling. Another scheduling algorithm based on finite block-length analysis of channel capacity is proposed in [70]. The proposed algorithm achieves better performance in terms of throughput as compared to the existing conventional technique for Long Term Evolution (LTE) system. A multidimentional QoS-based packet scheduling algorithm is proposed in [71] for providing optimized packet scheduling weights to fulfill the throughput requirements of the variety of applications and services. The proposed technique is applied to high speed packet data access (HSDPA) system and shown to achieve better throughput performance as compared to the existing methods. Orthogonal multicode transmission which is primarily used to enhance the data rate in the 3rd Generation Partnership Project (3GPP) standard [63, 72], has also been used for link adaptation.

A fundamental scheme for achieving variable data rates by changing the set of spreading sequences in multicode Code Division Multiple Access is proposed in [73]. The expressions for Multiple Access Interference (MAI) have also been derived. This paper lacks the scheduling algorithm for multicode transmission. A scheduling algorithm for both the Adaptive Modulation and Coding (AMC) and multicode transmission is proposed in [74], which maximizes the Carrier-to-Interference Ratio (CIR) to increase the throughput. A link adaptation for High Speed Packet Data Access (HSPDA) is presented in [75] by adaptive modulation and coding, multicode transmissions and Hybrid Automatic Repeat Request (HARQ). The paper also compares the throughput of MC-CDMA and DS-CDMA technologies using the proposed method. The average bit error rate performance of the AMC and multicode scheme for Nakagami fading channel is studied in [76].

For uplink CDMA system, the problem of maximizing the total throughput under a bit error rate constraint is investigated in [77]. The realization of variable data rate is achieved by parametrizing the number of signature waveforms (multicodes) and constellation points in Quadrature Amplitude Modulation (QAM) for each user. The solution is optimal and potentially complex. A sub-optimal approach of deriving the expressions for optimal resource allocation based on single user is proposed in [78]. The single user solution is then extended to form a sub-optimal sequential optimization procedure for multiple users.

Chapter 3

Sampling Clock Recovery

The timing synchronization at the physical layer of the proposed wideband waveform consists of two parts; (1) Sampling clock offset estimation and compensation, and (2) Burst detection. Both these operations are very important in wideband networking radio operation as they directly affect the adaptive time slot algorithm in ATDMA based Medium Access Control (MAC) protocol. Figure 3.1 shows the relation of adaptive time slot algorithm in wideband networking operation with the timing synchronization. The measurement of ATDMA time slots and thus the switching rate of MAC is affected by the time varying sampling clock offset. This sampling clock offset is caused by the inherent mismatch between the oscillators of transmitter and receiver [20]. Sampling clock recovery stage estimates and compensates this offset. Similarly, the start of each time slot depends on the burst detection stage and the switching rate of MAC. In this way, both these operations that constitute the timing synchronization, are very important for ATDMA and MAC protocol.

The Sampling Clock Offset (SCO) degrades the performance heavily, if not estimated and compensated properly. For multiuser CDMA system, it becomes more difficult to estimate the offset because each radio receives the composite signal from all the transmit radios. Moreover, this offset varies slowly with time due to thermal drift [21].

We propose Modified Square Timing Recovery (MSTR) algorithm[1] consisting of three stages for both the single and multiuser cases. The proposed MSTR algorithm consists of three stages. In the first stage, Sampling Clock Offset (SCO) is estimated at chip level by modifying square timing estimation. In the second stage, the SCO estimates are post-filtered to improve the tracking performance. We present a novel usage of Steady-State,

[1]Parts of this chapter appear in author's own publication, [20].

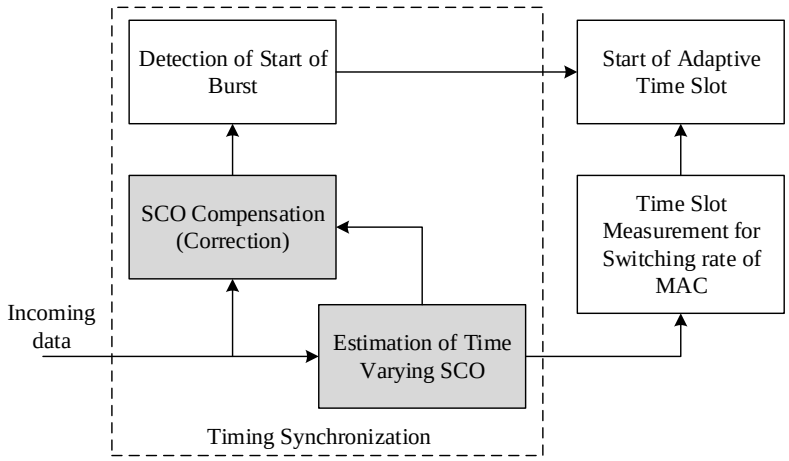

Figure 3.1: Adaptive time slot algorithm and its relation with timing synchronization

State-Space Recursive Least Squares with Adaptive Memory (S4RLSWAM) for the post-filtering of SCO estimate. The third stage compensates the estimated SCO by using a feedforward Lagrange interpolation based algorithm.

3.1 System Model and Problem Formulation

We consider K users at the physical layer of the wideband waveform. The spreading waveform of the k^{th} user is given by

$$\pi_k(t) = \sum_{n=0}^{G-1} c_k[n] g(t - nT_c) \tag{3.1}$$

where $c_k[n]$ is the n^{th} sample of the spreading code of k^{th} user, G is the spreading gain and $g(t)$ is the pulse shaping filter at chip level with period $T_c = T/G$ (T is the symbol duration). The transmitted signal $s_k(t)$ of k^{th} user is given by

$$s_k(t) = \sum_i d_k[i] \pi_k(t - iT) \tag{3.2}$$

where $d_k[i]$ is the i^{th} transmitted data symbol of k^{th} user and T is the symbol duration. For multipath fading environments, the channel impulse response is given by [79]

$$h_k(\tau, t) = \sum_{l=0}^{\gamma_k} \alpha_{kl}(t) e^{j2\pi f_{D,kl} t} \delta(t - \tau_{kl}) \tag{3.3}$$

where $\delta(t - \tau_{kl})$ is the Dirac delta function defined as

$$\delta(t - \tau_{kl}) = \begin{cases} +\infty, & \text{if } t = \tau_{kl} \\ 0, & \text{Otherwise} \end{cases}$$

and which is also constrained to satisfy the identity

$$\int_{-\infty}^{\infty} \delta(t - \tau_{kl})\, dt \ = 1$$

and $\alpha_{kl}(t)$, $f_{D,kl}$, τ_{kl} and γ_k are the time varying complex path gain, Doppler spread, delay spread corresponding to the l^{th} path and k^{th} user and number of multipath, respectively. After passing through the channel, the received composite continuous time baseband signal can be expressed as

$$r(t) = \sum_{k=1}^{K} e^{j2\pi \Delta f_k t} \sum_{i} d_k[i] q_k(t - iT) + w(t) \tag{3.4}$$

where

$$q_k(t) = \sum_{l=1}^{\gamma_k} \alpha_{kl}(t) \pi_k(t - \tau_{kl}) \tag{3.5}$$

and Δf_k is the k^{th} user's CFO caused due to the Doppler spread and/or frequency mismatch between the transmitter and receiver. The last term $w(t)$ in (3.4) represents White Gaussian Noise (WGN) with zero mean and variance σ^2. Let the length of each burst of data be BT, where B is the number of symbols in each burst. The parameter B is selected such that the channel behaves time invariant within burst duration. Therefore,

$$\alpha_{kl}(t) = \alpha_{kl} \qquad\qquad iT \leq t \leq (i + B)T$$

This constraint is satisfied if the time BT is less than or equal to the coherence time (T_{coh}). The coherence time is related with the Doppler spread. This relation is given as [80]

$$T_{coh} = \frac{0.423}{f_D}$$

After sampling the signal $r(t)$ at sampling rate of $f_s = 1/T_s = N_s/T_c$, we get

$$r(nT_s) = \sum_{k=1}^{K} e^{j2\pi\Delta f_k nT_s} \sum_i d_k[i] q_k(nT_s - iT - \epsilon_k(nT_s)T_c) + w(nT_s) \tag{3.6}$$

where N_s is the upsampling factor and $\epsilon_k(nT_s)$ is the n^{th} sample of the unknown slowly varying time delay corresponding to the k^{th} user, and represents the parameter to be estimated. This slowly varying time delay is produced due to frequency offset present between the oscillators of the two communicating devices. For single CDMA user case ($K = 1$), the subscript k is dropped, so that equation (3.6) becomes

$$r(nT_s) = e^{j2\pi\Delta f nT_s}.q(nT_s - iT - \epsilon(nT_s)T_c) + w(nT_s) \tag{3.7}$$

At the receiver, the analog received signal is first sampled by Analog-to-Digital Converter (ADC). The drift caused by the sampling clocks of the radios produces sampling clock errors at the ADC before timing and frequency estimation. Due to the sampling clock errors, ADC starts to sample at an unknown uncertain rate [29]. This uncertain rate is neither synchronous to the chip rate nor its oversampled rate. During the transmission of one burst, this clock error is accumulated. This causes excess or starvation of data samples at the output of ADC for slower or faster receiver sampling clocks, respectively. The situation is depicted in Figure 3.2. This problem becomes further complicated in case of multiple CDMA users where all the received signal is the sum of asynchronous transmissions from multiple users.

3.2 Modified Square Timing Recovery for Single User

In this section, the proposed Modified Square Timing Recovery (MSTR) algorithm for single user case has been presented. A three stage clock recovery algorithm has been proposed, including:

1. Modified Square Timing Estimation

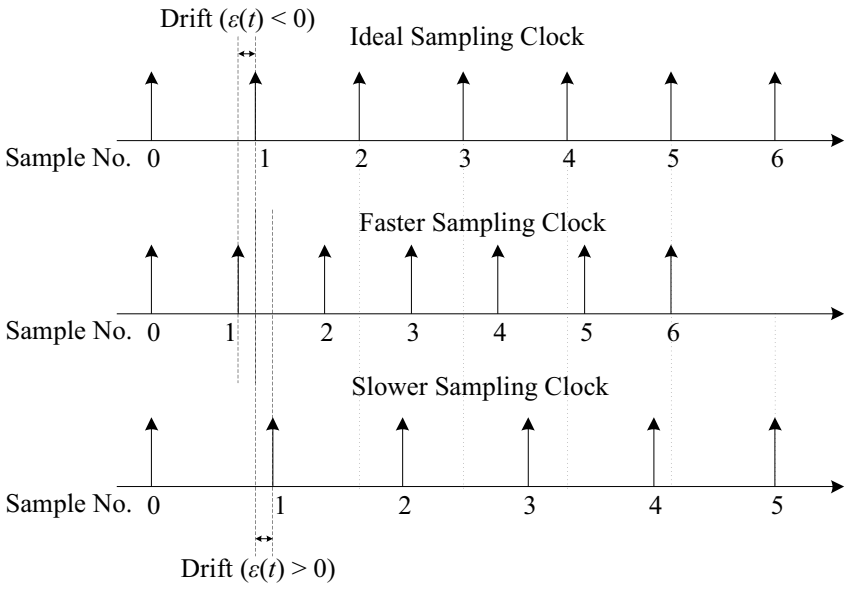

Figure 3.2: Concept of sampling clock drift

2. Post-filtering with State Space Recursive Least Squares with Adaptive Memory

3. Sampling Clock Offset Compensation

3.2.1 Modified Square Timing Estimation

The first stage of the algorithm finds the estimate of the slowly varying time delay $\epsilon[n] = \epsilon(nT_s)$ defined in (3.7). The received sequence is given as

$$r[n] = r(nT_c/N_s) \tag{3.8}$$

Let $f[n]$ be the filtered data after processing through receiving matched filter having impulse response of $g[n]$. Now, the sampling clock offset estimate $\hat{\epsilon}$ is found by computing the normalized phase of the complex Fourier coefficient of $K'N_s$ samples of the filtered sequence using [27]

$$\hat{\epsilon} = -\frac{N_s}{2\pi} \arg\left(\sum_{n=0}^{K'N_s-1} |f[n]|^2 e^{-j2\pi n/N_s} \right) \tag{3.9}$$

In (3.9), K' is the number of chip samples used for estimation. By splitting the summation on the right side of (3.9), we can write

$$\hat{\epsilon} = -\frac{N_s}{2\pi} \arg \left(\sum_{i=0}^{K'-1} \sum_{l=0}^{N_s-1} |f[iN_s + l]|^2 e^{-j2\pi(iN_s+l)/N_s} \right) \tag{3.10}$$

Since $e^{-j2\pi i} = 1 \; \forall \; i$, so

$$\hat{\epsilon} = -\frac{N_s}{2\pi} \arg \left(\sum_{i=0}^{K'-1} \sum_{l=0}^{N_s-1} |f[iN_s + l]|^2 e^{-j2\pi l/N_s} \right) \tag{3.11}$$

The sampling rate f_s must be chosen such that the spectral component of the downsampled data at $1/T_c$ can be represented. It means that we must have $N_s/T_c > 2/T_c$. So, $N_s = 4$ has been chosen. The SCO estimate for $N_s = 4$ is

$$\hat{\epsilon} = -\frac{2}{\pi} \arg \left(\sum_{i=0}^{K'-1} \left[|f[4i]|^2 - j|f[4i+1]|^2 - |f[4i+2]|^2 + j|f[4i+3]|^2 \right] \right) \tag{3.12}$$

or

$$\hat{\epsilon} = -\frac{2}{\pi} \arctan \left(\frac{\sum_{i=0}^{K'-1} |f[4i+3]|^2 - |f[4i+1]|^2}{\sum_{i=0}^{K'-1} |f[i]|^2 - |f[4i+2]|^2} \right) \tag{3.13}$$

The authors of [27] estimate ϵ section by section by assuming very slow variation in time. For each section $\Delta[n]$ (where ϵ is assumed to be constant), an estimate $\hat{\epsilon}[n]$ is found. This assumption is not practical in the presence of large clock offset. In our proposed estimator, the estimate $\hat{\epsilon}[n]$ for each incoming chip is found by computing the complex Fourier coefficient of the $K'N_s$ samples. The proposed sliding window computation of the SCO estimate for n^{th} chip is given by

$$\hat{\epsilon}[n] = -\frac{2}{\pi} \arctan \left(\frac{\sum_{i=n}^{K'+n-1} |f[4i+3]|^2 - |f[4i+1]|^2}{\sum_{i=n}^{K'+n-1} |f[i]|^2 - |f[4i+2]|^2} \right) \tag{3.14}$$

This proposed SCO estimator can be easily implemented using parallel processing and pipelining to achieve high data rates.

3.2.2 Post-filtering with State Space Recursive Least Squares with Adaptive Memory

The second stage of SCO estimation gives the post-filtered estimate $\tilde{\epsilon}[n]$ by post-filtering the estimate $\hat{\epsilon}[n]$ for n^{th} chip sample. The main advantage of post-filtering is the reduction of variance of the estimates. A novel usage of adaptive filter namely State Space Recursive Least Squares with Adaptive Memory (SSRLSWAM) for post-filtering of SCO estimates is proposed. SSRLSWAM has very good tracking performance especially in time-varying environments [81]. The reason for selecting SSRLSWAM instead of other adaptive filters (e.g. Least Mean Square filter, Kalman filter etc.) is the adaptive tuning of the forgetting factor, which is a key parameter in the SSRLSWAM algorithm. There is no concept of forgetting factor in Kalman filter, due to which its tracking performance varies with the time-varying behavior of the incoming estimates. On the other hand, the forgetting factor in SSRLSWAM is adaptively tuned to provide better tracking performance in time-varying scenarios by reducing the settling time and steady-state error as much as possible. This improvement in performance is achieved at the cost of computational complexity which results due to the fact that SSRLSWAM has a memory. Since SSRLSWAM is computationally extensive, an approximate solution is used which is termed as Steady State SSRLSWAM (or S4RLSWAM). The steady state algorithm is still time varying due to the time varying behavior of the forgetting factor.

Since the SCO estimate from the first stage is bounded by $-N_s/2 \leq \hat{\epsilon}[n] < N_s/2$ (see eq. 3.14), the post-filtered estimate $\tilde{\epsilon}[n]$ must also be bounded. Therefore, S4RLSWAM cannot be directly applied for the post-filtering of SCO estimates. A new idea of boundedness has been proposed within S4RLSWAM algorithm. The proposed idea is to apply modulo-N_s operation to the prediction error and a-posteriori states to restrict them to the interval $[-N_s/2, N_s/2)$.

Now, the summarized S4RLSWAM algorithm with the proposed modulo-N_s operation ($[.]_{N_s}$) is described which has been used to find the post-filtered SCO estimate $\tilde{\epsilon}[n]$ (de-

tailed generic algorithm of S4RLSWAM can be found in [81]). The S4RLSWAM algorithm requires a state-space model of the signal. We use the constant velocity model which is expressed in terms of continuous-time state space equations as

$$\begin{aligned} \dot{x_1}(t) &= x_2(t) \\ \dot{x_2}(t) &= 0 \\ y(t) &= x_1(t) \end{aligned} \tag{3.15}$$

such that

$$A = \begin{bmatrix} 0 & 1 \\ 0 & 0 \end{bmatrix}, \quad C = \begin{bmatrix} 1 & 0 \end{bmatrix} \tag{3.16}$$

The discrete-time equivalent of the model

$$\begin{aligned} \dot{x}(t) &= Ax(t) \\ y(t) &= Cx(t) \end{aligned} \tag{3.17}$$

is obtained by sampling at a period of T_s. Therefore,

$$\dot{x}(nT_s) = \frac{x((n+1)T_s) - x(nT_s)}{(n+1)T_s - nT_s} \tag{3.18}$$

Evaluating (3.17) for $t = nT_s$ and noting that $(n+1)T_s - nT_s = T_s$, we get

$$\begin{aligned} x((n+1)T_s) - x(nT_s) &= T_s A x(nT_s) \\ y(nT_s) &= Cx(nT_s) \end{aligned} \tag{3.19}$$

Rearranging gives,

$$\begin{aligned} x((n+1)T_s) &= [I + T_s A]x(nT_s) \\ y(nT_s) &= Cx(nT_s) \end{aligned} \tag{3.20}$$

Let the state and output matrices for discrete-time model be F and H, respectively. From (3.16) and (3.20), the matrices are

$$F = \begin{bmatrix} 1 & T_s \\ 0 & 1 \end{bmatrix}, \quad H = \begin{bmatrix} 1 & 0 \end{bmatrix} \tag{3.21}$$

So that the discrete-time constant velocity model becomes

$$\begin{aligned} x[n+1] &= Fx[n] \\ y[n] &= Hx[n] \end{aligned} \tag{3.22}$$

The algorithm then proceeds as follows. First of all, the predicted states are calculated based on previously estimated states by using

$$\bar{x}[n] = F\hat{x}[n-1] \tag{3.23}$$

By using the predicted states, the predicted SCO estimate is found by using the output equation

$$\bar{\epsilon}[n] = H\bar{x}[n] \tag{3.24}$$

So that the prediction error is

$$\xi[n] = [\hat{\epsilon}[n] - \bar{\epsilon}[n]]_{N_s} \tag{3.25}$$

Note that $\hat{\epsilon}[n]$ is the input to the post-filtering algorithm. The forgetting factor is updated using

$$\lambda[n] = \left[\lambda[m-1] + \alpha\psi[m-1]F^T H^T \xi[n]\right]_{\lambda_-}^{\lambda_+} \tag{3.26}$$

The bracket followed by λ_- and λ_+ in (3.26) indicates the restriction of the forgetting factor to the interval $[\lambda_-, \lambda_+]$. The limit λ_+ is usually set very close to 1, whereas λ_- is determined by the user. The matrix $\psi[n]$ used in (3.26) is given as,

$$\psi[n] = (F - K[n]HF)\,\psi[n-1] + S[n]H^T\xi[n] \tag{3.27}$$

where $K[n]$ is the S4RLSWAM gain, given as

$$K[n] = \lambda[n-1]^{-1}FP[n]F^T H^T \times \left[1 + \lambda[n-1]^{-1}HP[n]F^T H^T\right]^{-1} \tag{3.28}$$

The matrices $P[n]$ and $S[n]$ are given as,

$$P[n] = P_\lambda = \begin{bmatrix} 1-\lambda[n]^2 & (1-\lambda[n])^2 \\ (1-\lambda[n])^2 & (1-\lambda[n])^3/\lambda[n] \end{bmatrix} \tag{3.29}$$

and

$$S[n] = S_\lambda = \frac{\partial P_\lambda}{\partial \lambda} = \begin{bmatrix} -2\lambda[n] & -2(1-\lambda[n]) \\ -2(1-\lambda[n]) & (1-\lambda[n])^2(-1-2\lambda[n])/\lambda[n]^2 \end{bmatrix} \tag{3.30}$$

After the calculation of S4RLSWAM gain $K[n]$ and the estimation error, the a-posteriori estimate of states is calculated by

$$\hat{x}[n] = [F\hat{x}[n-1] + K[n]\xi[n]]_{N_s} \tag{3.31}$$

Using $\hat{x}[n]$, the post-filtered SCO estimate is finally given as

$$\tilde{\epsilon}[n] = H\hat{x}[n] \tag{3.32}$$

Since it is a recursive algorithm, it needs to be initialized. The method of regularization term has been used for initialization. Following initializations are taken to simplify the process.

$$\psi[0] = \mathbf{0}, \;\; \hat{x}[0] = \mathbf{0}$$

3.2.3 Sampling Clock Offset Compensation

The third stage of sampling clock recovery consists of compensation of the sampling clock offset using the post-filtered estimate found in the second stage. A feedforward compensation method based on polynomial-based Lagrange interpolation has been proposed for this stage. From (3.14) it can be seen that the possible range of $\hat{\epsilon}[n]$ is $-2 \leq \hat{\epsilon}[n] < 2$ (for $N_s = 4$), which will be the same for $\tilde{\epsilon}[n]$. With these bounds, figure 3.3 shows the method of selection of samples to be interpolated based on the estimated sampling clock offset. Note that rapid changes in the SCO estimate are shown to explain all the cases; this variation is relatively slower in practical systems. The offset is estimated with reference to the second sample in the set of four samples. A right headed arrow indicates a negative offset, whereas, left-headed arrow shows a positive offset. Let the integer and fractional parts of $\tilde{\epsilon}$ be α and δ respectively. Then, for $N_s = 4$, the samples for cubic interpolation

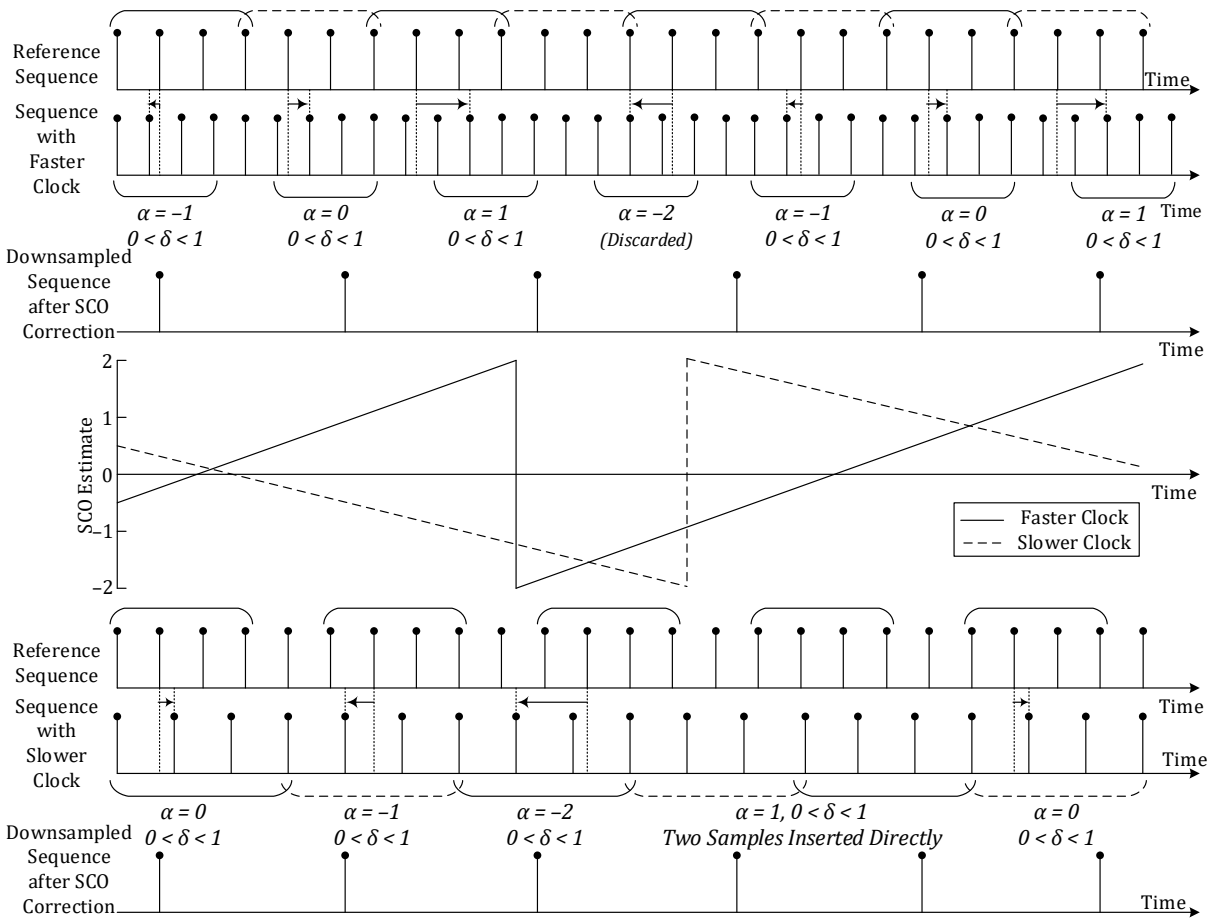

Figure 3.3: Proposed concept of SCO compensation using cubic interpolation

are given as

$$s_1 = x[i + \alpha - 1]$$

$$s_2 = x[i + \alpha]$$

$$s_3 = x[i + \alpha + 1]$$

$$s_4 = x[i + \alpha + 2]$$

where $i = 0, N_s, 2N_s, 3N_s, ...$ For faster sampling clock, a sample is skipped whenever the integer offset α is increased by 1. For slower sampling clocks, one latest sample in time

is used again in cubic interpolation whenever the integer offset α is decreased by 1. After selecting the samples for interpolation, the fractional part δ is used to perform the Lagrange polynomial based cubic interpolation. Let s_1, s_2, s_3, and s_4 be the 4 samples of the filtered signal corresponding to a specific chip on which cubic interpolation is to be performed. For each estimate $\tilde{\epsilon}[n]$, the fractional part $\delta[n]$ is used to interpolate the 4 samples. The compensated and downsampled sample $y[n]$ is given as

$$\begin{aligned} y[n] = &\left(-\frac{s_1}{6} + \frac{s_2}{2} - \frac{s_3}{2} + \frac{s_4}{6}\right)\delta^3[n] \\ &+ \left(\frac{s_1}{2} - s_2 + \frac{s_3}{2}\right)\delta^2[n] \\ &+ \left(-\frac{s_1}{3} - \frac{s_2}{2} + s_3 - \frac{s_4}{4}\right)\delta[n] + s_2 \end{aligned} \tag{3.33}$$

Another problem caused by the sampling clock drift is the excess or starvation of samples at the receiver due to faster or slower receiver sampling clocks respectively. In case of faster receiver clock, samples must be discarded whereas in case of slower receiver clock, extra samples must be put to avoid starvation of data samples.

A new technique to avoid starvation or excess of samples is proposed. The proposed technique works as follows (assuming $N_s = 4$). The integer part α of the SCO estimate decides whether the downsampler has to put required samples or discard extra samples. This is explained in Figure 3.3. It shows that if the receiver has faster sampling clock, the integer part α increases from -2 to 1 slowly. Since SCO estimate has an upper bound of $\tilde{\epsilon} < 2$ integer part jumps from 1 to -2. At this point a sample is discarded for the purpose of synchronization. Similarly, if the receiver has slower sampling clock, the integer part α decreases from 1 to -2 slowly. Since the SCO estimate is lower bounded by $\tilde{\epsilon} \geq -2$, integer part jumps from -2 to 1. At this point, the valid sample $x[i + \alpha - 3]$ is inserted directly without interpolation and an extra sample $x[i + \alpha + 1]$ is also inserted directly to avoid starvation of samples.

3.3 Modified Square Timing Recovery for Multiple Users

The estimation and compensation of sampling clock offset becomes more challenging in case of multiple CDMA users per slot. The reason is that the signal received by the receiving radio is the sum of all the users' transmissions. Therefore, valid signal needs to be decoupled from the composite signal prior to SCO estimation. The proposed modified square timing recovery algorithm is applied to multiuser case as follows.

From (3.7), $f[n]$ is the n^{th} sample of the sequence output from the receiving matched filter at $N_s/Tc = 4/T_c$. Before estimation of SCO, the desired user's data needs to be decoupled from the composite data. This requires correlation with the user specific spreading code. Since the spreading sequence c_k is at the sampling rate of $1/T_c$, it must be upsampled by 4 for chip sample-wise correlation with the sequence $f[n]$. This correlation is given as

$$f_k[n] = \sum_{j=0}^{4G-1} f[n+j]c_{u,k}[j] \tag{3.34}$$

where $f_k[n]$ is the n^{th} sample of the decoupled/correlated sequence and $c_{u,k}[j]$ is the j^{th} sample of the spreading sequence upsampled by 4, corresponding to the k^{th} user, respectively. The next stages of SCO estimation, post-filtering and compensation stages are applied on this sequence in a similar fashion as for single user case. Figure 3.4 elaborates the difference between the single user and multiuser cases. In Figure 3.4, the matched filtering, correlation and SCO estimation are collectively referred to as Modified Square Timing (MST) estimation. Note that the proposed scheme for multiuser SCO estimation reduces to single user SCO estimation when only one user is present. The reason is that there will be no multiple access interference (MAI) in the correlation result from (3.11) for single user.

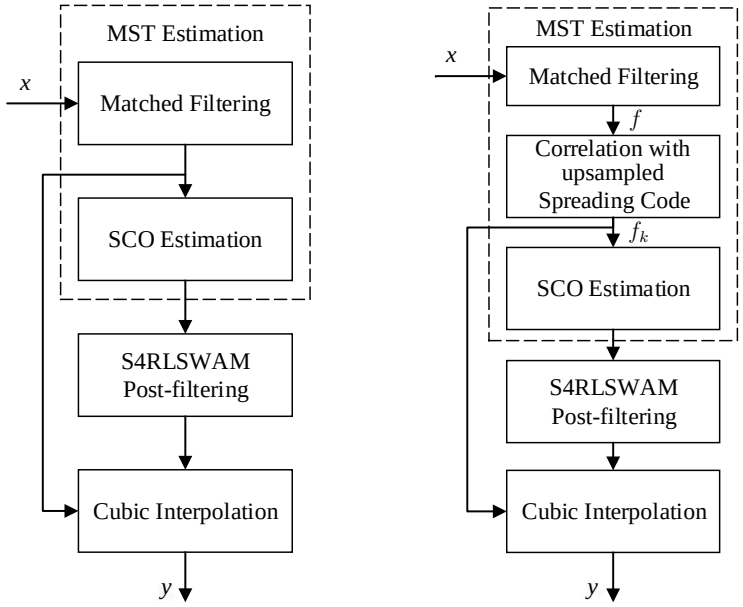

(a) Single user case (b) Multiple users case

Figure 3.4: Block diagram of the proposed MSTR algorithm

3.4 Simulation Results

In this section, simulation results of the proposed MSTR algorithm have been presented. The parameters used in the simulation are as follows.

- Number of modulated symbols in each (N_d) = 288
- RRC roll-off factor (R) = 0.65
- Number of samples used for SCO estimation (K') = 32
- Initial value of forgetting factor (λ_{init}) = 0.995
- Constant α = 0.000005

Golay sequences of length 16 have been used for spreading and QPSK has been used as the modulation technique. Figure 3.5 shows the tracking performance of the proposed

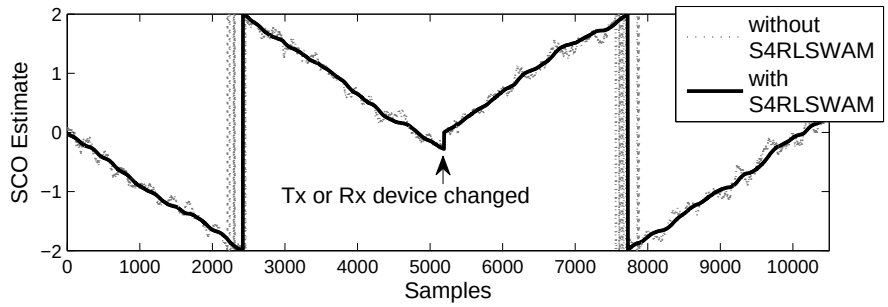

(a) Time varying SCO in both directions

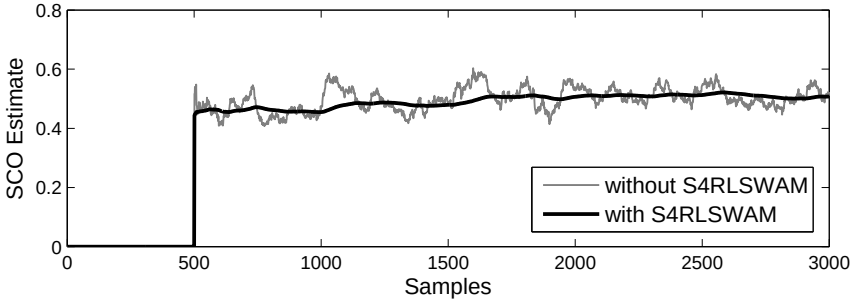

(b) Fixed fractional delay

Figure 3.5: Performance of the proposed SCO estimator for time varying and fixed clock offsets

estimator with and without S4RLSWAM post-filtering at SNR of 2 dB for single user case. S4RLSWAM has been initialized by the method of regularization term. In Figure 3.5(a), tracking performance is shown for a slowly varying time delay due to clock offsets of -200 ppm and $+200$ ppm. The sudden change of clock offset is common in communication networks due to the change of transmitting or receiving device. It can be seen that the proposed estimator efficiently tracks the varying time delay even after the sudden change in clock offset. The proposed estimator can cope with large sampling clock offsets in contrast to the algorithm given in [29] which assumes the inaccuracy of oscillators up to only 12 ppm. Figure 3.5(b) shows the tracking performance of the proposed estimator for a fixed fractional time delay of $0.5T$. It can be seen that the proposed estimator performs well for

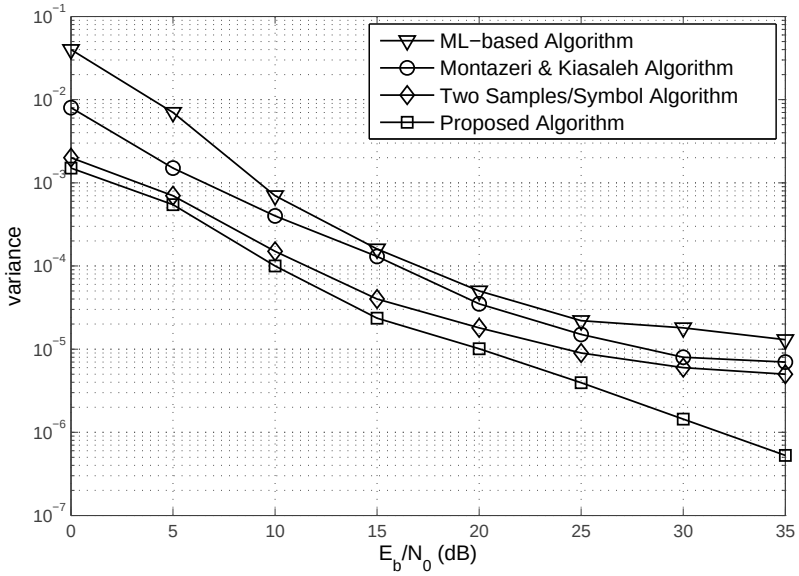

Figure 3.6: Performance comparison of the proposed estimator with other well-known estimators

both the fixed and varying time delays.

The comparison of variances of the proposed and other well-known SCO estimators is shown in Figure 3.6 for single user case. The performance metric (i.e. estimators variance) is given as

$$var(\tilde{\epsilon}) = \frac{1}{M}\sum_{i=1}^{M}\left(\tilde{\epsilon}_i - \hat{E}\left(\tilde{\epsilon}\right)\right) \tag{3.35}$$

where

$$\hat{E}\left(\tilde{\epsilon}\right) = \frac{1}{M}\sum_{i=1}^{M}\tilde{\epsilon}_i \tag{3.36}$$

is the sample mean of the post-filtered estimate $\tilde{\epsilon}_m$ and M is the number of realizations. In this simulation, we have taken $M = 2000$. For comparison, ML-based algorithm [55], Montazeri and Kiasaleh's estimator [26] and a two samples/symbol based feedforward algorithm given in [28] have been considered. It can be seen that the proposed estimator shows considerable performance improvement when compared to other estimators at all SNRs. It

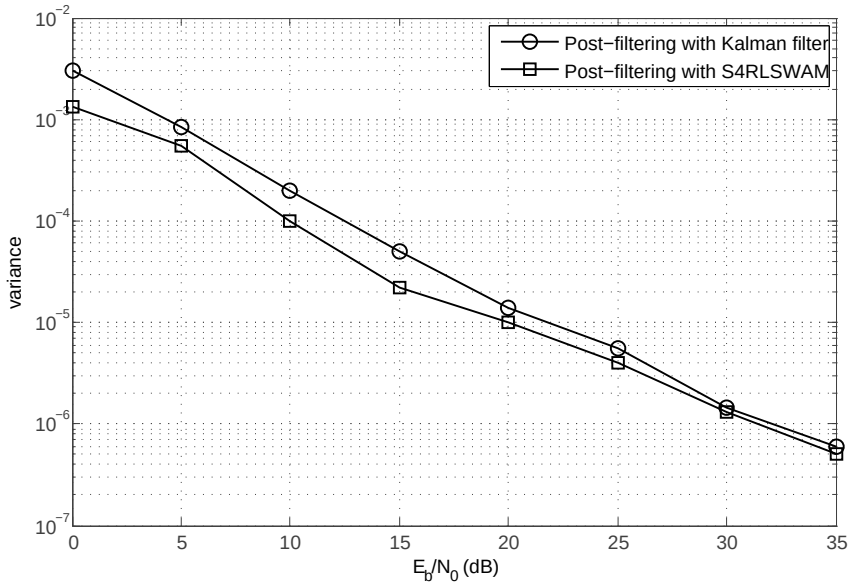

Figure 3.7: Performance comparison of the proposed estimator with Kalman filter and S4RLSWAM post-filtering

is also worth mentioning here that the algorithms given in [26] and [28] are applicable only when the time delay is fixed, whereas the proposed estimator is capable of estimating both the fixed and time varying delays efficiently. Furthermore, the proposed algorithm which uses S4RLSWAM as post-filtering method shows up to 3 dB performance improvement as compared to that with Kalman filter. This is shown in figure 3.7.

Table 3.1: SUI-3 channel model specifications

	Tap 1	**Tap 2**	**Tap 3**
Delay (μs)	0.0	0.4	0.9
Power (dB)	0	-5	-10
K-factor	1	0	0
Doppler (Hz)	0.40	0.30	0.50

Now, we present the performance of the proposed MSTR algorithm for single user in Stanford University Interim-3 (SUI-3) channel model [82]. These six Stanford University Interim (SUI) channels are modelled according to three terrain types and various values of delay spread, Doppler spread and Line of Sight (LOS)/Non Line of Sight (NLOS) conditions. The detailed specifications of all six SUI channel models are given in appendix A. We have used SUI-3 channel model in our simulations which models a terrain having moderate to high tree density and weak LOS. Other specifications of SUI-3 are given in table 3.1. In table 3.1, K-factor represents the ratio of LOS component to NLOS components. For NLOS case, K-factor is zero.

Figure 3.8 shows the estimation performance in terms of variance for AWGN and SUI-3 channel models. For multiuser case, we consider 4 radios, i.e. $K = 4$. Figure 3.9 shows the performance of the proposed MSTR algorithm in AWGN. The performance is compared to the single user case with the same SCO of +200 ppm. Without loss of generality, the first

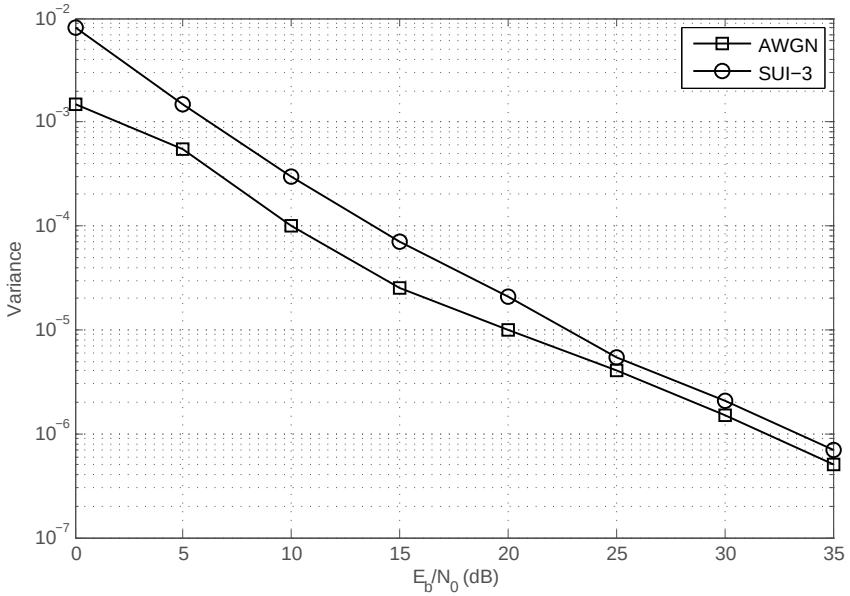

Figure 3.8: Performance of the proposed MSTR algorithm for single user in AWGN and SUI-3 channel model

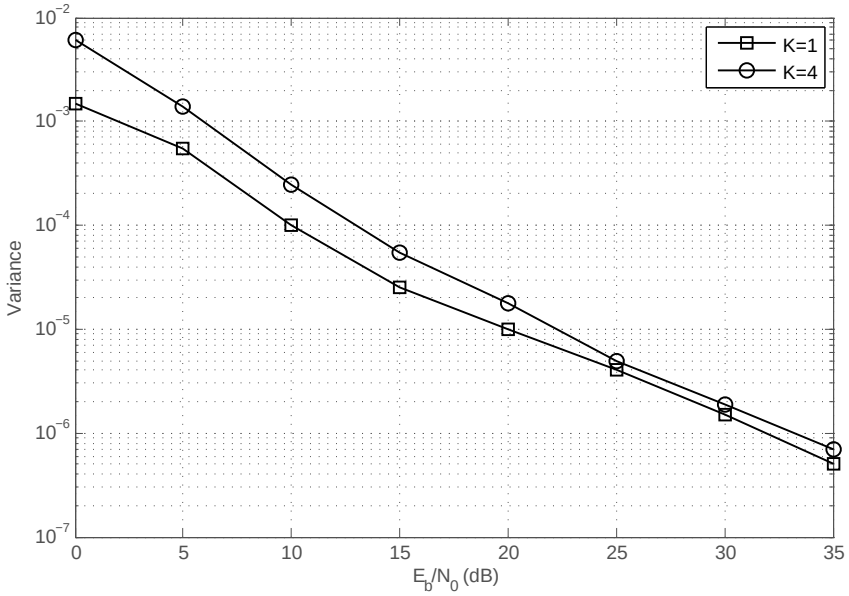

Figure 3.9: Performance of the proposed MSTR algorithm for single/multiple users in AWGN

user is considered as the desired user. It can be seen that the performance degradation is almost 2-3 dB at low SNRs, whereas it reduces to 0.5-1 dB at high SNRs. The performance degradation is due to the Multiple Access Interference present between multiple CDMA users.

3.5 Conclusion

In this chapter, a Modified Square Timing Recovery (MSTR) algorithm for the estimation and compensation of the sampling clock offset in the wideband waveform of SDR is proposed. The proposed algorithm consists of three stages for both the single and multiuser cases. The first stage estimates the Sampling Clock Offset (SCO) at chip level by modifying the well-known square timing estimation. The second stage post-filters the SCO estimates to improve the tracking performance. A novel usage of Steady-State, State-Space Recursive Least Squares with Adaptive Memory (S4RLSWAM) for the post-filtering of SCO estimate

is proposed. Finally, in third stage, the estimated SCO is compensated by using a feed-forward Lagrange interpolation method. It is shown through computer simulations that the proposed MSTR algorithm achieves better performance as compared to a set of known existing methods in terms of reduced estimator variance and overall BER performance.

Chapter 4

Burst Detection

To combat multipath fading effects, especially in fast fading channels, many communication systems use burst mode of transmission [83]. The size of each burst is selected such that the channel behaves time invariant within the duration of each burst [84]. Consequently, timing and frequency synchronization, channel estimation, equalization etc. are performed on each burst independently. In such systems, one of the major challenge at the receiver side is to detect the start of each valid burst of data.

The detection of burst is actually part of the proposed timing synchronization at the physical layer of the wideband networking waveform. The sampling clock recovery (chapter 3) and burst detection are very vital in wideband networking radio operation as they directly affect the adaptive time slot algorithm in ATDMA based Medium Access Control (MAC) protocol. Figure 4.1 shows the relation of adaptive time slot algorithm in wideband networking operation with the timing synchronization. The measurement of ATDMA time slots and thus the switching rate of MAC is affected by the time varying sampling clock offset. Similarly, the start of each time slot depends on the burst detection and the switching rate of MAC. In this way, both these operations that constitute the timing synchronization, are very important for ATDMA-based MAC protocol.

In this chapter, two robust algorithms for burst detection in wideband networking waveform are proposed[1] . The proposed algorithm I computes the decision metric on the basis of proposed Time Domain Repetitive (TDR) training sequence. The major contribution of the proposed algorithm II is a specifically designed training sequence containing two equal length sub-sequences. The design of training sequence involves the use of differential

[1]Parts of this chapter appear in author's own publications, [85], [86].

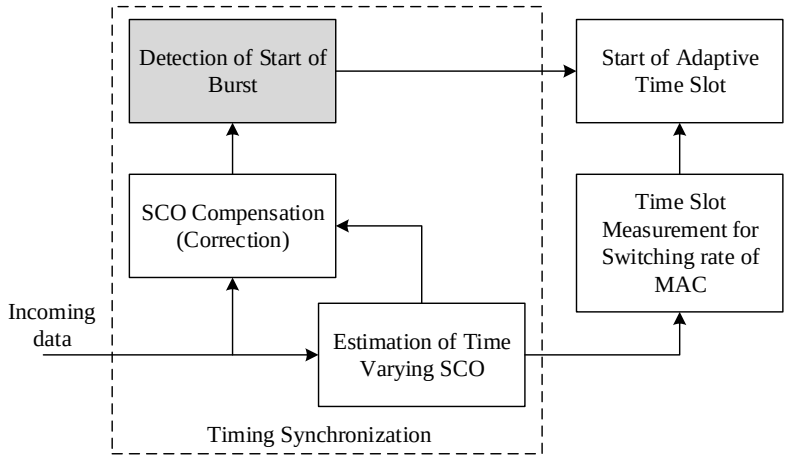

Figure 4.1: Adaptive time slot algorithm and its relation with burst detection

encoding through a precoding sequence. The training sequence structure and precoding sequence are exploited in the decision metric which is normalized by the signal energy. It is shown through computer simulations that the proposed burst detection is robust to carrier frequency offset and multipath fading effects.

4.1 Problem Formulation

The received sampled data (3.6) is re-written as

$$r(nT_s) = \sum_{k=1}^{K} e^{j2\pi\upsilon_k n} \sum_{i=0}^{B-1} d_k[i] q_k(nT_s - iT - \epsilon_k(nT_s)T_c) + w(nT_s) \tag{4.1}$$

where N_s is the upsampling factor and $\upsilon_k = \Delta f_k / f_s \in [-0.5, 0.5]$ is the normalized carrier frequency offset corresponding to the k^{th} user and $\epsilon_k(nT_s)$ is the slowly varying time delay due to SCO corresponding to k^{th} user (discussed in chapter 3). The SCO compensation stage compensates the estimated SCO by downsampling the sequence $r[n]$ by $N_s = 4$ through cubic interpolation and generates the sequence $y[n]$ at $1/T_c$ (equation (3.33)). For Data Aided (DA) burst detection algorithm, each burst contains a known training sequence extending over several samples. The receiver searches for this known training sequence for

the detection of data bursts. Normally the bursts are transmitted back to back without silent intervals, but in case of TDMA-based networking waveform, there can be silent intervals. In our case, let the number of spread samples of the known training sequence be N. Therefore, the valid number of spread data samples is $BG - N$, where G is the spreading gain.

4.2 Proposed Algorithm I

In this section, the proposed Time Domain Repetitive (TDR) training sequence design and the corresponding burst detection algorithm is presented.

4.2.1 Time Domain Repetitive Training Sequence

The design of training sequence can be done in either frequency domain or time domain. Frequency domain training sequences are mostly used in multicarrier systems, e.g. OFDM, multicarrier CDMA, etc [87]. Some training sequences [58] give a decision metric plateau resulting in high probability of false alarm. Therefore, a vital requirement of the training sequence design is that it should give a steep roll-off in the resulting timing/decision metric. Moreover, the training sequence data should also be uncorrelated with the valid data symbols.

To achieve both these requirements, we propose a Time Domain Repetitive (TDR) training sequence consisting of L identical parts. The basic repeated part is taken as a length M_0 sequence. This sequence must have good autocorrelation properties. Figure 4.2 shows the comparison of the autocorrelation of Golay sequence [88], Gold sequence [89] and m-sequence [90]. It can be seen that Golay sequence have better autocorrelation properties as compared to other sequences in terms of sharper peak and lower out-of-phase maxima. Therefore, we have chosen Golay complementary sequence to be used as basic repeated part of the TDR training sequence. Each repeated part is spread by the user specific spreading sequence, so that the length of each part now becomes $M = GM_0$, where G is the spreading

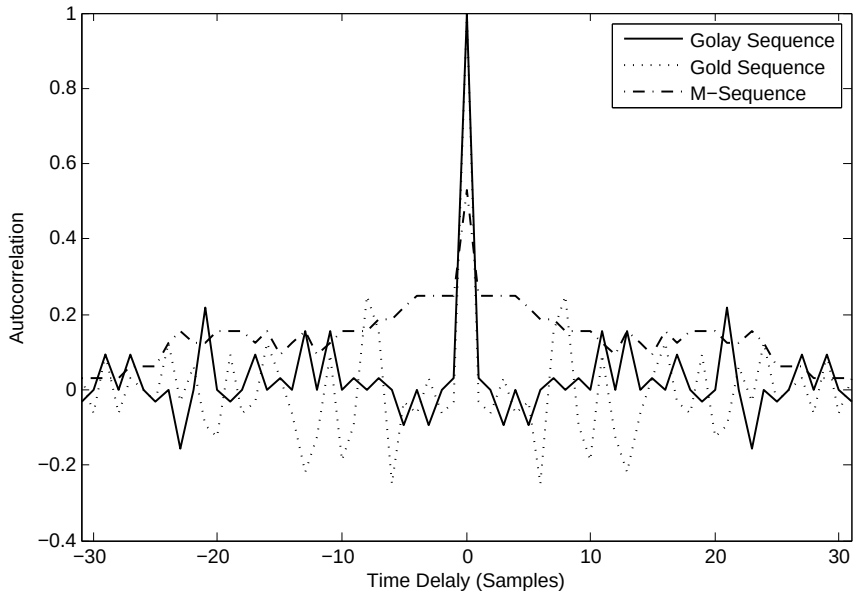

Figure 4.2: Autocorrelation comparison of Golay, Gold and m-sequences

gain. The L identical parts, each of length M are concatenated to form the TDR training sequence of length N, such that

$$M = \frac{N}{L} \tag{4.2}$$

Note that the L identical parts can have different sign patterns as given in [91]. These sign patterns are exploited in the calculation of timing metric for burst detection. As an example, for $L = 4$, the sign pattern can be $[- + - -]$. If the length M_0 repeated part is denoted by A, then the resulting training sequence becomes $[-A, A, -A, -A]$ for the given sign pattern. The concept is elaborated in Figure 4.3.

4.2.2 Burst Detection Algorithm based on TDR training

The proposed burst detection algorithm calculates decision timing metric on the data sequence $y[n]$ (output of SCO compensation stage) correlated with the user specific spreading sequence. The reason is that the received data is spread and the training sequence known at the receiver is also spread so there should be a method to indicate the start of each

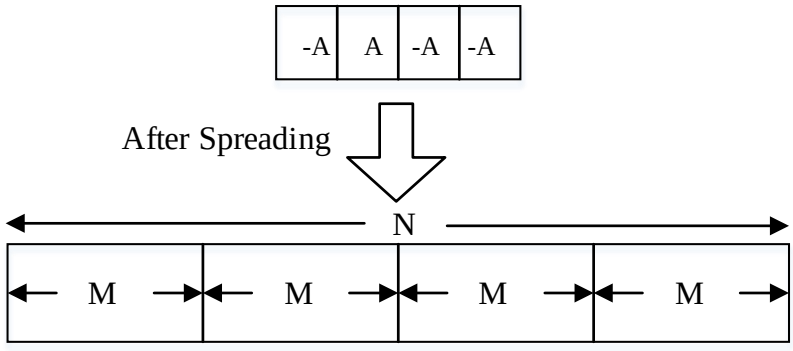

Figure 4.3: Concept of TDR training sequence for $L = 4$

spread symbol in time. For this purpose, the SCO compensated data is correlated with the spreading sequence of the corresponding user. The correlated data for k^{th} user is given as

$$y_{c,k}[n] = \sum_{j=0}^{G-1} y[n+j]c_k^*[j] \tag{4.3}$$

where G is the spreading gain, $y[n]$ is the n^{th} sample of the downsampled data from SCO recovery stage and c_k is the spreading sequence of k^{th} user. Note that this correlation is not needed in case of multiuser case, because of the correlation performed in sampling clock recovery stage. In that case, $y_{c,k}[n] = y[n]$. The correlated data found by using (4.3) is used to compute the timing metric and energy. The calculation of timing metric exploits the repeating structure of the training whereas the energy is calculated by squaring the samples of correlated data. The formulas for timing metric (P) and energy (E) are given as

$$P[d] = \sum_{k=0}^{L-2} b[k] \sum_{m=0}^{M_0-1} \left[\left(y_{c,k}^*[d + (kM_0 + m)G] \right) . \left(y_{c,k}[d + ((k+1)M_0 + m)G] \right) \right] \tag{4.4}$$

$$E[d] = \sum_{i=0}^{M-1} \sum_{k=0}^{L-1} |y_{c,k}[d + i + kM]|^2 \tag{4.5}$$

where $d = 1, 2, 3, ...$, $b[k] = p[k] \times p[k+1] = [--+]$, $p[k]$ is the length L sign pattern of the training sequence and $k = 0, 1, ..., L-2$. With the timing metric and energy defined

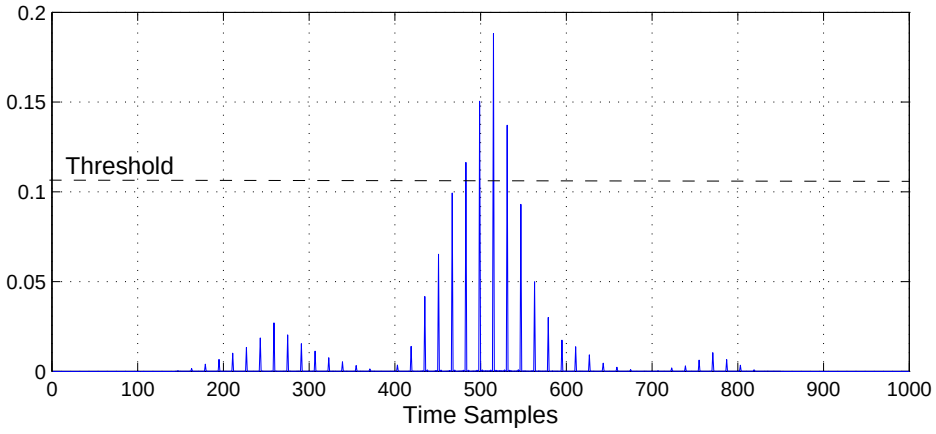

Figure 4.4: A typical normalized timing metric using TDR training sequence ($G = 16$)

in (4.4) and (4.5), the normalized timing metric for the burst detection is given as

$$T_1[d] = \left(\frac{L}{L-1} \frac{|P[d]|^2}{E[d]} \right) \tag{4.6}$$

The normalized timing metric given by (4.6) is similar to the one proposed in [91] for OFDM systems, but obviously the expressions for $P[d]$ and $E[d]$ given in [91] cannot be used directly for CDMA system. Therefore, a modified method for the calculation for $P[d]$ and $E[d]$ (given by (4.4) and (4.5)) is proposed in this paper which uses correlated data as input sequence and spreading gain G for the calculation of timing metric instead of using the received sequence directly. A typical normalized timing metric (or decision metric) T_1 for length 16 Walsh-hadamard spreading codes in AWGN obtained is shown in Figure 4.4. The normalized timing metric is the ratio of $P[d]$ to signal energy. It can be seen from figure 4.4 that the proposed burst detection method gives a timing metric having sharp peak at the burst start.

As mentioned earlier that timing metric calculation exploits the repeated structure of training sequence, so if burst is present, $T_1[d]$ will be high whereas in the absence of burst start, $T_1[d]$ will be low, since energy will be high in both the cases. Therefore, the start of

burst detection is a binary hypothesis problem which can be stated as

$$H_0 : T_1[d] < \gamma, \implies \text{No burst detected}$$

$$H_1 : T_1[d] > \gamma, \implies \text{Burst detected}$$

where γ is the threshold. If burst is detected, the next step is peak searching which finds the index corresponding to the maximum value of the normalized timing metric for next N_w samples. This is mathematically written as

$$\hat{n}_0 = arg \max_d T_1[d] \text{ for next } N_w \text{ samples} \tag{4.7}$$

The peak search can also be increased beyond N_w samples but it will cause unnecessary delay in the processing. The start of the burst index is given by (4.7). Starting from this burst index, the data $y_{c,k}$ is downsampled by G to get B symbols of the detected burst.

4.2.3 Simulation Results

In this section, we present the simulation results of the proposed burst detection algorithm based on TDR training sequence. The parameters used in the simulation are as follows.

- Number of modulated symbols in each burst (without spreading) $(N_d) = 288$
- Training sequence length $(N_0) = 32$
- RRC roll-off factor $(R) = 0.65$
- Threshold $(\gamma) = 0.1$

Golay sequences of length 16 have been used for spreading and QPSK has been used as the modulation technique. The performance of the proposed algorithm has been evaluated by finding the probability of correct burst detection (P_D). In this simulation, we have incorporated multipath fading effects by using SUI channel models [82]. The detailed SUI channel parameters can be found in appendix A. The probability of correct burst detection

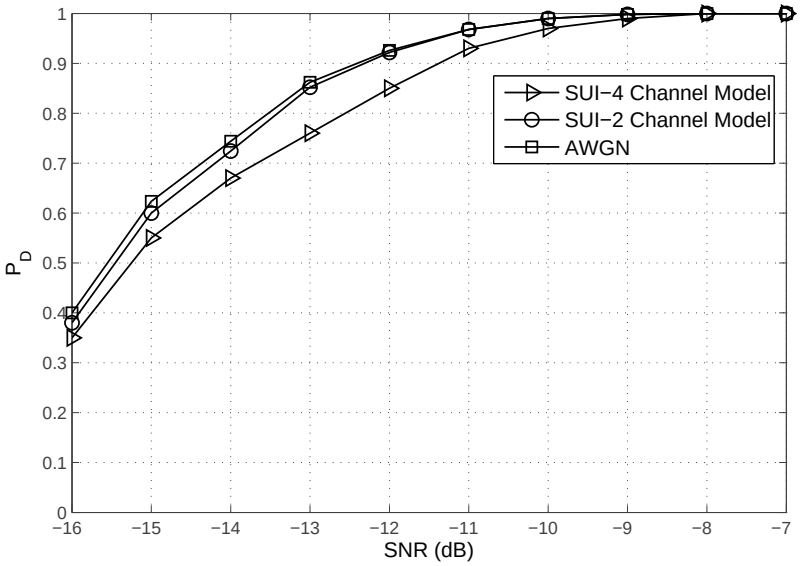

Figure 4.5: Probability of Burst detection versus SNR of the proposed TDR training based algorithm in different channel models

of the proposed algorithm by varying SNR in AWGN, SUI-2 and SUI-4 multipath fading channels is shown in Fig. 4.5. It can be seen that the probability in AWGN and SUI-2 channels is almost equal to that in AWGN whereas only a small difference is observed in case of SUI-4 channel model. This is due to zero line of sight and large delay spread values present in SUI-4 channel model (see appendix A). However, the detection probability is equal to unity at high SNR for all the channels. This shows that the proposed burst detection algorithm is robust against multipath fading effects.

The detection performance of the proposed burst detection algorithm has been compared with that of some existing algorithms. For this comparison, Zhao's algorithm [38] and Deng's algorithm [40] have been considered. The reason for selecting these algorithms is that they are superior to other detection algorithms described in chapter 2 in terms of detection performance. From Fig. 4.6, it can be seen that the proposed algorithm outperforms both these algorithms even at low SNR. The performance improvement is almost

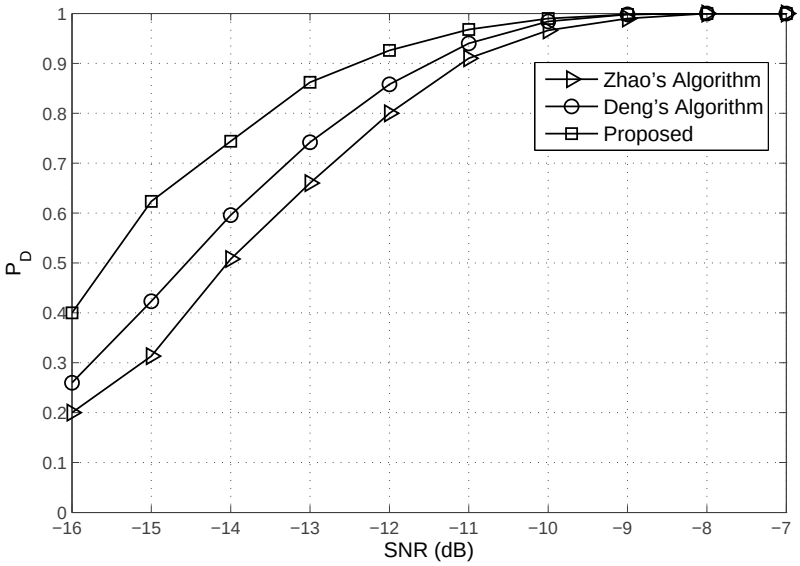

Figure 4.6: Detection performance comparison of the proposed TDR training based algorithm with other algorithms in AWGN channel

1dB at low SNRs ranging from -16dB to -9dB. Moreover, the proposed algorithm achieves $P_D = 1$ at -9dB. The performance of these three algorithms has also been compared in SUI-4 channel model with the same value of γ as used for AWGN channel. This comparison is shown in Fig. 4.7 which shows that P_D for the proposed algorithm is changed slightly, whereas P_D for the other two algorithms is decreased very much. In this case, the performance improvement is almost 2dB as compared to Deng's algorithm. Moreover, the proposed algorithm achieves $P_D = 1$ at -8.5dB.

4.3 Proposed Algorithm II

Although there is no timing metric plateau in the proposed TDR training based burst detection algorithm, the timing metric roll-off needs to be further increased so that the peak becomes sharper and more distinct. To achieve this, we propose a novel Differentially

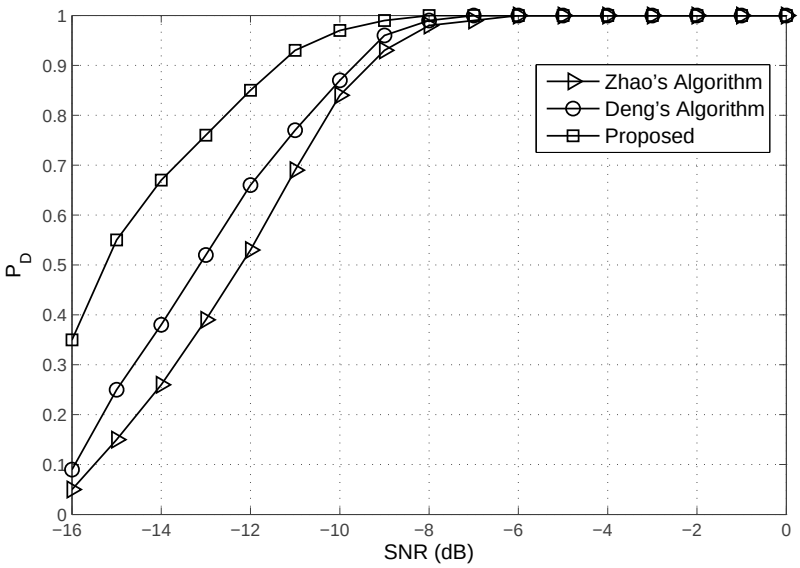

Figure 4.7: Detection performance comparison of the proposed TDR training based algorithm with other algorithms in SUI-4 channel model

Modulated (DM) training sequence and burst detection with precoding algorithm.

4.3.1 Differentially Modulated Training Sequence

We propose a novel training sequence which is based on differential encoding using a precoding sequence. This is why it is termed as Differentially Modulated (DM) training sequence. The idea is to concatenate two equal length sub-sequences $\mathbf{p_1}$ and $\mathbf{p_2}$, each of length $L_0 = N/2G$, where N is the length of spread training sequence and G is the spreading gain. The second sub-sequence $\mathbf{p_2}$ is obtained by differentially modulating the first sub-sequence $\mathbf{p_1}$. This is achieved by using a precoding sequence $\mathbf{p_w}$ of length L_0. Therefore,

$$p_2[j] = p_1[j].p_w[j] \qquad j = 0, 1, 2, ..., L_0 - 1 \tag{4.8}$$

where $p_1[j]$, $p_2[j]$ and $p_w[j]$ are the j^{th} samples of $\mathbf{p_1}$, $\mathbf{p_2}$ and $\mathbf{p_w}$, respectively. By concatenating the two sub-sequences $\mathbf{p_1}$ and $\mathbf{p_2}$, the unspread sequence $\mathbf{v_u}$ of length $N_0 = N/G$ is

given as

$$\mathbf{v_u} = [\mathbf{p_1}\ \ \mathbf{p_2}] \tag{4.9}$$

The sequence given in (4.9) has no user specific information. Therefore, the sequence $\mathbf{v_u}$ is spread by the user specific spreading code to distinguish it from that of other users. So, the proposed spread training signal for k^{th} user becomes

$$v_k(t) = \sum_{i=0}^{N_0-1} v_u[i] z_k(t - iT) \tag{4.10}$$

The choice of sub-sequence $\mathbf{p_1}$ and precoding sequence $\mathbf{p_w}$ is the most important step in the design. These sequences must be intelligently chosen to have specific correlation properties. An important property that the sequences $\mathbf{p_1}$ and $\mathbf{p_w}$ must have is the minimum value of maximum out-of-phase autocorrelation. The accuracy of the correct detection performance of the proposed algorithm is directly related with the value of maximum out-of-phase autocorrelation. The lower the out-of-phase maxima of the chosen sequence, the more will be the accuracy.

Figure 4.2 shows the comparison of the autocorrelation of Golay sequence, Gold sequence and m-sequence. It can be seen that Golay sequence [88] have better autocorrelation properties as compared to other sequences. It can be noted that;

i. The out-of-phase maxima of the Golay sequence autocorrelation is lower than other two sequences, and

ii. The out-of-phase maxima of the Golay sequence autocorrelation is not near the main peak as compared to other two sequences

These two properties govern the selection of Golay sequences for the training sequence design. Furthermore, the proposed training sequence has even better autocorrelation properties. Figure 4.8 compares the autocorrelation of a Golay complementary sequence and the proposed training sequence of length 32. It can be seen that the out-of-phase maxima of the Golay sequence autocorrelation is 21.88% of the peak value in case of Golay

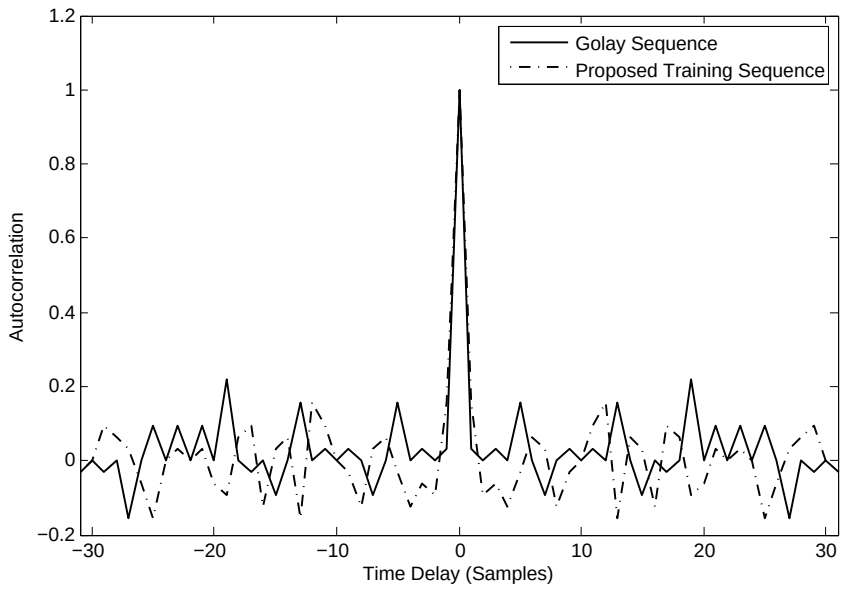

Figure 4.8: Autocorrelation comparison of Golay sequence and the proposed training sequence

sequence, whereas the out-of-phase maxima of the proposed training sequence autocorrelation is 15.6% of the peak value. It also affirms the better correlation properties of the proposed training sequence as compared to the typical Golay sequences. The sequences $\mathbf{p_1}$, $\mathbf{p_w}$ and $\mathbf{p_2}$ chosen from the Golay sequence set of length $N_0/2$ are

$$\mathbf{p_1} = [1, -1, -1, -1, -1, 1, -1, -1, 1, -1, -1, -1, 1, -1, 1, 1],$$

$$\mathbf{p_w} = [1, -1, 1, 1, 1, -1, -1, -1, -1, 1, -1, -1, 1, -1, -1, -1],$$

and

$$\mathbf{p_2} = [1, 1, -1, -1, -1, -1, 1, 1, -1, -1, 1, 1, 1, 1, -1, -1].$$

4.3.2 Burst Detection Algorithm with Precoding

For burst detection, we follow the method of S&C [58] with appropriate modifications. The main modification is in the training sequence design. So, firstly, the proposed differentially

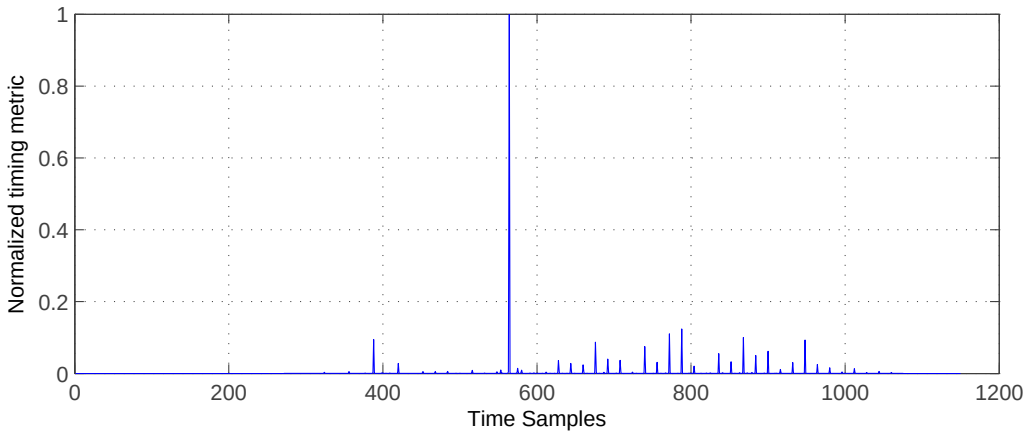

Figure 4.9: A typical normalized timing metric using DM training sequence ($G = 16$)

modulated training sequence is designed according to the procedure mentioned in section 4.3.1. Then the method presented in [58] is applied as follows. Since the received data given by (4.1) is spread and the training sequence known at the receiver is also spread, therefore the SCO compensated data is first correlated with the user specific spreading sequence. This is necessary to indicate the start of each spread symbol in time. If k^{th} user is receiving data, than m^{th} chip of the correlated data is given by

$$y_{c,k}[n] = \sum_{j=0}^{G-1} r[n+j]c_k[j] \tag{4.11}$$

where $y[n]$ is the n^{th} sample of the SCO compensated data. Note that this correlation is not required in case of multiuser case because of the correlation performed in the SCR stage. The correlated data from (4.11) is used to compute the decision metric. Note that the method given in [40] uses the absolute value of correlated data (similar to (4.11)) followed by peak search for detection process. The peaks are separated by the period $T = GT_c$. A major problem in this approach is that these peaks are submerged at low SNRs. To overcome this problem, we propose a decision metric for burst detection which uses the correlated data given in (4.11) and exploits the structure of the proposed training sequence (see section 4.3.1). The algorithm operates in sliding window mode, where the window

size is equal to the spread training sequence length N. The proposed normalized decision metric is given as

$$T_2[d] = \frac{\left|\sum_{m=0}^{L_0-1} y_{c,k}[d+mG].y_{c,k}[d+(m+L_0)G].p_w[m]\right|^2}{|E(d)|^2} \tag{4.12}$$

where

$$E[d] = \sum_{m=0}^{L_0-1} |y_{c,k}[d+(m+L_0)G]|^2 \tag{4.13}$$

is the energy of the current batch of correlated data of k^{th} user. Also, let

$$P[d] = \sum_{m=0}^{L_0-1} y_{c,k}[d+mG].y_{c,k}[d+(m+_0 L)G].p_w[m] \tag{4.14}$$

where $d = 0, 1, 2, 3, ...$ and L_0 is the length of precoding sequence equal to $N_0/2$ and $p_w[m]$ is the m^{th} sample of the precoding sequence (see section 4.3.1). The inclusion of the proposed precoding sequence is the main difference between our modified decision metric and the metric of [58]. A typical normalized timing metric (or decision metric) T_2 of length 16 Walsh-hadamard spreading codes in AWGN obtained by proposed modification is shown in Figure 4.9. The normalized timing metric is the ratio of $P[d]$ to signal energy. It can be seen from figure 4.9 that the proposed burst detection method produces a timing metric having sharp peak at the correct burst start.

From (4.12) and (4.13), the modified decision metric consists of two parts; (1) Timing metric, P, which exploits the training sequence structure and precoding sequence, and (2) Normalization factor, E, which doesn't exploit the training sequence structure. As mentioned earlier that timing metric calculation exploits the differential modulated structure of training sequence, so if burst is present, $T_2[d]$ will be high whereas in the absence of burst start, $T_2[d]$ will be low, since energy will be high in both the cases. Therefore, the start of burst detection is a binary hypothesis problem which can be stated as

$$H_0 : T_2[d] < \gamma, \implies \text{No burst detected}$$
$$H_1 : T_2[d] > \gamma, \implies \text{Burst detected}$$

where γ is the threshold. If burst is detected, the next step is peak searching which finds the index corresponding to the maximum value of the normalized timing metric for next N_w samples. This is mathematically written as

$$\hat{n}_0 = arg \max_d T_2[d] \text{ for next } N_w \text{ samples} \tag{4.15}$$

The peak search can also be increased beyond N_w samples but it will cause unnecessary delay in the processing. The start of the burst index is given by (4.15). Starting from this burst index, the data $y_{c,k}$ is downsampled by G to get B symbols of the detected burst.

4.3.3 Simulation Results

In this section, we present simulation results of the proposed burst detection algorithm based on DM training sequence. The parameters used in the simulation are as follows.

- Number of modulated symbols in each burst (without spreading) $(B) = 288$
- Training sequence length in symbols $(N_0) = 32$
- RRC roll-off factor $(R) = 0.65$
- Spreading gain $(G) = 16$
- Precoding sequence length $(L_0) = 16$
- Training sequence length in chips $(N) = 512$

For different values of false alarm probability (P_{FA}), the detection probability (P_D) of the proposed algorithm in Additive White Gaussian Noise (AWGN) has been shown in Figure 4.10. Since P_{FA} is a Q-function of SNR and threshold [92], it can be fixed for each curve by decreasing the value of threshold as SNR increases. To change the fixed value of P_{FA} for other curve, threshold is adequately increased which decreases the detection probability (P_D). The detection performance of the proposed burst detection algorithm has been compared with that of Zhao's [38] and Deng's [40] algorithms. All the

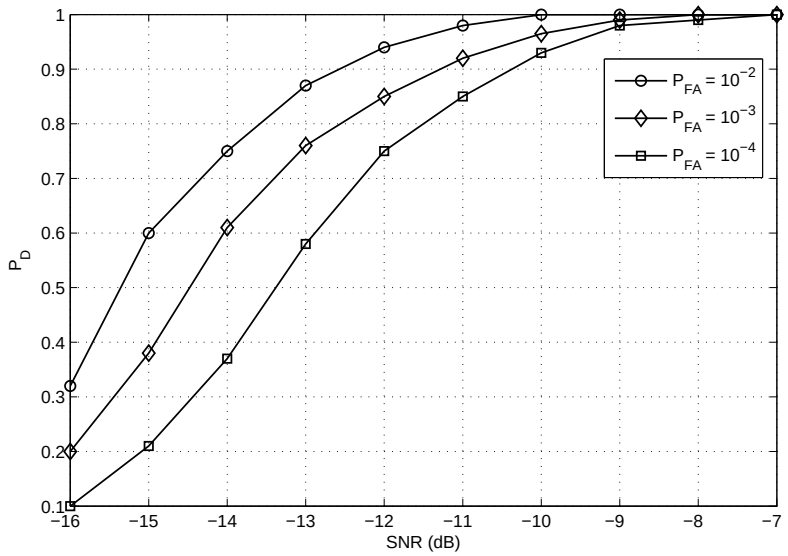

Figure 4.10: Detection performance of the proposed DM training based algorithm in AWGN channel for different values of P_{FA}

simulation parameters have been kept the same and P_{FA} is set to be 10^{-2}. Since the two algorithms [38] and [40] are applicable only to single user system, the proposed algorithm is also simulated for single user case for true comparison. From Figure 4.11, it can be seen that the proposed algorithm outperforms both these algorithms even at low SNR. The performance improvement is almost 1dB at low SNRs ranging from -16dB to -9dB. Moreover, the proposed algorithm achieves $P_D = 1$ at -10dB.

The performance of these three algorithms has also been compared in Stanford University Interim (SUI) channel model [82]. We have used SUI-4 channel model in our simulations which models a terrain having moderate to high tree density and weak LOS. The comparison is shown in Figure 4.12 which shows that the proposed DM training based algorithm achieves a performance improvement of almost 2dB as compared to Deng's algorithm and also achieves $P_D = 1$at -9dB. Moreover, the detection performance of the proposed algorithm is decreased only about 0.5dB as when compared with its performance over AWGN. On the other hand, the performance degradation for Deng's algorithm is almost 1-1.5dB.

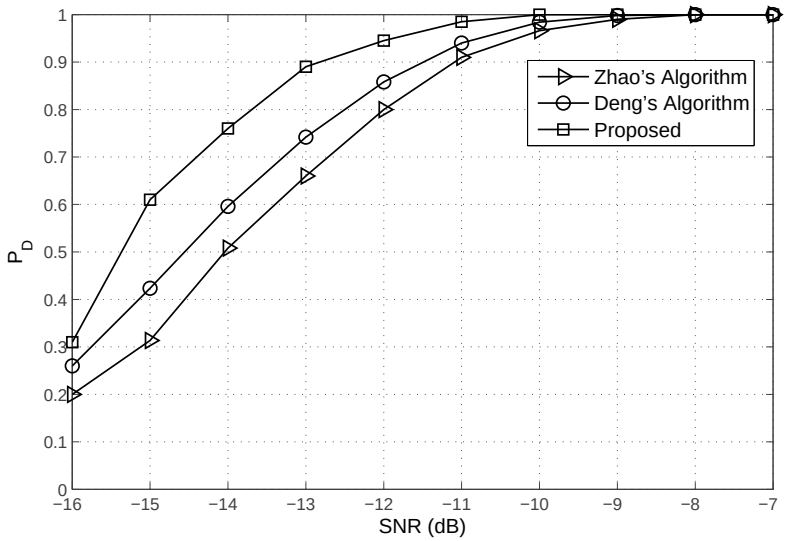

Figure 4.11: Detection performance comparison of the proposed DM training based algorithm with other algorithms in AWGN channel

This shows that the proposed algorithm is very robust against multipath fading effects.

Finally, the performance of proposed burst detection algorithm for multiuser case has been evaluated by finding the probability of correct burst detection (P_D) for different number of users. The simulation is performed over AWGN channel for 1, 4, and 8 CDMA users. Figure 4.13 shows the detection probabilities versus SNR for different number of users. It can be seen that for 1 and 4 users' case, P_D becomes 1 at -10dB, whereas for 8 users P_D becomes 1 at -9dB which shows that by increasing number of users from 1 to 4, the proposed algorithm can still achieve $P_D = 1$ at the same SNR. The detection performance for multiuser case is also evaluated over SUI-4 channel model and shown in figure 4.14. It can be seen that there is almost 1-2dB difference between 1 user and 8 users' cases. It affirms that the proposed DM training based burst detection algorithm is very effective for multiuser CDMA based wideband networking waveform in multipath fading environment.

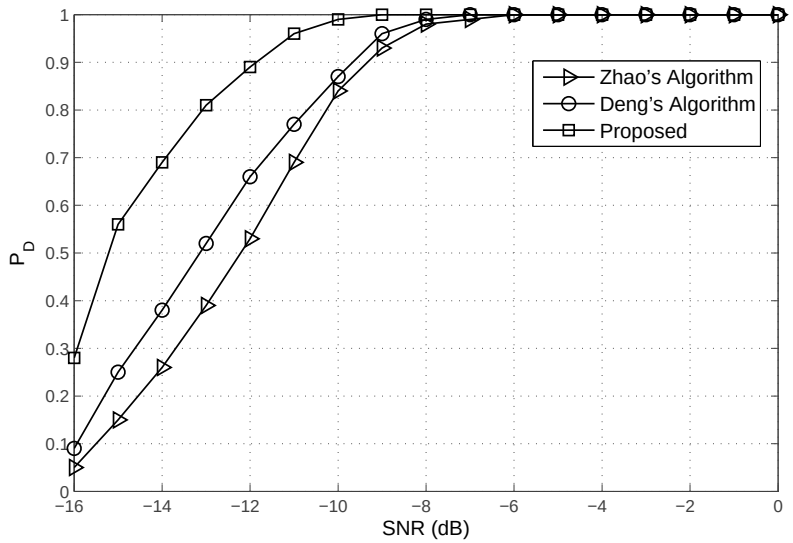

Figure 4.12: Detection performance comparison of the proposed DM training based algorithm with other algorithms in SUI-4 channel model

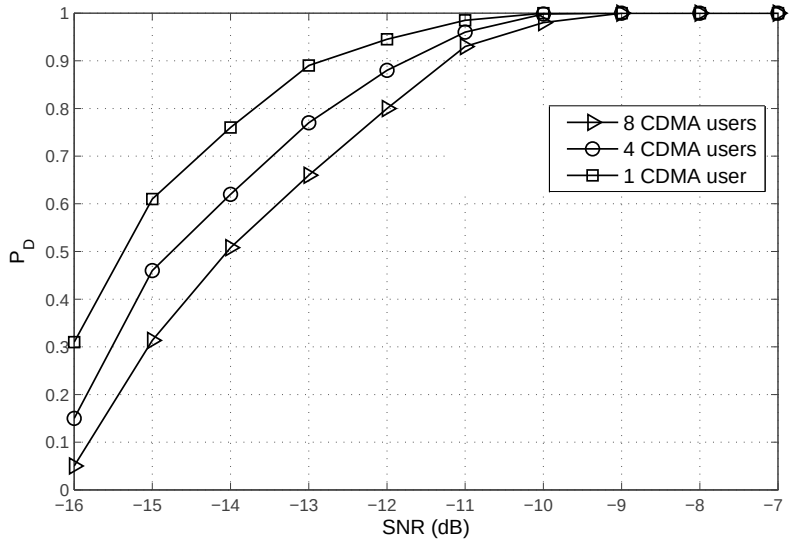

Figure 4.13: Detection performance of the proposed DM training based algorithm for multiple CDMA users in AWGN

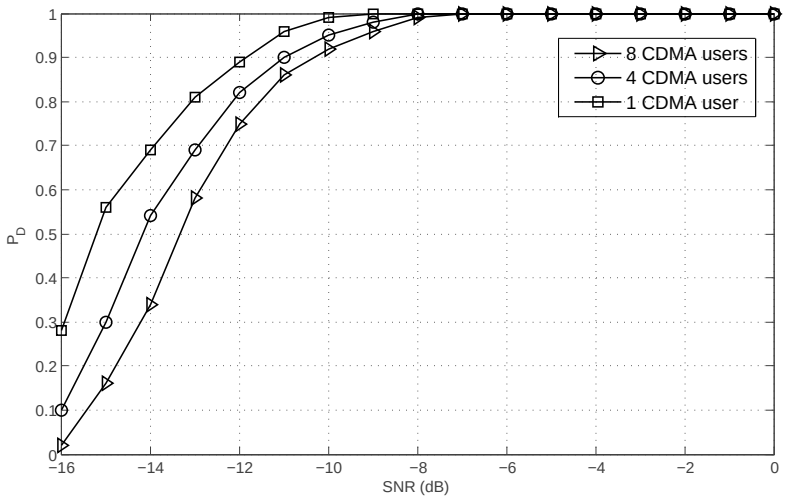

Figure 4.14: Detection performance of the proposed DM training based algorithm for multiple CDMA users in SUI-4 channel

4.4 Comparison of TDR training and DM training based Burst Detection

In this chapter, we have presented two novel data aided algorithms for burst detection at the physical layer of the wideband networking waveform. The first algorithm (section 4.2) is based on TDR training and exploits a specific sign pattern for identical parts in the calculation of timing metric. The resulting timing metric, normalized by the signal energy, has a steep roll-off pattern. The second algorithm (section 4.3) is based on DM training and exploits the precoding sequence used in the design of training sequence for the calculation of timing metric. Due to the use of two sub-sequences formed through differential modulation, the occurrence of data similar to training sequence becomes very less probable. Furthermore, the sub-sequences are selected from Golay complementary sequences and it is shown that the proposed DM training sequence has better correlation properties as compared to that of Golay sequence. The resulting timing metric of the DM training based algorithm has a very sharp peak at the correct detection point. Due to

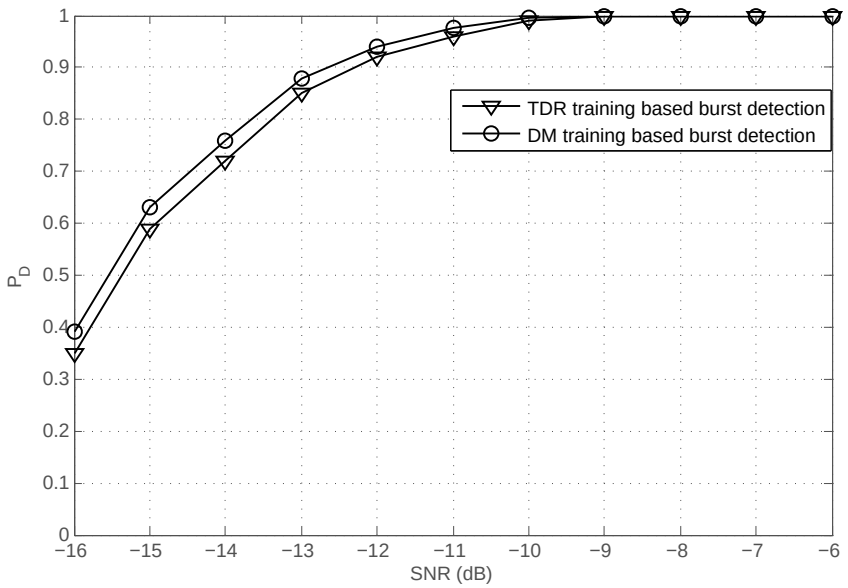

Figure 4.15: Performance comparison of the two proposed burst detection algorithms in SUI-2 channel

this reason, the DM training based algorithm gives slight improvement in the detection performance as compared to the TDR training based algorithm. This is shown in Figure 4.15 for SUI-2 channel model. Figure 4.16 shows the detection performance of the two proposed algorithms in SUI-4 channel. It can be seen that the DM training based algorithm outperforms the other by almost $0.25 - 0.5$dB.

4.5 Conclusion

This chapter presented two proposed novel algorithms for burst detection in wideband networking waveform. A Time Domain Repetitive (TDR) training sequence is proposed and used for the computation of decision metric for algorithm I. For the proposed algorithm II, a specifically designed training sequence containing two equal length sub-sequences is proposed. It is termed as differentially modulated (DM) training sequence. The design of DM training sequence involves the use of differential encoding through a precoding sequence.

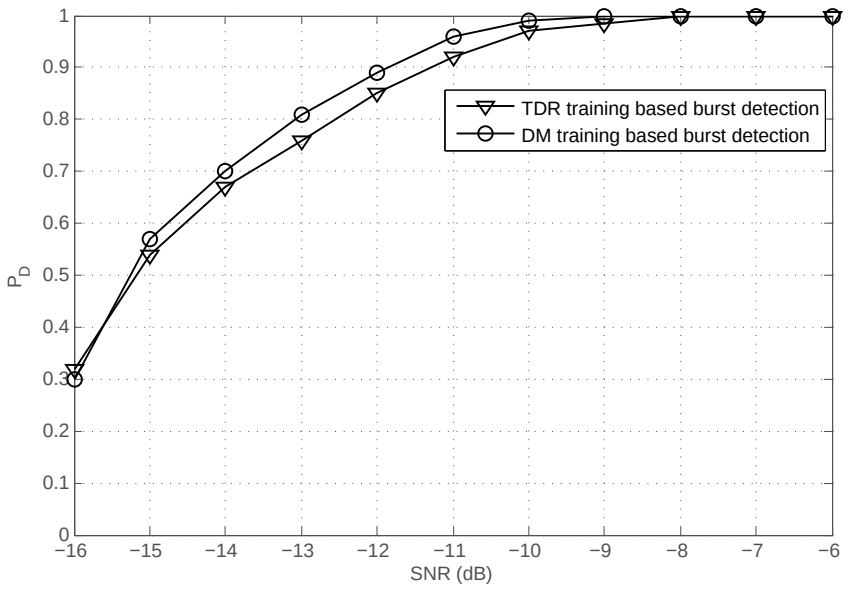

Figure 4.16: Performance comparison of the two proposed burst detection algorithms in SUI-4 channel

The training sequence structure and precoding sequence are exploited in the decision metric which is normalized by the signal energy. It is shown through computer simulations that the proposed burst detection is superior to a set of known existing algorithms in terms of the probability of detection. The detection performance is also evaluated in the presence of multipath fading effects generated by using SUI channel models.

Chapter 5

Carrier Frequency Offset Estimation

Carrier Frequency Offset (CFO) is caused due to the inherent mismatch between the oscillator frequencies of the transmitter and receiver. As a result of CFO, the received signal's phase is distorted. The digital data can't be properly detected if the CFO is not correctly estimated and compensated at the receiver side [93]. Since the software defined radio networks are mostly infrastructureless, each radio has a carrier frequency oscillator that is independent to those of other radios. Therefore, the CFO introduced at each receiver side is independent from all other receivers. So each radio should estimate and compensate the CFO for the incoming signal individually.

Due to the burst mode of transmission of the proposed wideband waveform, each burst may be affected by a different Doppler spread in case of relative motion between transmitter and receiver [94]. Moreover, each incoming burst may come from a different radio in the network due to the TDMA-based networking operation. Therefore, CFO needs to be estimated and compensated for each burst individually and independently.

In this chapter, we propose two types of novel CFO estimation and compensation algorithms[1]. The first algorithm is based on Fast Fourier Transform (FFT) and interpolation. Firstly, a basic estimation algorithm has been proposed which uses FFT and quadratic interpolation. Secondly, an enhanced CFO estimator has been proposed which is based on modified FFT and biquadratic interpolation technique. A detailed computational complexity analysis of both the basic and enhanced algorithms is also presented. The second algorithm is a novel two stage algorithm for CFO estimation and compensation. The first stage (coarse estimation) provides a coarse estimate of CFO by using Maximum Likeli-

[1]Parts of this chapter appear in author's own publications, [22], [23].

hood Data Aided (MLDA) correlation based algorithm. The second stage (fine estimation) estimates the residual offset error for each burst on sample by sample basis using blind estimation approach. The estimation range of the proposed estimator is almost full. It will be shown that the proposed algorithm has better performance and lower computational complexity as compared to a set of known two stage CFO estimation algorithms.

5.1 Problem Formulation

The received sampled data (3.6) is re-written as

$$r(nT_s) = \sum_{k=1}^{K} e^{j2\pi\upsilon_k n} \sum_{i=0}^{B-1} d_k[i] q_k(nT_s - iT - \epsilon_k(nT_s)T_c) + w(nT_s) \tag{5.1}$$

where $\upsilon_k = \Delta f T = \Delta f_k / f_s$ is the normalized carrier frequency offset for k^{th} user and $\epsilon_k(nT_s)$ is the slowly varying time delay due to SCO corresponding to k^{th} user. Since Δf can vary from $-f_s/2$ to $f_s/2$, the range of the normalized CFO is from -0.5 to 0.5. The received sequence $r(nT_s)$ is downsampled after SCO estimation in the sampling clock recovery stage by $N_s = 4$ followed by further downsampling by G in the burst detection stage to result in the downsampled and despread sequence $z[n]$. This downsampled data sequence in the form of bursts is input to the CFO estimation stage which estimates the symbol-level normalized CFO for k^{th} user ($\upsilon_{o,k} = GN_s\upsilon_k$). Since the CFO of each user is to be estimated independently, the subscript k is dropped for simplicity. The aim of CFO estimation algorithm is to find an estimate of CFO (υ_o) and then correct it.

5.2 Proposed FFT and Interpolation based Algorithms

5.2.1 FFT and Quadratic Interpolation

This section presents the proposed basic algorithm for CFO estimation using FFT and Lagrange quadratic interpolation. In burst mode of communication, each burst is affected

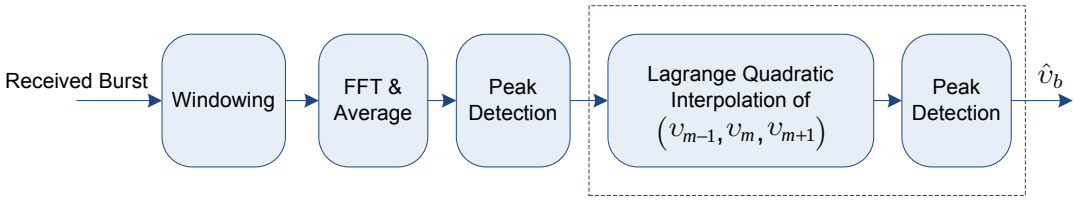

Figure 5.1: Block diagram of the proposed FFT and Quadratic interpolation based algorithm

by a different frequency offset, so the proposed estimator finds the CFO estimate for each burst independently.

Let the number of samples in each received burst is denoted by B. Firstly, each received burst of length B is divided into $N_{0,basic}$ windows, each of length $W = 2^R$, where R is an integer such that $1 \leq R \leq \log_2(B)$. A greater window size results in better FFT resolution. Fast Fourier Transform is then applied to each window and average of FFT coefficients for all windows is calculated. The frequency corresponding to the maximum value FFT coefficient is a coarse frequency offset estimate with an error of $e_{FFT} = \upsilon_o - \upsilon_m$, where υ_m is the normalized frequency corresponding to the maximum FFT amplitude. This error is very large due to the limited resolution of FFT. It is then reduced by the use of quadratic interpolation. Figure 5.1 shows the block diagram of the proposed basic estimator.

The quadratic interpolation is applied to the peaks of the resulting FFT of the received burst. Figure 5.2 illustrates the technique for finding the peak of the spectrum from three adjacent spectral lines. Point $B(\upsilon_m, a_m)$ is the point of maximum FFT energy detected by the receiver, whereas points $A(\upsilon_{m-1}, a_{m-1})$ and $C(\upsilon_{m+1}, a_{m+1})$ are the spectral lines adjacent to it. The index m represents the position of the FFT peaks. The true frequency υ_o is located at Point D. A quadratic polynomial is then applied between the spectral peaks A, B and C to estimate the true peak which is located at point D. A quadratic polynomial obtained using these three points is obtained by using Lagrange polynomial

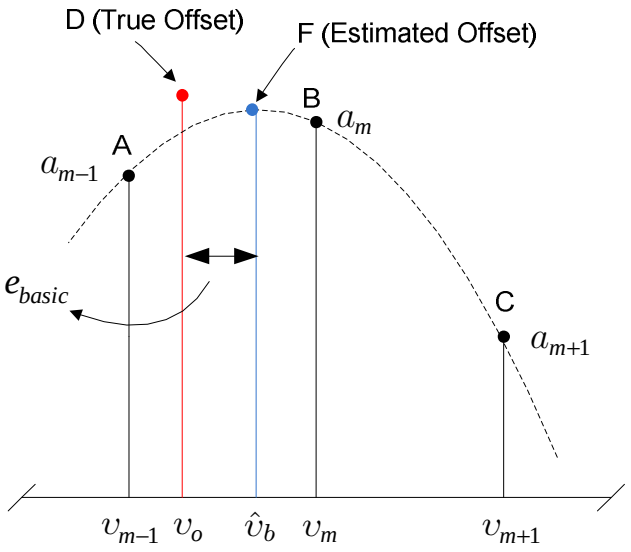

Figure 5.2: Quadratic interpolation applied to the FFT peaks

interpolation [95]. This polynomial is given as

$$\begin{aligned} L(\upsilon) = &\frac{(\upsilon-\upsilon_m)(\upsilon-\upsilon_{m+1})}{(\upsilon_{m-1}-\upsilon_m)(\upsilon_{m-1}-\upsilon_{m+1})}a_{m-1} + \frac{(\upsilon-\upsilon_{m-1})(\upsilon-\upsilon_{m+1})}{(\upsilon_m-\upsilon_{m-1})(\upsilon_m-\upsilon_{m+1})}a_m \\ &+ \frac{(\upsilon-\upsilon_{m-1})(\upsilon-\upsilon_m)}{(\upsilon_{m+1}-\upsilon_{m-1})(\upsilon_{m+1}-\upsilon_m)}a_{m+1} \end{aligned} \tag{5.2}$$

The point of maximum amplitude can be found by differentiating (5.2) with respect to υ such that,

$$\begin{aligned} \frac{dL(\upsilon)}{d\upsilon} = &\frac{[2\upsilon-(\upsilon_m+\upsilon_{m+1})]}{(\upsilon_{m-1}-\upsilon_m)(\upsilon_{m-1}-\upsilon_{m+1})}a_{m-1} + \frac{[2\upsilon-(\upsilon_{m-1}+\upsilon_{m+1})]}{(\upsilon_m-\upsilon_{m-1})(\upsilon_m-\upsilon_{m+1})}a_m \\ &+ \frac{[2\upsilon-(\upsilon_{m-1}+\upsilon_m)]}{(\upsilon_{m+1}-\upsilon_{m-1})(\upsilon_{m+1}-\upsilon_m)}a_{m+1} \end{aligned} \tag{5.3}$$

Now the point of maximum amplitude can be obtained by letting

$$\left.\frac{dL(\upsilon)}{d\upsilon}\right|_{\upsilon=\hat{\upsilon}_b} = 0$$

If the frequency resolution of FFT is $\upsilon_{res} = \upsilon_m - \upsilon_{m-1}$, then the following simplifications

can be made accordingly.

$$\upsilon_m - \upsilon_{m+1} = \upsilon_{res}$$

$$\upsilon_{m-1} - \upsilon_m = -\upsilon_{res}$$

$$\upsilon_{m+1} - \upsilon_{m-1} = 2\upsilon_{res}$$

By using these simplifications, (5.3) can be written as

$$\begin{aligned} 0 = \frac{[2\hat{\upsilon}_b - (\upsilon_m + \upsilon_{m+1})]}{2\upsilon_{res}^2} a_{m-1} - \frac{[2\hat{\upsilon}_b - (\upsilon_{m-1} + \upsilon_{m+1})]}{\upsilon_{res}^2} a_m \\ + \frac{[2\hat{\upsilon}_b - (\upsilon_{m-1} + \upsilon_m)]}{2\upsilon_{res}^2} a_{m+1} \end{aligned} \tag{5.4}$$

which is further simplified as

$$2\hat{\upsilon}_b(a_{m-1} - 2a_m + 2a_{m+1}) = (\upsilon_m + \upsilon_{m+1})a_{m-1} - 2(\upsilon_{m-1} + \upsilon_{m+1})a_m + (\upsilon_m + \upsilon_{m-1})a_{m+1}$$

$$\hat{\upsilon}_b = \frac{\upsilon_m a_{m-1} + \upsilon_{m+1}a_{m-1} - 2\upsilon_{m-1}a_m + 2\upsilon_{m+1}a_m + \upsilon_m a_{m+1} + \upsilon_{m-1}a_{m+1}}{2(a_{m-1} - 2a_m + a_{m+1})} \tag{5.5}$$

Adding and subtracting $\upsilon_m a_{m-1}$, $\upsilon_m a_{m+1}$ and $4\upsilon_m a_m$ to the numerator of the right side of 5.5, collecting similar terms and using $\upsilon_{res} = \upsilon_m - \upsilon_{m-1} = \upsilon_{m+1} - \upsilon_m$, we get

$$\hat{\upsilon}_b = \frac{2\upsilon_m a_{m-1} - 4\upsilon_m a_m + 2\upsilon_m a_{m+1} + (a_{m-1} - a_{m+1})\upsilon_{res} + 2a_m(2\upsilon_m - \upsilon_{m-1} - \upsilon_{m+1})}{2(a_{m-1} - 2a_m + a_{m+1})} \tag{5.6}$$

As $2\upsilon_m - \upsilon_{m-1} - \upsilon_{m+1} = 0$, so the CFO estimate $\hat{\upsilon}_b$ using the basic FFT and quadratic interpolation is given as

$$\hat{\upsilon}_b = \upsilon_m + \frac{(a_{m-1} - a_{m+1})\upsilon_{res}}{2(a_{m-1} - 2a_m + a_{m+1})} \tag{5.7}$$

The error between the estimated and true frequency offset is

$$e_b = \upsilon_o - \hat{\upsilon}_b \tag{5.8}$$

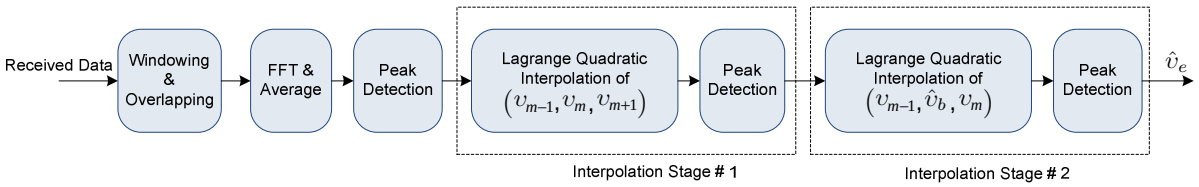

Figure 5.3: Block diagram of the proposed modified FFT and biquadratic interpolation based CFO estimator

5.2.2 Modified FFT and Biquadratic Interpolation

The estimation performance of the CFO using FFT and quadratic interpolation depends on the maxima/minima of the quadratic curve which depends heavily on the amplitude difference of the points A and B in Figure 5.2. To further improve the performance of the estimator, we propose an enhanced algorithm which is based on overlapping windows based FFT and successive use of quadratic interpolation (termed as biquadratic interpolation) on the FFT coefficients of the received data. Figure 5.3 shows the block diagram representation of the proposed CFO estimation algorithm. It consists of the following three steps;

Step I

Each received burst of size B is divided into $N_{0,enh}$ overlapped windows, each of size W, such that

$$N_{0,enh} = \frac{B}{rW} - 1 \tag{5.9}$$

where r is the overlapping factor. The reason for using overlapped windows is to avoid the loss of data near the window boundaries [96]. Moreover, to avoid the spectral leakage effect, Hamming windows can be used instead of rectangular windows [97]. The concept of overlapping windows is illustrated in Figure 5.4. Now, applying a similar procedure as mentioned in the basic algorithm, frequency corresponding to the maximum absolute FFT coefficient is found.

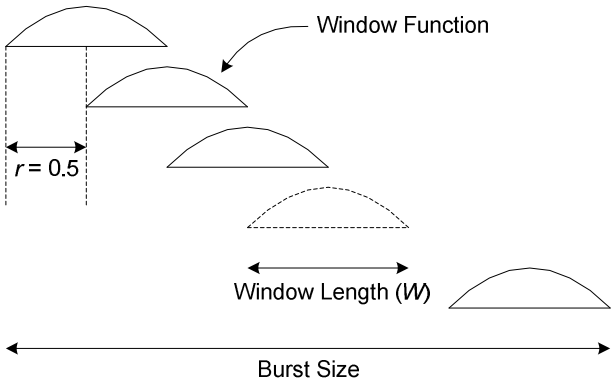

Figure 5.4: Concept of overlapping windows for modified FFT

Step II

After detecting the point of highest energy (υ_m, a_m) in the FFT data, Lagrange quadratic interpolation is applied to this highest energy point (υ_m, a_m) and its two adjacent points $(\upsilon_{m-1}, a_{m-1})$ and $(\upsilon_{m+1}, a_{m+1})$. The CFO estimate $\hat{\upsilon}_b$ is calculated by the procedure mentioned in section 5.2.1.

Step III

The frequency point $(\hat{\upsilon}_b)$ obtained in step II using (5.7) is considered as the center point and quadratic interpolation is again applied to the point $(\hat{\upsilon}_b, a_b)$ and its two adjacent points $(\upsilon_{m-1}, a_{m-1})$ and (υ_m, a_m) as shown in Figure 5.5.

Now, for applying quadratic interpolation again, first we have to find a_b. It can be calculated by using equation 5.2 and putting $\upsilon = \hat{\upsilon}_b$ such that

$$a_b = L(\hat{\upsilon}_b) \tag{5.10}$$

After calculation of this FFT energy, we interpolate these points by Lagrange polynomial

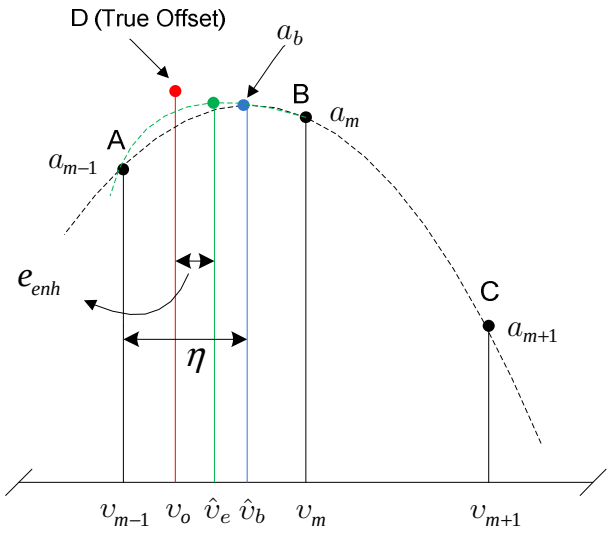

Figure 5.5: Biquadratic interpolation applied to the FFT peaks

method. The Lagrange polynomial will now be

$$L_2(\upsilon) = \frac{(\upsilon - \hat{\upsilon}_b)(\upsilon - \upsilon_m)}{(\upsilon_{m-1} - \hat{\upsilon}_b)(\upsilon_{m-1} - \upsilon_m)} a_{m-1} + \frac{(\upsilon - \upsilon_{m-1})(\upsilon - \upsilon_m)}{(\hat{\upsilon}_b - \upsilon_{m-1})(\hat{\upsilon}_b - \upsilon_m)} a_b + \frac{(\upsilon - \upsilon_{m-1})(\upsilon - \hat{\upsilon}_b)}{(\upsilon_m - \upsilon_{m-1})(\upsilon_m - \hat{\upsilon}_b)} a_m \tag{5.11}$$

The point of maximum amplitude can be obtained by letting,

$$\left. \frac{dL_2(\upsilon)}{d\upsilon} \right|_{\upsilon = \hat{\upsilon}_e} = 0$$

It is worth mentioning here that the data points for this interpolation are not uniformly spaced, so we cannot use the FFT resolution thoroughly in this case. However if we define η as the fractional distance of the peak $\hat{\upsilon}_b$ from υ_{m-1} and also use $\upsilon_m - \upsilon_{m-1} = \upsilon_{res}$, then we can write

$$\hat{\upsilon}_b - \upsilon_{m-1} = \eta \upsilon_{res}$$

$$\upsilon_m - \hat{\upsilon}_b = (1 - \eta) \upsilon_{res}$$

Using these simplifications, the enhanced CFO estimate $\hat{\upsilon}_e$ by the proposed modified FFT and biquadratic interpolation becomes

$$\hat{\upsilon}_e = \frac{\upsilon_{m-1}[\eta a_m - a_b] + \hat{\upsilon}_b[(1-\eta)a_{m-1} + \eta a_m] + \upsilon_m[(1-\eta)a_{m-1} - a_b]}{2[(1-\eta)a_{m-1} - a_b + \eta a_m]} \tag{5.12}$$

From Figure 5.5, it is clear that the estimation error of the enhanced algorithm is less than that of the basic algorithm.

5.2.3 Computational Complexity

In this section, we describe the computational complexity of the basic and enhanced CFO estimation algorithms proposed in sections 5.2.1 and 5.2.2, respectively. The computational complexities of the proposed basic and enhanced algorithms in terms of number of additions, multiplications and divisions for burst size B are shown in Tables 5.1 and 5.2. For a burst size B, window overlapping factor of r and window size of W, the total number of FFT windows for the proposed basic and enhanced algorithm is given by

$$N_{0,basic} = \frac{B}{W}$$

$$N_{0,enh} = \frac{B}{rW} - 1$$

Since, a W-point FFT requires $(W/2)\log_2(W)$ complex additions and $W\log_2(W)$ complex multiplications [98], therefore the total number of operations for the FFT computation in the both the algorithms will be calculated as follows.

Table 5.1: Computational complexity of proposed basic CFO estimation algorithm

Operations	**Additions**	**Multiplications**	**Divisions**
FFT computation	$\frac{B}{2}\log_2(W)$	$B\log_2(W)$	-
FFT averaging	$B - W$	-	W
Quadratic interpolation	4	3	1
Total	$\frac{B}{2}\log_2(W) + B - W + 4$	$B\log_2(W) + 3$	$W + 1$
Total operations: $\frac{3B}{2}\log_2(W) + B + 8$			

Table 5.2: Computational complexity of proposed enhanced CFO estimation algorithm

Operations	**Additions**	**Multiplications**	**Divisions**
FFT computation	$\frac{B-rW}{2r}\log_2(W)$	$\frac{B-rW}{r}\log_2(W)$	-
FFT averaging	$\frac{B}{r}-2W$	-	W
1^{st} quadratic interpolation	4	3	1
2^{nd} quadratic interpolation	8	6	1
Total	$\frac{B-rW}{2r}\log_2(W)+\frac{B}{r}-2W+12$	$\frac{B-rW}{r}\log_2(W)+9$	$W+2$
Total operations: $\frac{3(B-rW)}{2r}\log_2(W)+\frac{B}{r}-W+23$			

For basic algorithm:

$$\text{Complex additions: } \left(\frac{B}{W}\right)\left(\frac{W}{2}\right)\log_2(W) \Rightarrow \frac{B}{2}\log_2(W)$$

$$\text{Complex multiplications: } \left(\frac{B}{W}\right)W\log_2(W) \Rightarrow B\log_2(W)$$

For enhanced algorithm:

$$\text{Complex additions: } \left(\frac{B-rW}{rW}\right)\left(\frac{W}{2}\right)\log_2(W) \Rightarrow \frac{B-rW}{2r}\log_2(W)$$

$$\text{Complex multiplications: } \left(\frac{B-rW}{rW}\right)W\log_2(W) \Rightarrow \frac{B-rW}{r}\log_2(W)$$

The next step is the averaging of FFT windows which results in $B-W$ and $(B/r)-2W$ additions for basic and enhanced algorithms, respectively. The number of divisions for averaging operation is W for both the cases. The number of multiplications, additions and divisions for the two stages of interpolation is calculated by using (5.7) and (5.12). Table 5.4 shows the numerical values of all the operations for the basic and enhanced algorithms for the parameters listed in Table 5.3. It can be seen that the major contribution towards the complexity is due to the overlapping windowed FFT operation. The inclusion of second stage of quadratic interpolation contributes very less towards the total computations. Also, the percentage increase in the total computational complexity for enhanced estimation algorithm is about 15.5%.

Table 5.3: Parameters used in the simulation

Parameter	**Value/Description**
Spreading gain (G)	16
Number of users (K)	8
Window size (W)	32
Window type	Hamming
FFT size	32
Burst length in samples (B)	320
Overlapping factor (r)	0.8

5.2.4 Simulation Results

In this section, we present the simulation results of the proposed basic and enhanced CFO estimation algorithms. The simulation parameters used for this purpose are summarized in Table 5.3. To model the fading channel with variety of terrain types, SUI channel models are also used in the simulation.

Figure 5.6 presents the BER performance of the two proposed CFO estimation algorithms. We have introduced 20% CFO (i.e. normalized offset = 0.2). It is clear that the basic algorithm is almost 2-3 dB deviant from the ideal case, where CFO is assumed to be known at the receiver. This degradation is much reduced by the used of modified FFT and biquadratic interpolation based algorithm which improves the estimation performance, resulting in the BER performance close to that of the ideal case. Similar is the case with

Table 5.4: Computational complexity comparison of the basic and enhanced algorithms for parameters listed in Table 5.3

Operations	**Additions**	**Multiplications**	**Divisions**	**Total**
Basic algorithm	1092	1603	33	2728
Enhanced algorithm	1268	1849	34	3151

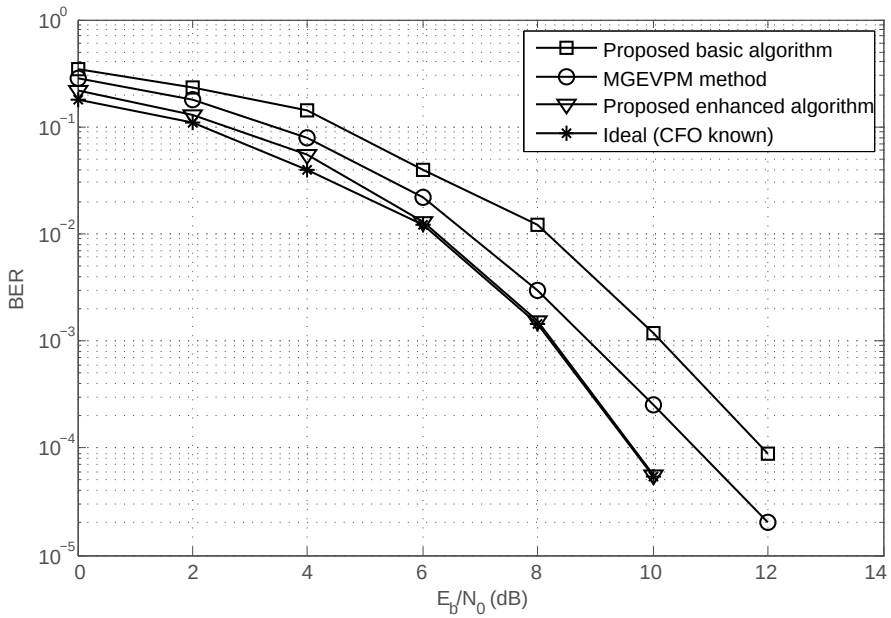

Figure 5.6: BER performance analysis of the proposed FFT and interpolation based algorithms in AWGN

the simulation in SUI-2 channel model shown in Figure 5.7. The deviation of the proposed basic algorithm is observed to be 1-2 dB from the ideal curve. Again, the enhanced algorithm improves the BER performance and makes it very close to that of the ideal case. The performance of the proposed estimator is also compared to that of MGEVPM method [48]. It can be seen that the proposed enhanced algorithm gives a performance improvement of almost 0.5-1 dB in both the AWGN and SUI-2 channel models.

5.3 Proposed Two Stage Data Aided Algorithm

The carrier frequency offset is often estimated in two stages; coarse estimation and fine estimation. Some of these algorithms are reviewed in chapter 2. Before presenting our proposed two stage CFO estimation algorithm, we briefly explain two well-known existing algorithms.

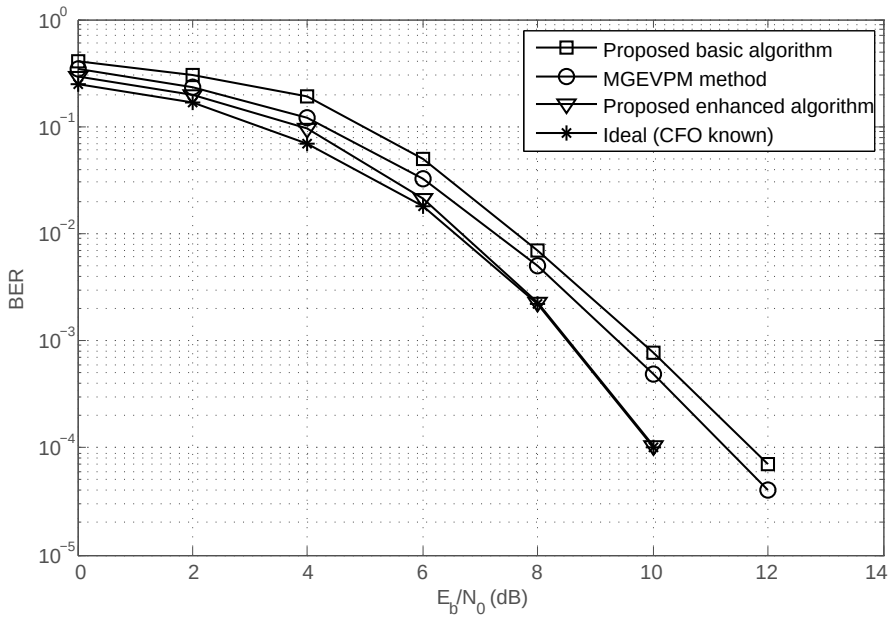

Figure 5.7: BER performance analysis of the proposed FFT and interpolation based algorithms in SUI-2 channel model

Casini's algorithm

In Casini's algorithm [54], the first stage of coarse estimation is based on Mengali's conventional CFO estimation [55]. The coarse estimator exploits the autocorrelation of the known preamble sequence to find the frequency offset and is given as

$$\hat{v}_{coarse} = \frac{1}{2\pi DT} \arg \left[\sum_{k=D}^{N_0} z[k] z^*[k-D] \right] \tag{5.13}$$

where $\hat{v}_{coarse}$ is the coarse estimate of CFO, $z[k]$ is the k^{th} sample of the sequence input to the CFO estimation stage, T is the sampling period, D is the loop delay and N_0 is the number of symbols in the training sequence. The drawback of this estimator is that it can estimate up to 20% normalized frequency offset for $D = 2$. For larger values of D, the estimation range is further decreased.

For fine estimation of CFO, a suboptimal estimator providing variance close to Cramer-

Rao Lower Bound (CRLB) has been used [56]. The estimate is given as

$$\hat{v}_{fine} = \frac{1}{\pi T(M'+1)} \arg\left[\sum_{k=1}^{M'} R[k]\right] \tag{5.14}$$

where $\hat{v}_{fine}$ is the fine estimate of CFO, M' is a positive constant such that $M' \leq N_0 - 1$ and $R[k]$ is the autocorrelation estimate defined as

$$R[k] = \frac{1}{N_0 - k} \sum_{i=k+1}^{N_0} z_c[i].z_c^*[i-k], \;\; 0 \leq k \leq N_0 - 1 \tag{5.15}$$

where $z_c[i]$ is the i^{th} sample of the compensated data after coarse CFO estimation. Due to the sub-optimum implementation assumptions, the mean square error between the Maximum Likelihood (ML) estimate and the suboptimal estimate increases as Signal-to-Noise Ratio (SNR) decreases. Moreover, the closed form expression for the frequency estimate given by (5.14) is obtained under the assumptions of high SNR and low frequency deviations (i.e. $M'T\hat{v}_{fine} \ll 1$) which are not practical especially in SDR networks. Also, the variance of the estimate approaches CRLB when the value of M' is approximately $N_0/2$ (for $N_0 \gg 1$) [56], which increases the computational complexity of the overall algorithm. The performance of the fine estimation algorithm can be increased by accumulating training sequences of consecutive bursts. Let B be the number of symbols in each burst, then the fine estimate will become

$$\hat{v}_{fine} = \frac{1}{\pi T(M'+1)} \arg\left[\sum_{n=0}^{K_a-1} \sum_{k=1}^{M'} R[n,k]\right] \tag{5.16}$$

where K_a is the number of autocorrelation summations and

$$R[n,k] = \frac{1}{N_0 - k} \sum_{i=k+1}^{N_0} z_c[i+nB].z_c^*[i-k+nB]. \tag{5.17}$$

This accumulation operation requires large memory for the autocorrelation summations.

Oh's Algorithm

The coarse CFO estimator proposed by Oh and Kim [57] is a modified version of the Extended Schmidl and Cox Algorithm (ESCA) [58,59]. The smoothing function is removed

from and arg() operation is re-positioned in ESCA to reduce the computational complexity [60]. The modified estimator exploits the correlation between the samples of the received signal to find the frequency estimate. The frequency estimate is given as

$$\hat{\upsilon}_{coarse} = \frac{1}{2\pi T}\arg\left[\sum_{k=1}^{M_a}\{R[k].R^*[k-1]\}\right] \tag{5.18}$$

where M_a is the number of autocorrelators and

$$R[k] = \frac{1}{N_0 - k}\sum_{i=k}^{N_0-1} z[i].z^*[i-k]. \tag{5.19}$$

The estimation range of this coarse CFO estimation algorithm is almost full irrespective of the value of M_a, but the choice of M_a is related to the variance of the estimator. The authors of [57] has chosen $M_a = 9$ to reduce the computations. For $M_a = 9$, the estimator outperforms the estimator of [55], but shows large deviation from CRLB at low values of SNR, as will be shown in simulation results.

For fine estimation of CFO, a simple correlation scheme between the training sequences of consecutive bursts is used [61]. This estimator can be expressed as

$$\hat{\upsilon}_{fine} = \frac{1}{2\pi B}\arg\left[\sum_{k=0}^{N_0-1} z_{c,current}[k].z^*_{c,previous}[k]\right] \tag{5.20}$$

where $z_{c,current}[k]$ and $z_{c,previous}[k]$ are the k^{th} samples of the current and previous data bursts after coarse CFO compensation, respectively. This estimator works well except a problem that it uses two data bursts to estimate the residual CFO correctly.

Now we present our proposed novel two stage algorithm for carrier frequency offset estimation. The first stage (coarse estimation) provides a coarse estimate of CFO by using Maximum Likelihood Data Aided (MLDA) correlation based algorithm. The second stage (fine estimation) estimates the residual offset error for each burst on sample by sample basis using blind estimation approach. The estimation range of the proposed estimator is almost full.

5.3.1 Stage I: Maximum Likelihood Data Aided Estimation

In this section, we derive the Maximum Likelihood Data Aided (MLDA) algorithm for as the first stage of the proposed two stage CFO estimator. The estimation range of the proposed MLDA algorithm is full i.e. $-0.5 \leq \hat{\upsilon}_o \leq 0.5$. The likelihood function for the estimation of υ_o is given by [99]

$$L(\upsilon_o) = \mathrm{Re}\left\{\sum_{i=-\frac{N_0-1}{2}}^{\frac{N_0-1}{2}} e^{-j2\pi\upsilon_o i} d^*[i]z[i]\right\} \tag{5.21}$$

where $d[i]$ and $z[i] = z(iT)$ are the i^{th} samples of the transmitted and received symbols, respectively, and N_0 is the unspread training sequence length.

In order to find CFO estimate $\hat{\upsilon}_o$, we have to maximize the likelihood function given by (5.21)

$$\max_{\upsilon_o} \{L(\upsilon_o)\}$$

Here, we follow a similar approach to [99], where $|L(\upsilon_o)|^2 = L(\upsilon_o)L^*(\upsilon_o)$ has been maximized instead of $L(\upsilon_o)$. So, taking derivative of $|L(\upsilon_o)|^2$ with respect to υ_o and setting it equal to zero yields $\hat{\upsilon}_o$. So,

$$2|L(\upsilon_o)|\mathrm{Re}\left\{\sum_{i=-\frac{N_0-1}{2}}^{\frac{N_0-1}{2}} (-j2\pi i) e^{-j2\pi\hat{\upsilon}_o i} d^*[i]z[i]\right\} = 0. \tag{5.22}$$

As $L(\upsilon_o)$ is not zero, we need only to put the real term part equal to zero in (5.22). Hence

$$\mathrm{Re}\left\{\sum_{i=-\frac{N_0-1}{2}}^{\frac{N_0-1}{2}} (-j2\pi i) e^{-j2\pi\hat{\upsilon}_o i} d^*[i]z[i]\right\} = 0. \tag{5.23}$$

Equation 5.23 can be re-written as

$$0 = \mathrm{Re}\left\{j\sum_{i=-\frac{N_0-1}{2}}^{\frac{N_0-1}{2}} i d^*[i]z[i]e^{-j2\pi\hat{\upsilon}_o i}\right\} \tag{5.24}$$

$$\begin{aligned} 0 &= \mathrm{Re}\left\{j\sum_{i=-\frac{N_0-1}{2}+1}^{\frac{N_0-1}{2}} i d^*[i]z[i]e^{-j2\pi\hat{\upsilon}_o i} - \left(\frac{N_0-1}{2}\right) d^*\left[-\tfrac{N_0-1}{2}\right] z\left[-\tfrac{N_0-1}{2}\right] e^{-j2\pi\hat{\upsilon}_o\left(-\frac{N_0-1}{2}\right)}\right\} \\ &= \mathrm{Re}\left\{j\sum_{i=-\frac{N_0-1}{2}+1}^{\frac{N_0-1}{2}} i d^*[i]z[i]e^{-j2\pi\hat{\upsilon}_o i} \right. \\ &\qquad \left. \left(\frac{N_0-1}{4}\right)\left[\frac{N_0-3}{2} - \frac{N_0+1}{2}\right] d^*\left[-\tfrac{N_0-1}{2}\right] z\left[-\tfrac{N_0-1}{2}\right] e^{-j2\pi\hat{\upsilon}_o\left(-\frac{N_0-1}{2}\right)}\right\} \end{aligned} \tag{5.25}$$

By further expanding the terms on right side of (5.25) and, adding and subtracting the term

$$\left(\frac{N_0^2-1}{8}\right) d^*\big[\tfrac{N_0-1}{2}+1\big] z\big[\tfrac{N_0-1}{2}+1\big] e^{-j2\pi\hat{v}_o\left(\frac{N_0-1}{2}+1\right)}$$

we get

$$\begin{aligned}
0 = \mathrm{Re}\Bigg\{ j \Bigg\{ & \left(\frac{N_0^2-1}{8}\right) d^*\big[\tfrac{N_0-1}{2}+1\big] z\big[\tfrac{N_0-1}{2}+1\big] e^{-j2\pi\hat{v}_o\left(\frac{N_0-1}{2}+1\right)} \\
& - \left(\frac{N_0-1}{4}\right)\left(\frac{N_0+1}{2}\right) d^*\big[-\tfrac{N_0-1}{2}\big] z\big[-\tfrac{N_0-1}{2}\big] e^{-j2\pi\hat{v}_o\left(-\frac{N_0-1}{2}\right)} \\
& - \sum\nolimits_{i=-\frac{N_0-1}{2}+1}^{\frac{N_0-1}{2}} i(i-1) d^*[i] z[i] e^{-j2\pi\hat{v}_o i} \\
& + \sum\nolimits_{i=-\frac{N_0-1}{2}+1}^{\frac{N_0-1}{2}} i(i+1) d^*[i] z[i] e^{-j2\pi\hat{v}_o i} - \left(\frac{N_0^2-1}{8}\right) d^*\big[\tfrac{N_0-1}{2}+1\big] z\big[\tfrac{N_0-1}{2}+1\big] e^{-j2\pi\hat{v}_o\left(\frac{N_0-1}{2}+1\right)} \\
& + \left(-\frac{N_0-1}{2}+1\right)\left(-\frac{N_0-1}{2}\right) d^*\big[-\tfrac{N_0-1}{2}\big] z\big[-\tfrac{N_0-1}{2}\big] e^{-j2\pi\hat{v}_o\left(-\frac{N_0-1}{2}\right)} \Bigg\} \Bigg\}.
\end{aligned} \tag{5.26}$$

By noting that

$$\frac{N_0^2-1}{8} = \left(\frac{N_0-1}{2}+1-1\right)\left(\frac{N_0-1}{2}+1\right)$$

and combining the 5^{th} and 6^{th} terms on the right side of (5.26) with 3^{rd} and 4^{th} summation terms, respectively, we get

$$\begin{aligned}
0 = \mathrm{Re}\Bigg\{ j \Bigg\{ & \left(\frac{N_0^2-1}{8}\right) d^*\big[\tfrac{N_0-1}{2}+1\big] z\big[\tfrac{N_0-1}{2}+1\big] e^{-j2\pi\hat{v}_o\left(\frac{N_0-1}{2}+1\right)} \\
& - \left(\frac{N_0^2-1}{8}\right) d^*\big[-\tfrac{N_0-1}{2}\big] z\big[-\tfrac{N_0-1}{2}\big] e^{-j2\pi\hat{v}_o\left(-\frac{N_0-1}{2}\right)} \\
& - \sum\nolimits_{i=-\frac{N_0-1}{2}+1}^{\frac{N_0-1}{2}+1} i(i-1) d^*[i] z[i] e^{-j2\pi\hat{v}_o i} + \sum\nolimits_{i=-\frac{N_0-1}{2}}^{\frac{N_0-1}{2}} i(i+1) d^*[i] z[i] e^{-j2\pi\hat{v}_o i} \Bigg\} \Bigg\}.
\end{aligned} \tag{5.27}$$

Adding and subtracting the term

$$\left(\frac{N_0^2-1}{8}\right) \sum\nolimits_{i=-\frac{N_0-1}{2}+1}^{\frac{N_0-1}{2}} d^*[i] z[i] e^{-j2\pi\hat{v}_o i}$$

on the right side of (5.27) and combining the 1^{st} and 2^{nd} terms with the two added/subtracted

summations, we get

$$
\begin{aligned}
0 = \mathrm{Re}\Bigg\{ j \Bigg\{ & \left(\frac{N_0^2-1}{8}\right) \sum\nolimits_{i=-\frac{N_0-1}{2}+1}^{\frac{N_0-1}{2}+1} d^*[i]z[i]e^{-j2\pi\hat{v}_o i} \\
& -\{\left(\frac{N_0^2-1}{8}\right) \sum\nolimits_{i=-\frac{N_0-1}{2}}^{\frac{N_0-1}{2}} d^*[i]z[i]e^{-j2\pi\hat{v}_o i} \\
& - \sum\nolimits_{i=-\frac{N_0-1}{2}+1}^{\frac{N_0-1}{2}+1} i(i-1)d^*[i]z[i]e^{-j2\pi\hat{v}_o i} + \sum\nolimits_{i=-\frac{N_0-1}{2}}^{\frac{N_0-1}{2}} i(i+1)d^*[i]z[i]e^{-j2\pi\hat{v}_o i} \Bigg\} \Bigg\} \\
0 = \mathrm{Re}\Bigg\{ j \Bigg\{ & \left(\frac{N_0^2-1}{8}\right) \sum\nolimits_{i=-\frac{N_0-1}{2}}^{\frac{N_0-1}{2}} d^*[i+1]z[i+1]e^{-j2\pi\hat{v}_o (i+1)} \\
& - \left(\frac{N_0^2-1}{8}\right) \sum\nolimits_{i=-\frac{N_0-1}{2}}^{\frac{N_0-1}{2}} d^*[i]z[i]e^{-j2\pi\hat{v}_o i} \\
& - \sum\nolimits_{i=-\frac{N_0-1}{2}}^{\frac{N_0-1}{2}} i(i+1)d^*[i+1]z[i+1]e^{-j2\pi\hat{v}_o (i+1)} \\
& + \sum\nolimits_{i=-\frac{N_0-1}{2}}^{\frac{N_0-1}{2}} i(i+1)d^*[i]z[i]e^{-j2\pi\hat{v}_o i} \Bigg\} \Bigg\} \\
0 = \mathrm{Re}\Bigg\{ & \sum\nolimits_{i=-\frac{N_0-1}{2}}^{\frac{N_0-1}{2}} \frac{j}{2} \left(\frac{N_0^2-1}{2} - i(i+1)\right) \\
& \left\{ d^*[i+1]z[i+1]e^{-j2\pi\hat{v}_o (i+1)} - d^*[i]z[i]e^{-j2\pi\hat{v}_o i} \right\} \Bigg\}.
\end{aligned}
\tag{5.28}
$$

or

$$
\begin{aligned}
0 = \mathrm{Re}\Bigg\{ & \sum\nolimits_{i=-\frac{N_0-1}{2}}^{\frac{N_0-1}{2}} \frac{j}{8} \left(N_0^2 - (2i+1)^2\right) \\
& \left\{ d^*[i+1]z[i+1]e^{-j2\pi\hat{v}_o (i+1)} - d^*[i]z[i]e^{-j2\pi\hat{v}_o i} \right\} \Bigg\}.
\end{aligned}
\tag{5.29}
$$

which can be written as

$$
\mathrm{Re}\left\{ \sum\nolimits_{i=-\frac{N_0-1}{2}}^{\frac{N_0-1}{2}} jc[i] \left\{ d^*[i+1]z[i+1]e^{-j2\pi\hat{v}_o (i+1)} - d^*[i]z[i]e^{-j2\pi\hat{v}_o i} \right\} \right\} = 0 \tag{5.30}
$$

where

$$
c[i] = \frac{1}{8}\left(N_0^2 - (2i+1)^2\right) \tag{5.31}
$$

is a special filter function which performs windowing operation. The following relationship [100] is a good approximation at high SNRs.

$$
\frac{z^*[i]}{d^*[i]e^{-j2\pi\hat{v}_o i}} \approx 1 \tag{5.32}
$$

Multiplying each term in the summation of (5.30) with the term on left hand side of (5.32), we get

$$\mathrm{Re}\left\{\sum_{i=-\frac{N_0-1}{2}}^{\frac{N_0-1}{2}} jc[i]\left\{\frac{d^*[i+1]z[i+1]z^*[i]}{d^*[i]}e^{-j2\pi\hat{v}_o} - z^*[i]z[i]\right\}\right\} = 0. \tag{5.33}$$

Noting that $z^*[i]z[i] = |z[i]|^2$ (a real sequence), (5.33) becomes

$$\mathrm{Re}\left\{\sum_{i=-\frac{N_0-1}{2}}^{\frac{N_0-1}{2}} jc[i]\left\{\frac{d^*[i+1]z[i+1]z^*[i]}{d^*[i]}e^{-j2\pi\hat{v}_o}\right\}\right\} = 0. \tag{5.34}$$

From (5.34), we directly get the coarse CFO estimate as

$$\hat{v_{o(coarse)}} = \frac{1}{2\pi}\arg\left\{\sum_{i=-\frac{N_0-1}{2}}^{\frac{N_0-1}{2}} c[i]\frac{d^*[i+1]}{d[i]}z[i+1]z^*[i]\right\}. \tag{5.35}$$

Here, we explain the technical differences between the MLDA estimator (5.35) and the estimators [54] and [57]. The proposed estimator makes use of the phase difference between successive samples $z[i]$ and $z[i+D]$, where $D = 1$. For $D = 1$, the estimation range of the estimator is almost full. For $D \geq 1$, the variance of the estimator is increased due to the reduced number of samples to be averaged in a given window; however, the computational complexity is accordingly decreased. On the other hand, Casini's algorithm [54] can estimate only 20% normalized CFO for $D = 2$. The most important contribution of the MLDA estimator is the introduction of a special filter function $c[i]$ which is in the form of a symmetric window function. The variance of this estimator meets Cramer-Rao Bound due to the use of the filter $c[i]$ (at-least at high SNRs due to approximation of (5.32)) [101]. At low SNRs, the variance of the estimate can be reduced by using the residual offset estimation stage (to be discussed in the next section). The basic idea behind the coarse estimation stages of the proposed algorithm and the Casini's algorithm is similar, but the difference is that the proposed MLDA estimator uses transmitted training sequence and along with the filter function $c[i]$ to reduce the variance by windowing. On the other hand, Oh's algorithm [57] exploits the correlation of the received samples for coarse CFO estimation.

5.3.2 Stage II: Sample-by-Sample Residual Offset Estimation

After obtaining coarse frequency estimate by the MLDA algorithm, CFO compensation has to be applied on the received data. The coarse compensated data is given as

$$z_c[i] = z[i]e^{-j2\pi\hat{\upsilon}_{o(coarse)}i}, \quad i = 0, 1, ..., B-1. \tag{5.36}$$

Now, we present the algorithm for residual offset estimation. The approach is quite similar to the phase estimation algorithm for PSK signals [102] with some modifications. This approach is based on estimating the residual offset of each sample in the burst by using a sliding window approach. For M-ary PSK modulated system, the phase of i^{th} symbol (assuming perfect frequency synchronization) is given as

$$\phi_i = \theta + k_i(2\pi/M) \tag{5.37}$$

where θ is the initial phase and k_i is the modulation index. Due to the estimation error of from stage I, the phase ϕ_i becomes

$$\phi_i = \theta + 2\pi\upsilon_\epsilon i + k_i(2\pi/M). \tag{5.38}$$

In (5.38), the term υ_ϵ is the residual offset that needs to be estimated.

To estimate the residual offset of the i^{th} symbol of any burst, let $R_E = 2P + 1$ be the number of symbols in the estimation interval, where P is the number of symbols before/after the i^{th} symbol. Therefore, the estimation window for the estimation of residual offset $\upsilon_\epsilon[i]$ for $z_c[i]$ will be

$$z_c[i-P], ..., z_c[i-1], z_c[i], z_c[i+1], ..., z_c[i+P].$$

The structure of the estimator for the estimation of residual offset of the i^{th} symbol is shown in Figure 5.8.

To incorporate the moving window estimation, we insert P zeros on both sides of the burst, so that the modified zero-padded burst becomes

$$\mathbf{z_0} = [\mathbf{0}_{1\times P}, z_c[0], z_c[1], ..., z_c[B-1], \mathbf{0}_{1\times P}]\,. \tag{5.39}$$

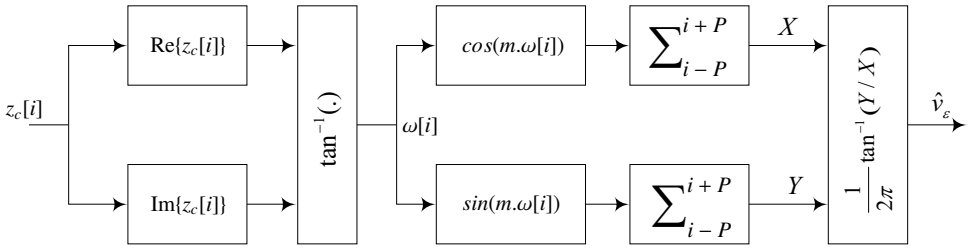

Figure 5.8: Block diagram of the 2^{nd} stage of the proposed CFO estimator

The residual frequency offset for $(i-P)^{th}$ M-ary PSK symbol using the residual frequency estimator is given as

$$\hat{\upsilon}_\epsilon[i-P] = \left[\frac{1}{2\pi M}\arg\left\{\sum_{k=\max(i-P,P+1)}^{\min(i+P-1,B+P)} e^{jM\arg(z_0[k])}\right\}\right]_{\frac{2\pi}{M}} \tag{5.40}$$

where $i = P, P+2, ..., P+B-1$ and $[.]_{\frac{2\pi}{M}}$ is the modulu-$2\pi/M$ operation.

After the estimation of residual offset $\hat{\upsilon}_\epsilon = \hat{\upsilon}_{fine}$ using (5.40), the final compensated data r_f will be

$$z_f[i] = z_c[i]e^{-j2\pi i\hat{\upsilon}_\epsilon[i]}, \quad i = 0, 1, ..., B-1$$

5.3.3 Simulation Results

In this section, we present the simulation results of the proposed two stage CFO estimation algorithm. The training sequence length N_0 for MLDA algorithm is taken 32 whereas the estimation interval R_E for the 2^{nd} stage is taken 23. The length of burst B including training sequence is 320 samples.

It has been mentioned in earlier sections that the proposed algorithm is capable of estimating large frequency offsets. Figure 5.9 and 5.10 show the relative CFO estimate vs the actual normalized CFO for $SNR = -10$ dB and $SNR = 0$ dB respectively. The actual normalized CFO (υ_o) varies from 0 to 0.5. Each point has been obtained by averaging over 5,000 statistically independent frequency estimates. It can be seen that the proposed

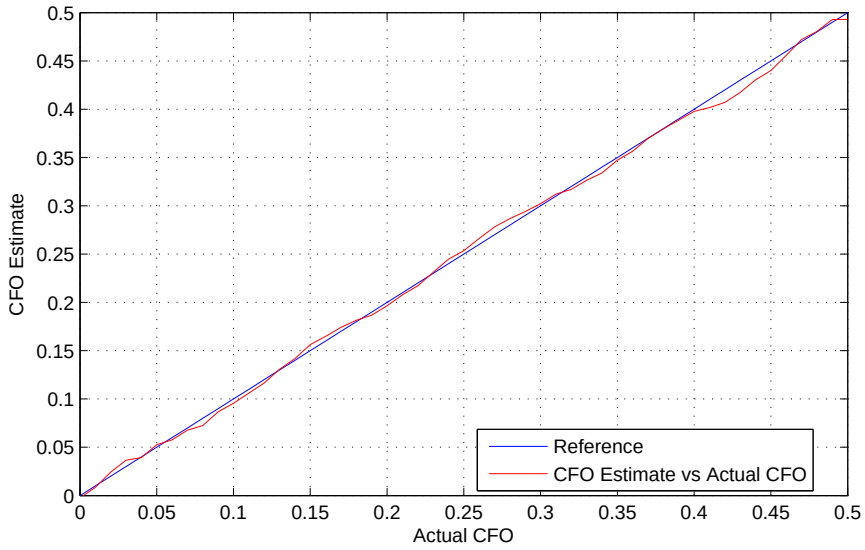

Figure 5.9: Estimate of CFO vs actual CFO using the MLDA estimator ($SNR = -10$ dB).

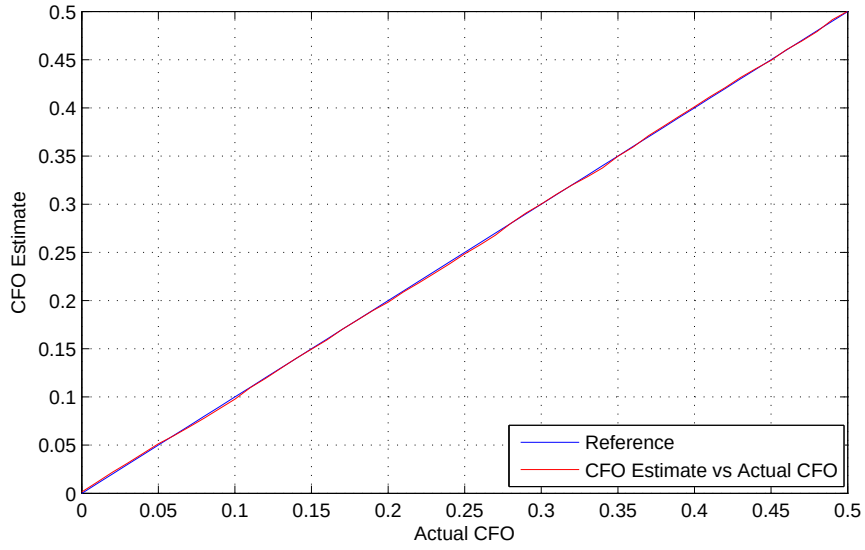

Figure 5.10: Estimate of CFO vs actual CFO using the MLDA estimator ($SNR = 0$ dB).

frequency estimator efficiently estimates CFO throughout its range even at $SNR = -10$ dB. This observation makes the proposed estimator valid for estimating a wide range of frequency offsets efficiently.

The variance of the proposed two stage frequency estimator has been compared with the Cramer-Rao Bound (CRB). The proposed algorithm uses N_0 samples in the first stage and a maximum of $2P+1$ samples in the second stage for the estimation of CFO. Therefore the overall length of estimation interval will be $N_{est} = N_0 + 2P + 1$. For frequency estimation, CRB is given as [55]

$$CRB(\upsilon_o) = \frac{3}{8\pi^2 N_{est}^3} \frac{1}{SNR}. \tag{5.41}$$

Figure 5.11 shows the Mean Square Error (MSE) performance of the proposed two stage estimator compared with the Cramer-Rao Bound (CRB). It can be seen that the estimator approaches CRB with a little deviation at low SNR. In this simulation, 30% frequency offset (i.e. normalized CFO = 0.3) is assumed. With this frequency offset, the MSE of the proposed estimator has been compared with Casini's CFO estimator [54] and Oh's CFO estimator [57]. For [54], $M' = 18$ is chosen, whereas for [57], $M_a = 9$ and training sequence length $N_0 = 32$ are used. The simulation result is shown in Figure 5.12. It can be seen that the proposed estimator outperforms both the algorithms at all SNRs.

The 2^{nd} stage of the proposed estimation algorithm involves windowing and averaging operation. The effect of changing the window length R_E on MSE performance of the proposed estimator is shown in figure 5.13. It can be seen that there is an MSE performance degradation of 2 dB at low SNRs and less than 1 dB at high SNRs if window length is changed from 23 to 11. Even with the reduced window length (which also reduces the computational complexity), the proposed estimator is superior to the Oh's estimator in terms of MSE performance.

Now we compare the Bit Error Rate (BER) performance of the proposed two stage algorithm with the ideal case where CFO is known to the receiver. The BER curves have been obtained by Monte Carlo simulations with a Monte Carlo index of 1000. Figure 5.14 shows the BER comparison of the MLDA estimator (1^{st} stage only), proposed two stage estimator

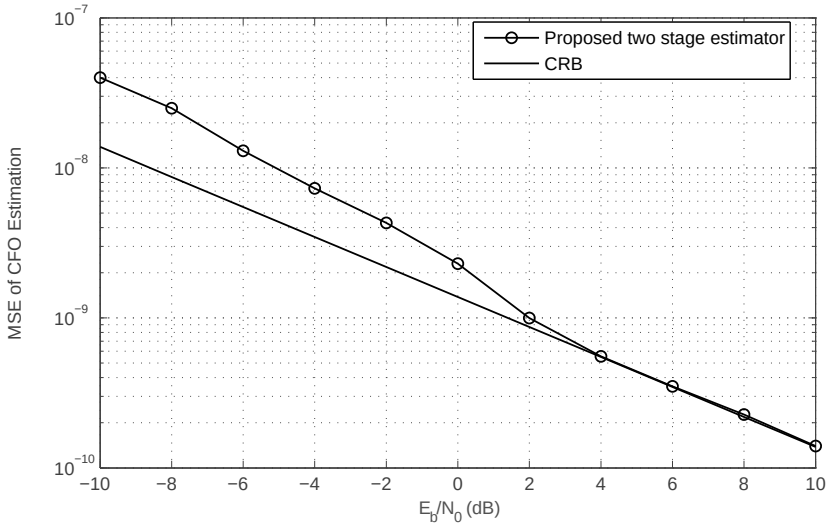

Figure 5.11: MSE for frequency estimation in AWGN with 30% frequency offset (Comparison with CRB).

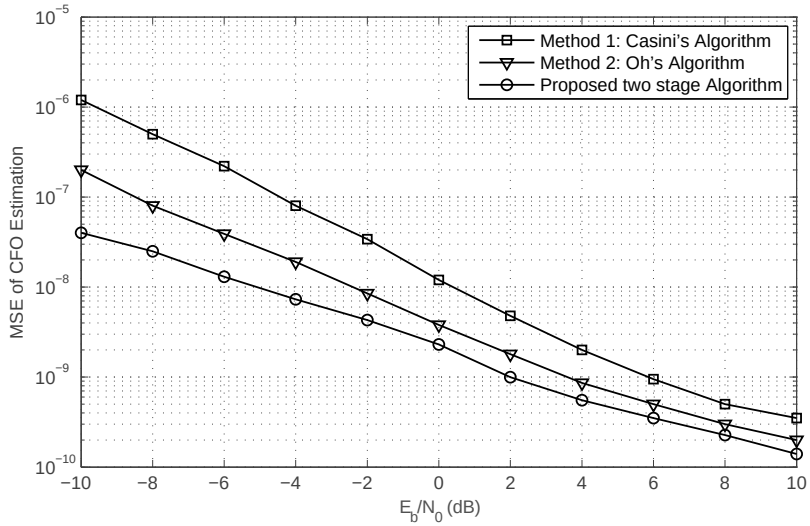

Figure 5.12: MSE comparison for frequency estimation in AWGN with 30% frequency offset.

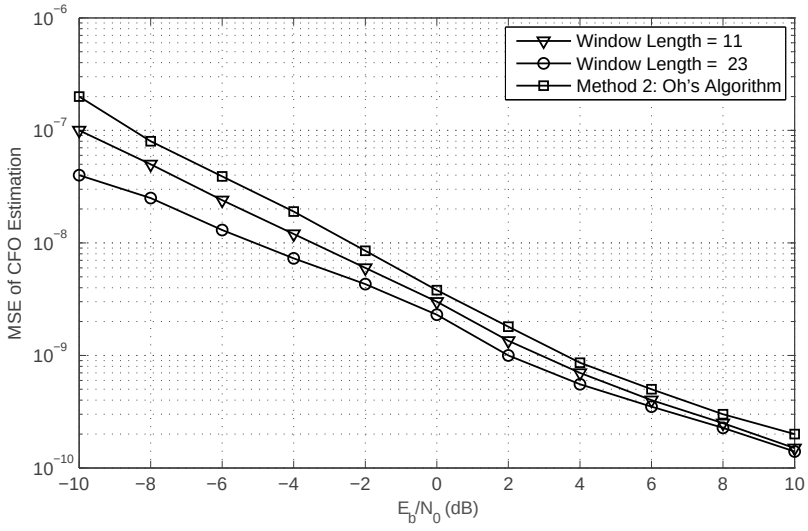

Figure 5.13: MSE comparison for frequency estimation in AWGN with different window lengths

and the ideal case. It can be seen that the proposed two stage estimator approaches the BER performance of the ideal case at all SNRs. In this simulation, 30% frequency offset has been introduced which is successfully estimated and compensated by the proposed estimator. Figure 5.15 compares the BER performance of the proposed estimator to that of the Oh's estimator. A performance improvement of almost 3 dB can clearly be observed.

To demonstrate the effectiveness of the proposed estimator in multipath fading channel, the performance is evaluated over Stanford University Interim (SUI) channel models. In the simulation, we have used SUI-3 channel model with three taps and having a Doppler spread of 0.5 Hz. Figure 5.16 shows the BER performance comparison of the proposed estimator and Oh's estimator. It can be seen that the proposed algorithm outperforms the Oh's algorithm at all SNRs while approaching to the ideal case where CFO is known. This result affirms the viability of the proposed algorithm to be used for CFO estimation in multipath fading channels.

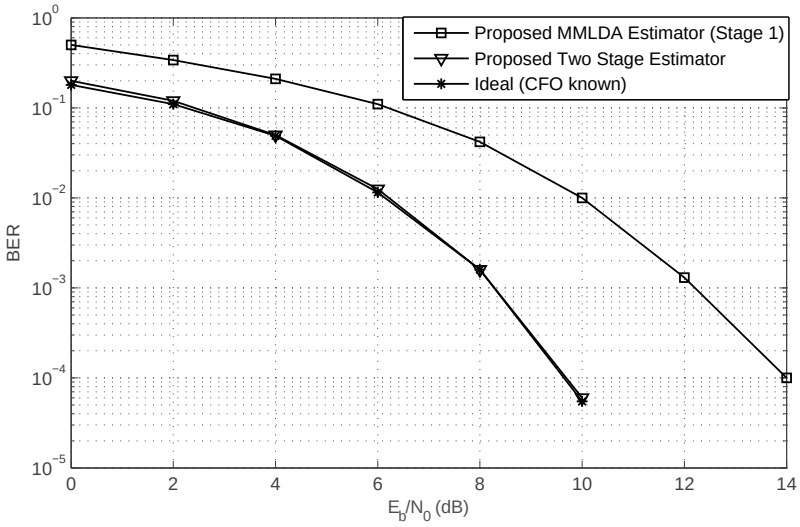

Figure 5.14: BER performance of the proposed algorithm in AWGN

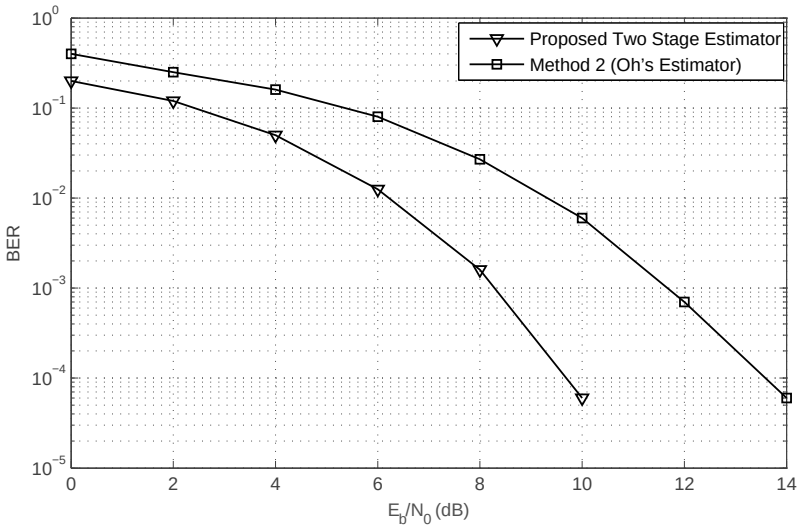

Figure 5.15: BER performance comparison in AWGN

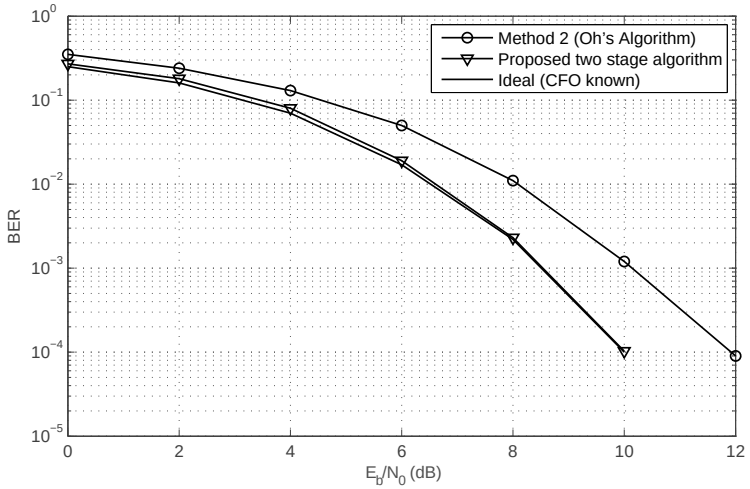

Figure 5.16: BER performance comparison in SUI-3 channel model

5.4 Channel Estimation

For channel impulse response estimation, we follow the method given in [91] with some modification. The modification is required because of the absence of the cyclic prefix in CDMA systems. The received training sequence after correct detection of burst is sampled at $T = GN_sT_s$. This is given in vector form as (dropping subscript k for simplicity)

$$\mathbf{v_R} = [y_c(0), y_c(G), y_c(2G), ..., y_c((N_0 - 1)G)]^T$$

The channel to be estimated $\mathbf{h}$, the matrix $\mathbf{W}$ and the white noise $\mathbf{n}$ are given as;

$$\mathbf{h} \triangleq [h_0, h_1, ..., h_{K_c-1}]^T$$

$$\mathbf{W}(\upsilon_o) \triangleq \text{diag}[1, e^{j2\pi\hat{\upsilon}_o/N_0}, ..., e^{j2\pi(N_0-1)\hat{\upsilon}_o/N_0}]$$

$$\mathbf{n} \triangleq [n(0), n(1), ..., n(N_0 - 1)]^T$$

where K_c is the number of coefficients to be estimated. If the transmitted training sequence is given by $\mathbf{v_T}$, then we form a matrix $\mathbf{V_T}$, given as,

$$\mathbf{V_T} = \begin{bmatrix} v_T(0) & v_T(-1) & \cdots & v_T(-K+1) \\ v_T(1) & v_T(0) & \cdots & v_T(-K+2) \\ \vdots & \vdots & \ddots & \vdots \\ v_T(N_0-1) & v_T(N_0-2) & \cdots & v_T(N_0-K_c) \end{bmatrix} \tag{5.42}$$

where $v_T(-1) = v_T(-2) = \cdots = v_T(-K_c+1) = 0$. The Maximum Likelihood (ML) channel impulse response estimate can be realized by,

$$\hat{\mathbf{h}} = [\mathbf{V_T}^H.\mathbf{V_T}]^{-1}\mathbf{V_T}^H.\mathbf{W}^H(\hat{\upsilon}_o).\mathbf{v_R}(0) \tag{5.43}$$

where

$$\mathbf{v_R}(0) = \mathbf{W}(\hat{\upsilon}_o)\mathbf{V_T}.\mathbf{h} + \mathbf{n} \tag{5.44}$$

To combat multipath fading effects, RAKE receiver with Maximal Ratio Combining (MRC) has been implemented.

5.5 Conclusion

In this chapter, two types of novel CFO estimation and compensation algorithms for the wideband SDR waveform are proposed. The first algorithm is based on Fast Fourier Transform (FFT) and interpolation. Firstly, a basic estimation algorithm has been proposed in which FFT and quadratic interpolation are used sequentially to estimate CFO. The estimation performance of this algorithm is improved by proposing an enhanced CFO estimator which uses modified FFT and biquadratic interpolation. A detailed computational complexity analysis of both the basic and enhanced algorithms is also presented. A novel two stage algorithm for CFO estimation and compensation is also proposed and presented in this chapter. The first stage (coarse estimation) of this algorithm provides a coarse estimate of CFO by using Maximum Likelihood Data Aided (MLDA) correlation based

algorithm. In the second stage (fine estimation),the residual offset error for each burst on sample by sample basis using blind estimation approach is estimated and compensated. The estimation range of the proposed estimator is almost full. It is shown through computer simulations that the proposed algorithm has better performance as compared to a set of known two stage CFO estimation algorithms.

Chapter 6

Link Adaptation

The future SDR-based networks will have to support a variety of high data rate applications such as streaming video, biometrics, IP data, voice, situational awareness, while offering a high degree of survivability, mobility and security. Due to these requirements, the future network developments are moving toward wideband and digital signal based networking capable of providing adaptive and high speed communication. Efficient algorithms for resource allocation/utilization are required to optimize the use of scarce SDR resources. This involves adapting the transmission parameters of the SDR waveform to varying channel conditions, QoS and data rate requirements. This process is called link adaptation. A simple example is the transmit power control algorithm, in which the transmission power is altered based on channel variations and fading, because a low transmit power is sufficient under good channel conditions. The requirement of link adaptation increases when the transmissions are in the form of network packets. A low value of bit error rate can drastically increase the packet error rate and thus packet re-transmissions, if the signal and protocol parameters are not dynamically changed according the channel conditions and tolerable bit error rate.

In this chapter, a novel algorithm for link adaptation using fuzzy rule based system (FRBS) for the physical layer of the wideband networking waveform of SDR is proposed[1]. To reduce the packet re-transmissions overhead, the configurable system parameters need to be changed dynamically according to the channel conditions. Moreover, different applications (e.g. Push To Talk (PTT), position tracking, point-to-point calls, messages, file transfer, video communication etc) have different QoS requirements. This varying QoS re-

[1]Parts of this chapter appear in author's own publication, [103]

quirement in a networking waveform is fulfilled by link adaptation which usually comprises of two parts; 1) Varying the waveform parameters at the physical layer, and 2) Adaptive TDMA. The focus of this thesis is on the first part with multicode CDMA at the physical layer. A novel scheme based on fuzzy rules is proposed which is capable of selecting the most suitable parameters based on the heuristics. The required Quality of Service (QoS) and throughput constraints are met by dynamically changing the modulation technique and the number of multicodes assigned to each user through fuzzy inference system. The proposed algorithm reduces the complexity and thus the power consumption by restricting the throughput to the value required by user or application, even if the channel conditions are fair enough to allow higher throughput. Results have been presented to demonstrate the effectiveness of the proposed algorithm. It has been shown that the proposed link adaptation scheme achieves better throughput by efficiently reducing the packet re-transmissions overhead.

6.1 System Model

Considering a maximum of K users at the physical layer of wideband waveform, the spreading waveform corresponding to the m^{th} code assigned to k^{th} user is given by

$$\pi_{k,m}(t) = \sum_{n=0}^{G-1} c_{k,m}[n] g(t - nT_c) \qquad m = 0, 1, ..., I_{M,k} - 1 \tag{6.1}$$

where $c_{k,m}[n]$ is the n^{th} sample of the m^{th} spreading code of k^{th} user, $I_{M,k}$ is the multicode index (i.e. number of codes) assigned to k^{th} user). The transmitted signal of k^{th} user is given by

$$s_k(t) = \sum_{i} \sum_{m=0}^{I_{M,k}-1} d_k[I_{M,k}(i-1) + m] \pi_{k,m}(t - iT) \tag{6.2}$$

where $d_k[.] \in e^{j2m_k\pi/M_k}$ are the M-PSK symbols of k^{th} user, M_k is the modulation index and $m_k = 0, 1, ..., M_k - 1$. After passing through the multipath fading channel, the received

composite continuous-time baseband signal is

$$r(t) = \sum_{k=1}^{K} e^{j2\pi\Delta f_k t} . \sum_{i} . \sum_{m=0}^{I_{M,k}-1} . \sum_{l=1}^{\gamma_k} \alpha_{kl} d_k[I_{M,k}(i-1)+m] \pi_{k,m}(t - iT - \tau_{kl}) + w(t) \tag{6.3}$$

and $f_{D,kl}$, α_{kl} and τ_{kl} are the Doppler spread, constant complex path gain (considering $BT \leq T_{coh}$) and delay spread corresponding to the l^{th} path and k^{th} user, respectively, γ_k is the number of multipath and Δf_k be the k^{th} user's CFO. Let the waveform $q_{k,m}(t)$ for k^{th} user's m^{th} spreading code be defined as

$$q_{k,m}(t) = \sum_{l=1}^{\gamma_k} \alpha_{kl} \pi_{k,m}(t - iT) \tag{6.4}$$

so that considering first burst of data, (6.3) becomes

$$r(t) = \sum_{k=1}^{K} e^{j2\pi\Delta f_k t} . \sum_{i=0}^{B-1} \sum_{m=0}^{I_{M,k}-1} . \sum_{l=1}^{\gamma_k} \alpha_{kl} d_k[I_{M,k}(i-1)+m] q_{k,m}(t - iT) + w(t) \tag{6.5}$$

After sampling the received signal given by (6.5) at N_s/T_c, timing and frequency synchronization is achieved. The aim of the proposed link adaptation scheme is to dynamically change the modulation index M and multicode index I_M through Fuzzy Rule based System (FRBS) which takes QoS and throughput requirements and estimated received SNR as inputs as shown in Figure 6.1. The first two inputs (i.e. QoS and throughput) are either specified by user or as required by a specific application, whereas the received SNR needs to be estimated at the receiver. Several SNR estimation algorithms are present in the literature, e.g. see [104–106]. The proposed link adaptation algorithm uses higher modulation index M up to 16. Due to this reason, a moment-based algorithm for estimating SNR for higher order modulation given in [106] has been chosen. The estimation performance of this estimator is superior to other existing moment-based algorithms.

6.2 Problem Formulation

The effective throughput of any waveform depends on the both the waveform parameters and channel conditions. The waveform parameters include RF bandwidth, modulation

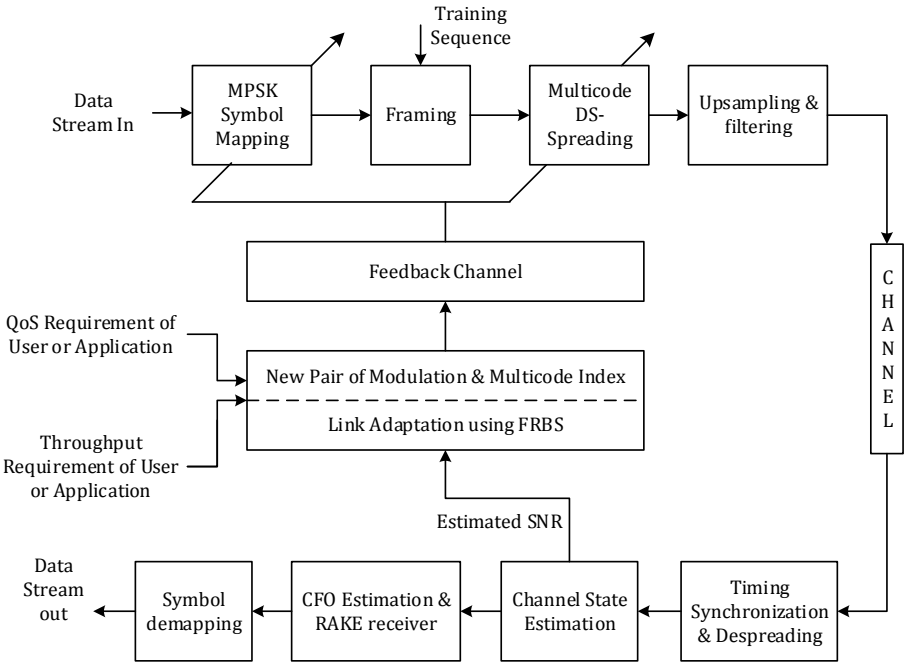

Figure 6.1: Overview of the proposed link adaptation scheme based on fuzzy rule based system

scheme, number of samples per symbol, forward error correction etc. For a wideband waveform based on multicode CDMA, these parameters also include spreading gain and multicode index. Wideband networking waveforms suffer heavily by re-transmissions overhead due to erroneous received packets in case of harsh channel conditions. This overhead reduces the effective throughput. The aim of a good link adaptation scheme should be to provide maximum possible data throughput as required by a user or application by reducing the packet re-transmissions overhead through the use of optimum waveform parameters. The computational complexity and thus the power consumption need to be reduced by restricting the throughput to the required value even if the channel conditions are fair enough to allow higher throughput. Thus, the problem of link adaptation at the physical layer of

wideband networking waveform is formulated as

$$\max R_k = \frac{2BI_{M,k}\log_2(M_k)}{B_{norm}N_sG}.\frac{N_d}{N_0+N_d} \tag{6.6}$$

subject to the constraints

$$\text{BER} \leq \text{BER}_{max}$$

$$R_k = \begin{cases} R_{max}, & \text{if } R_{max} \leq R_{req} \\ R_{req}, & \text{if } R_{max} > R_{req} \end{cases}$$

where

B_{RF} = RF bandwidth in MHz

$\log_2(M_k)$ = Bits per M-PSK symbol for k^{th} user

$I_{M,k}$ = Multicode index for k^{th} user

B_{norm} = Normalized two-sided bandwidth

N_s = Number of samples per symbol (upsampling factor)

N_d = Number of data symbols/burst

N_0 = Number of symbols in training sequence

R_k = Data rate of k^{th} user in Mbps

BER = Bit Error Rate

BER_{max} = Maximum allowed BER as per QoS requirement

$R_{k,req}$ = Throughput requirement of k^{th} user/application in Mbps

R_{max} = Maximum throughput possible for given QoS bound and SNR

We have assumed $10^{-4} \leq \text{BER}_{max} \leq 10^{-1}$ and 0.25Mbps$\leq R_{k,req} \leq$ 17.5Mbps. Note that the effective throughput depends on packet error rate. As packet error rate increases, the effective throughput is decreased due to the increase in number of packet re-transmissions.

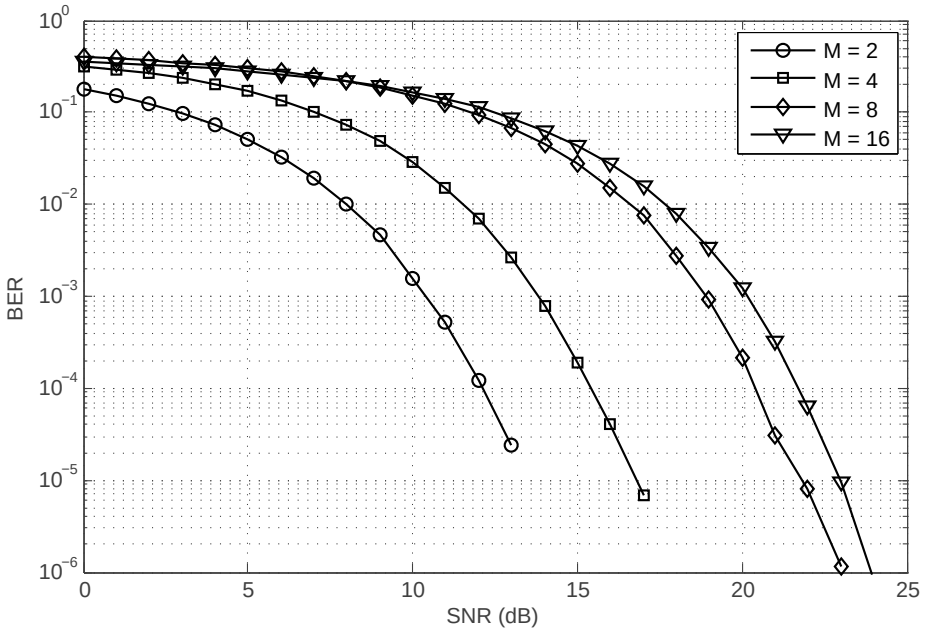

Figure 6.2: BER for various values for multicode index $I_M = 8$ and modulation indices (M) varying from 2 to 16

6.3 Data Acquisition for Fuzzy Rules Formation

The first step of the proposed algorithm is the acquisition of data from BER performance curves of the system for all the possible modes of operation. BER performance of the system is analyzed for all the possible pairs of modulation and multicode indices. Figure 6.2 shows an example with a set of BER curves for a multicode index $I_M = 8$ and modulation indices (M) varying from 2 to 16. In similar way, BER curves for all other pairs are obtained through simulation.

The data is then acquired from the set of BER curves by drawing horizontal line (for a specific QoS requirement) for each BER curve and noting the intersection point. This will give the minimum SNR that guarantees the BER to be within maximum allowable value along with the achievable throughput for a specific Modulation and Multicode Index (MMI) pair. This process is repeated for the complete set of BER curves obtained through

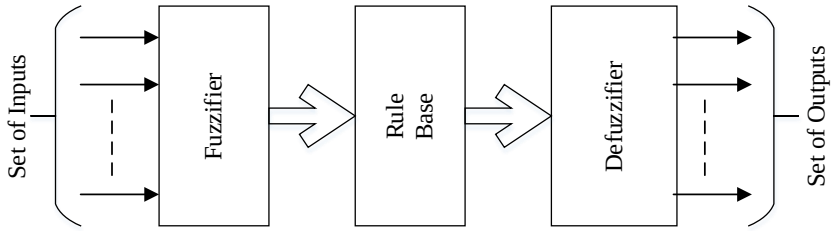

Figure 6.3: Block diagram of a typical fuzzy inference system

simulation to obtain the data acquisition table 6.1. Note that the subscript k is dropped for simplicity.

6.4 Proposed Fuzzy Rule based Link Adaptation

In this section, we present the proposed algorithm for creating the FRBS which selects the best MMI pair for the next transmission. Fuzzy logic depends heavily on human thinking in spirit and is much closer to natural language as compared to conventional logic systems. By adjusting the input signal, the fuzzy logic controller executes similar actions as a human operator executes. A typical fuzzy system comprises of these stages; Fuzzification, Rule Base and Defuzzification (see Figure 6.3). In Fuzzification stage, these inputs are first converted to fuzzy numbers. The next stage, rule base, generates fuzzy number of the compensated output signal by using the fuzzified input variables. The fuzzy numbers corresponding to the compensated output signal are converted to crisp values in the defuzzifier stage. Collectively, these three stages are referred to as Fuzzy Inference System (FIS).

6.4.1 Selection of Fuzzy Sets

After completing the data acquisition from BER curves, fuzzy sets and the corresponding Membership Functions (MF) are now selected to cover the complete range of inputs and

Table 6.1: Data acquired from the BER curves (Minimum SNR values that guarantee the BER to be within maximum allowable value)

	$\mathbf{BER}_{max}$	**M=2**	**M=4**	**M=8**	**M=16**
$I_M = 1$	10^{-1}	-	0.35	5.02	5.6
	10^{-2}	1.28	4.87	9.85	10.68
	10^{-3}	3.76	7.07	12.2	13.2
	10^{-4}	5.31	8.63	13.72	14.8
		M=2	**M=4**	**M=8**	**M=16**
$I_M = 2$	10^{-1}	-	3	7.6	8.27
	10^{-2}	3.9	7.43	12.42	13.45
	10^{-3}	6.38	9.7	14.82	15.97
	10^{-4}	7.83	11.21	16.43	17.48
		M=2	**M=4**	**M=8**	**M=16**
$I_M = 4$	10^{-1}	1.06	5.23	9.95	10.53
	10^{-2}	6.15	9.67	14.74	15.7
	10^{-3}	8.55	12.02	17.14	18.2
	10^{-4}	10.3	13.45	18.68	19.78
		M=2	**M=4**	**M=8**	**M=16**
$I_M = 8$	10^{-1}	2.85	7.1	11.73	12.46
	10^{-2}	8.01	11.55	16.58	17.64
	10^{-3}	10.41	13.8	18.93	20.15
	10^{-4}	12.2	15.41	20.4	21.72
		M=2	**M=4**	**M=8**	**M=16**
$I_M = 16$	10^{-1}	4.2	8.4	13.03	13.85
	10^{-2}	9.38	12.92	17.89	19.1
	10^{-3}	11.81	15.18	20.3	21.59
	10^{-4}	13.32	16.56	21.77	23.14

outputs. The inputs to the proposed FIS are QoS requirement (taken as negative logarithm of BER, denoted as $nLogBER$) throughput requirement ($R_{k,req}$) and estimated SNR. The generated output is Modulation and Multicode Index (MMI) pair. Triangular membership function is used with min-max (and-or) as implication and aggregation operation. The triangular membership function $M(x)$ is with endpoints $(a, 0)$ and $(b, 0)$ and the high point (c, α) is given as

$$M(x) = \begin{cases} \alpha\left(\frac{x-a}{c-a}\right), & a \leq x \leq c \\ \alpha\left(\frac{x-b}{c-b}\right), & c \leq x \leq b \\ 0, & \text{otherwise} \end{cases}$$

The third input ($R_{k,req}$) uses non-uniform triangular MF, whereas the other two inputs and the output use the standard uniform triangular MF. The MFs of the inputs and output of the proposed FIS are shown in Figure (6.4). Sufficient number of fuzzy sets are used to represent the inputs and output. The input variable $nLogBER$ is simply calculated as

$$nLogBER = -\log(\text{BER})$$
$$\text{BER} = 10^{-b}$$
$$nLogBER = -\log(10^{-b}) = b$$

The number of fuzzy sets used for the inputs are 4, 6 and 9 for $nLogBER$, received SNR and $R_{k,req}$, respectively. For the output MMI pair, the possible values of M_k are 2, 4, 8, 16 and the possible values of $I_{M,k}$ are 1, 2, 4, 8, 16. So, the maximum 20 possible fuzzy sets are used for the output MMI pair.

6.4.2 Fuzzy Rule Matrix for Multicode and Modulation Indices Selection

The Fuzzy Rule Matrix (FRM) is the main processing stage of any FIS. It is based on a collection of logic rules in the form of IF-THEN statements. The 'IF' part of the rule is called 'antecedent' and the 'THEN' part of the rule is called 'consequent'. As mentioned

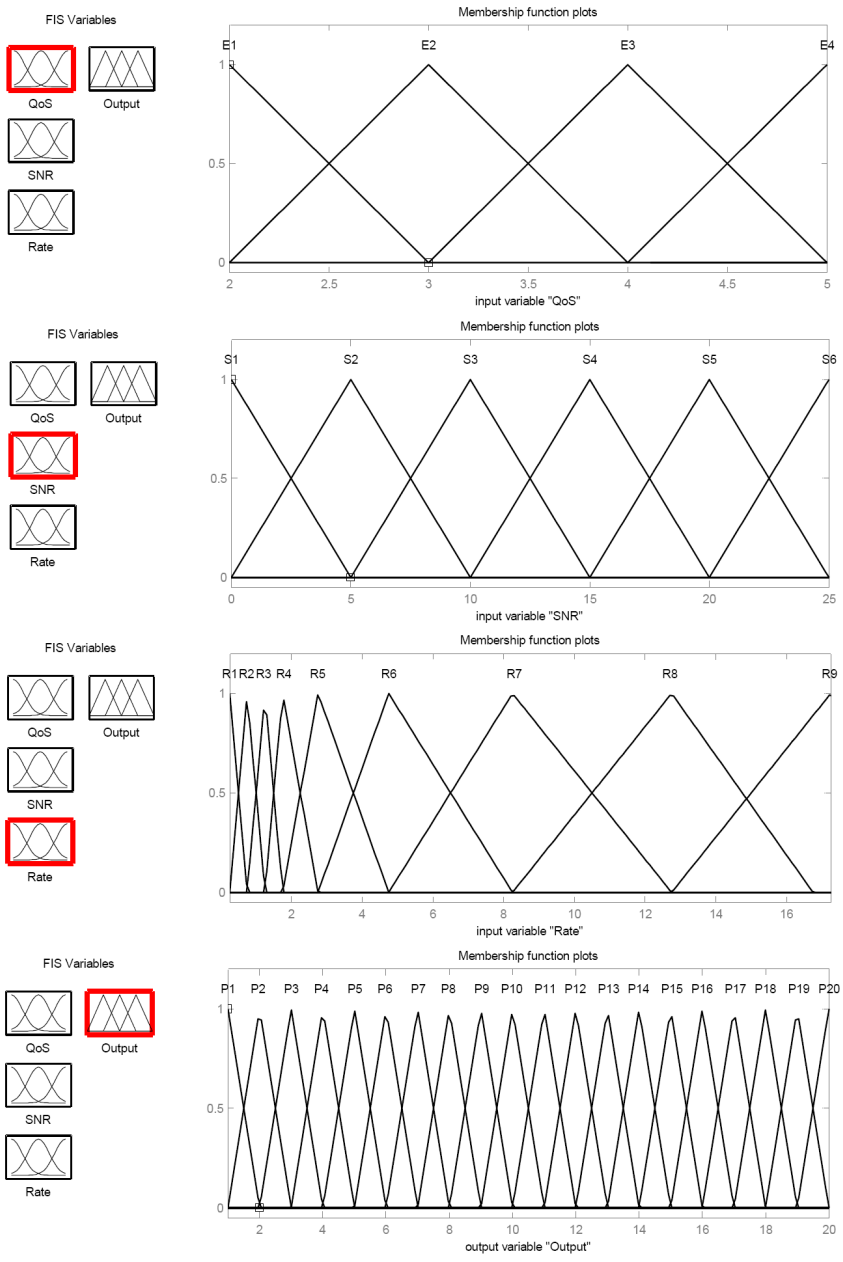

Figure 6.4: Membership functions of the inputs and output of the proposed FIS using fuzzy systems toolbox

earlier, the FIS of the proposed system takes three inputs (QoS requirement, throughput requirement and estimated SNR) and generates an output Modulation and Multicode Index pair. Let the total number of fuzzy rules be N_R. The possible input-output pairs for the proposed FRBS can be represented as

$$(x_1^r, x_2^r, x_3^r; y^r) \qquad r = 1, 2, 3, ..., N_R$$

where x_1^r, x_2^r, x_3^r and y^r denote the desired $nLogBER$, received SNR, $R_{k,req}$ and the output MMI pair for the r^{th} rule respectively.

Letting $\{E_1, E_2, E_3, E_4\}$, $\{S_1, S_2, ..., S_6\}$, $\{R_1, R_2, ..., R_9\}$ and $\{P_1, P_2, ..., P_{20}\}$ be the fuzzy set values for the required $nLogBER$, SNR, $R_{k,req}$ and the output MMI pair, respectively, an example fuzzy rule can be stated as

IF $\{(x_1$ is $E_2)$ AND $(x_2$ is $S_8)$ AND $(x_3$ is $R_3)\}$ THEN (y is P_{12})

The output MMI pairs for the 20 fuzzy set values are shown in table 6.2. Based on the number of fuzzy set values used for the inputs and output of the FIS, a total number of $N_R = 216$ fuzzy rules are formed using the acquired data from the BER curves. Some rules have same antecedent (IF part) but different consequents (THEN parts). Such rules are called conflicting rules. For conflicting rules, the consequent resulting in higher throughput is selected. Similarly, if two or more consequents result in same throughput, the consequent with lower value of modulation and/or multicode indices is selected since it will result in lower computational complexity and thus lower power consumption. If some input/output pairs are not available in the acquired data, then those parts are filled by human intuition or expert knowledge. For example, if an MMI pair fulfills the given specifications at a lower SNR, then it is certainly valid for higher SNR. If the throughput specification is not achievable by the available MMI pairs under a given QoS requirement, then the MMI pair resulting in the highest possible throughput is selected. The complete Fuzzy Rule Matrix (FRM) is given table 2.

Table 6.2: Output MMI pairs (modulation index, multicode index) for the 20 fuzzy set values

Value	MMI Pair	Value	MMI Pair	Value	MMI Pair	Value	MMI Pair
P_1	(2,1)	P_6	(4,2)	P_{11}	(8,4)	P_{16}	(16,8)
P_2	(4,1)	P_7	(8,2)	P_{12}	(16,4)	P_{17}	(2,16)
P_3	(8,1)	P_8	(16,2)	P_{13}	(2,8)	P_{18}	(4,16)
P_4	(16,1)	P_9	(2,4)	P_{14}	(4,8)	P_{19}	(8,16)
P_5	(2,2)	P_{10}	(4,4)	P_{15}	(8,8)	P_{20}	(16,16)

Table 6.3: Human intuition based FRM for MMI pair selection

QoS	SNR	Required data rate ($R_{k,req}$)								
		$\boldsymbol{R_1}$	$\boldsymbol{R_2}$	$\boldsymbol{R_3}$	$\boldsymbol{R_4}$	$\boldsymbol{R_5}$	$\boldsymbol{R_6}$	$\boldsymbol{R_7}$	$\boldsymbol{R_8}$	$\boldsymbol{R_9}$
$\boldsymbol{E_1}$	$\boldsymbol{S_1}$	P_1	P_5	P_5	P_5	P_5	P_5	P_5	P_5	P_5
	$\boldsymbol{S_2}$	P_2	P_6	P_9	P_{13}	P_{17}	P_{17}	P_{17}	P_{17}	P_{17}
	$\boldsymbol{S_3}$	P_3	P_4	P_7	P_8	P_{11}	P_{18}	P_{18}	P_{18}	P_{18}
	$\boldsymbol{S_4}$	P_3	P_4	P_7	P_{10}	P_{12}	P_{15}	P_{16}	P_{19}	P_{20}
	$\boldsymbol{S_5}$	P_3	P_4	P_7	P_{10}	P_{12}	P_{15}	P_{16}	P_{19}	P_{20}
	$\boldsymbol{S_6}$	P_3	P_4	P_7	P_{10}	P_{12}	P_{15}	P_{16}	P_{19}	P_{20}
$\boldsymbol{E_2}$	$\boldsymbol{S_1}$	P_1	P_1	P_1	P_1	P_1	P_1	P_1	P_1	P_1
	$\boldsymbol{S_2}$	P_1	P_5	P_5	P_5	P_5	P_5	P_5	P_5	P_5
	$\boldsymbol{S_3}$	P_2	P_3	P_{10}	P_{13}	P_{17}	P_{17}	P_{17}	P_{17}	P_{17}
	$\boldsymbol{S_4}$	P_2	P_4	P_7	P_8	P_{11}	P_{18}	P_{18}	P_{18}	P_{18}
	$\boldsymbol{S_5}$	P_2	P_4	P_7	P_8	P_{12}	P_{15}	P_{16}	P_{19}	P_{20}
	$\boldsymbol{S_6}$	P_2	P_4	P_7	P_8	P_{12}	P_{15}	P_{16}	P_{19}	P_{20}
	$\boldsymbol{S_1}$	P_1	P_1	P_1	P_1	P_1	P_1	P_1	P_1	P_1

Continued on next page

Table 6.3 – *Continued from previous page*

QoS	SNR	$\boldsymbol{R_1}$	$\boldsymbol{R_2}$	$\boldsymbol{R_3}$	$\boldsymbol{R_4}$	$\boldsymbol{R_5}$	$\boldsymbol{R_6}$	$\boldsymbol{R_7}$	$\boldsymbol{R_8}$	$\boldsymbol{R_9}$
$\boldsymbol{E_3}$	$\boldsymbol{S_2}$	P_1	P_1	P_1	P_1	P_1	P_1	P_1	P_1	P_1
	$\boldsymbol{S_3}$	P_5	P_6	P_6	P_6	P_6	P_6	P_6	P_6	P_6
	$\boldsymbol{S_4}$	P_2	P_4	P_7	P_{10}	P_{14}	P_{14}	P_{14}	P_{14}	P_{14}
	$\boldsymbol{S_5}$	P_2	P_4	P_7	P_8	P_{11}	P_{15}	P_{18}	P_{18}	P_{18}
	$\boldsymbol{S_6}$	P_2	P_4	P_7	P_8	P_{11}	P_{15}	P_{16}	P_{19}	P_{20}
$\boldsymbol{E_4}$	$\boldsymbol{S_1}$	P_1	P_1	P_1	P_1	P_1	P_1	P_1	P_1	P_1
	$\boldsymbol{S_2}$	P_1	P_1	P_1	P_1	P_1	P_1	P_1	P_1	P_1
	$\boldsymbol{S_3}$	P_1	P_5	P_5	P_5	P_5	P_5	P_5	P_5	P_5
	$\boldsymbol{S_4}$	P_2	P_3	P_{10}	P_{10}	P_{17}	P_{17}	P_{17}	P_{17}	P_{17}
	$\boldsymbol{S_5}$	P_2	P_4	P_7	P_8	P_{11}	P_{18}	P_{18}	P_{18}	P_{18}
	$\boldsymbol{S_6}$	P_2	P_4	P_7	P_8	P_{11}	P_{15}	P_{16}	P_{19}	P_{20}

6.4.3 Defuzzification

In the fuzzification stage, all the three inputs are converted into fuzzy numbers $\mu_{nLogBER}$, μ_{SNR} and $\mu_{R_{k,req}}$. The fuzzy inference stage generates a fuzzy output value Δu by using the FRM. This fuzzy value is then defuzzified in to a crisp value in the form of MMI pair number. For defuzzification, Centroid of Area (COA) method [107] is used in the proposed FRBS. For discrete number of fuzzy rules the defuzzified output $\Delta u(k)$ by COA method will be

$$\Delta u(k) = \frac{\sum_i \mu_{R_i}(\Delta u)\Delta u(R_i)}{\sum_i \Delta u(R_i)} \tag{6.7}$$

where $\Delta u(R_i)$ is the representative crisp value corresponding to the peak value of the membership degree of the fuzzy set which is an output from the FRM for the rule R_i.

6.5 Simulation Results

This section presents the simulation results of the proposed link adaptation algorithm. The parameters used in the simulations are as follows.

- RF bandwidth (B_{RF}) = 8 MHz
- Pulse shaping roll-off factor (α) = 0.65
- Spreading sequence length (G) = 16

The proposed algorithm is applicable to the systems with a maximum of K active users at the physical layer in the current time slot, where $K \leq G$. Note that if $K = G$ in a single time slot, then I_M will always be unity which results in a maximum data throughput of 1.08 Mbps. The aim of the proposed link adaptation algorithm is to provide either maximum possible data rate (R_{max}) depending upon the QoS and throughput requirements (if $R_{max} \leq R_{req}$) or restrict the data rate to that required by the user or application (if $R_{max} > R_{req}$). The data rate is restricted to the throughput required by the user or a specific application to reduce the computational load and thus the power consumption and allow more active users to communicate.

Figures 6.5-6.6 show the resulting throughput versus E_b/N_0 for QoS requirements of 10^{-1} and 10^{-3}, respectively, plotted for R_{req} ={0.25, 1.75, 4.25, 8.25, 17.25} Mbps. The Stanford University Interim channel model is used in the simulations to investigate the performance in the presence of Doppler spread and multipath fading. It can be seen that the proposed algorithm achieves the required throughput for all the QoS and data rate requirements at various E_b/N_0 values by maintaining the BER less than or equal to BER_{max}. The higher throughput requirements are met at higher values of E_b/N_0 because of the selection of higher modulation and multicode indices. However, maximum possible throughput is achieved at lower values of E_b/N_0 by the selection of appropriate MMI pair.

Figure 6.7 shows the effect of QoS demands on the maximum achieved data throughput. As expected, R_{req} is achieved at lower values of E_b/N_0 for relatively lower QoS

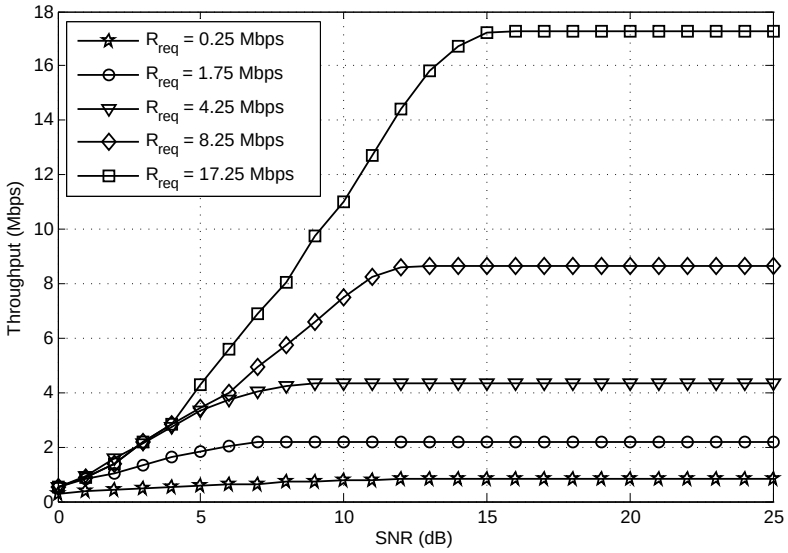

Figure 6.5: Throughput performance of the proposed algorithm for QoS demand of 10^{-1}

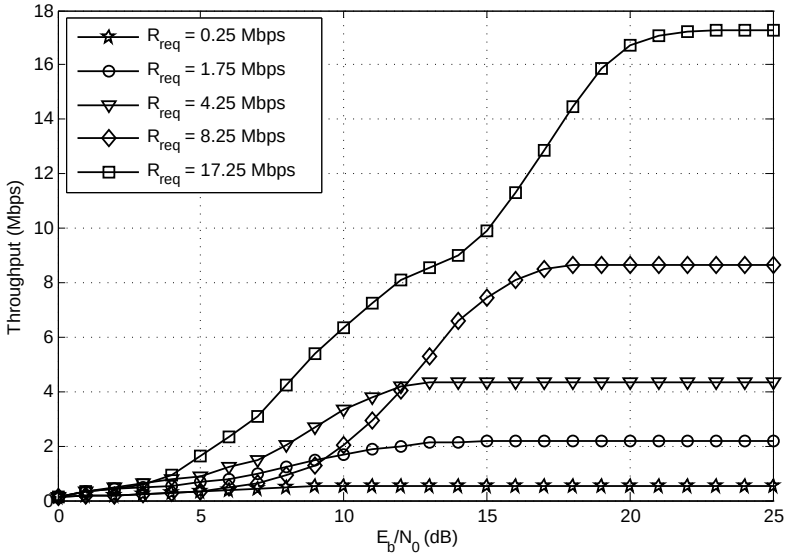

Figure 6.6: Throughput performance of the proposed algorithm for QoS demand of 10^{-3}

demands. The QoS demands are taken in $nLogBER$ format defined earlier in the paper. For $BER_{max} = 3$ and 4, the effect on throughput is small. This is due to less difference in BER performance between $M = 8$ and $M = 16$, as shown in figure 6.2.

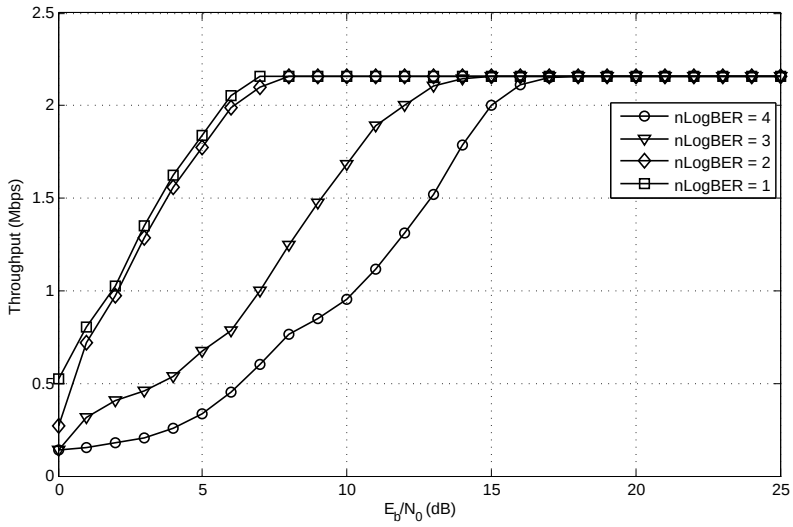

Figure 6.7: Throughput performance of the proposed algorithm for various QoS requirements and $R_{req} = 1.75$ Mbps

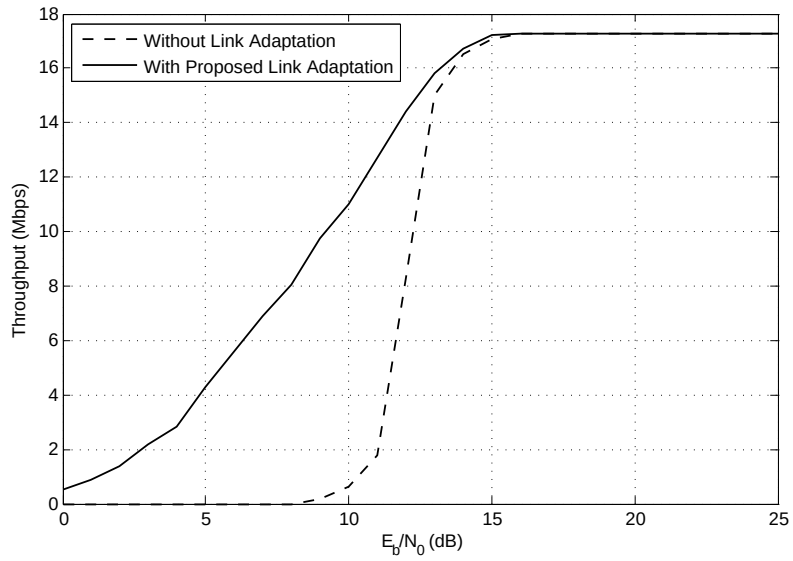

Figure 6.8: Throughput with and without proposed link adaptation (QoS = 10^{-1} and $R_{req} = 17.25$ Mbps)

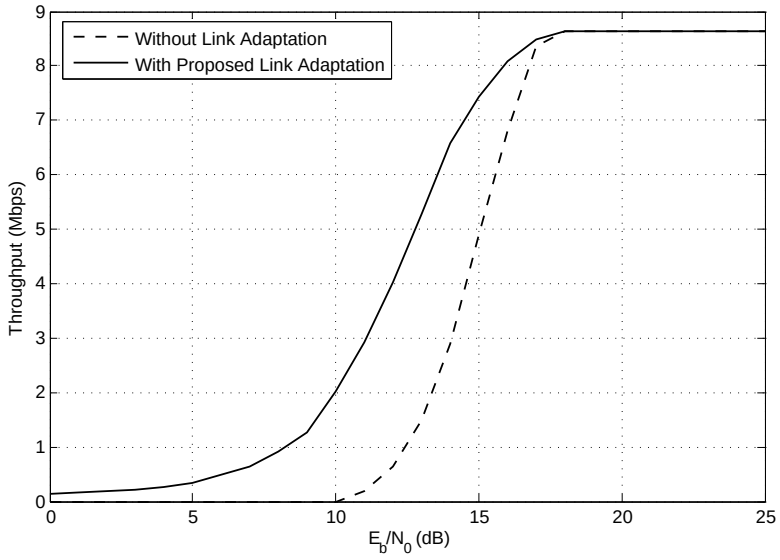

Figure 6.9: Throughput with and without proposed link adaptation (QoS = 10^{-3} and $R_{req} = 8.25$ Mbps)

Mostly, the wideband networking waveforms use network packet-based communication. In the absence of link adaptation, a lower value of BER drastically increases the packet error rate, thereby increasing the packet re-transmission rate. The proposed link adaptation algorithm reduces packet re-transmissions rate by switching the modulation scheme and multicode index to provide maximum possible throughput for lower E_b/N_0 values. Figures 6.8-6.9 show the throughput comparison with two different QoS requirements with and without the proposed link adaptation algorithm. For both the throughput requirements without link adaptation, the modulation scheme and modulation index are chosen which provide the required throughput in perfect channel conditions. In the absence of link adaptation, the throughput drastically reduces at lower E_b/N_0 values because most of the network packets need re-transmissions due to very high packet error rate. On the other side, the proposed link adaptation provides maximum possible throughput for lower E_b/N_0 values and restricts throughput to the required value in good channel conditions.

6.6 Conclusion

This chapter prsents a novel algorithm for link adaptation using fuzzy rule based system (FRBS) for the physical layer of the wideband networking waveform of SDR. The varying QoS requirement of different applications in a networking waveform is fulfilled by link adaptation which is usually achieved by varying the waveform parameters at the physical layer and/or implementing adaptive TDMA. This chapter focussed on the first part with multicode CDMA at the physical layer. A novel scheme based on fuzzy rules is proposed which is capable of selecting the most suitable parameters based on the heuristics. The required Quality of Service (QoS) and throughput constraints are met by dynamically changing the modulation technique and the number of multicodes assigned to each user through fuzzy inference system. The proposed algorithm reduces the complexity and thus the power consumption by restricting the throughput to the value required by user or application, even if the channel conditions are fair enough to allow higher throughput. It is shown through computer simulations that the proposed link adaptation scheme achieves better throughput by efficiently reducing the packet re-transmissions overhead.

Chapter 7

Implementation and Results

Software defined radio is a radio transceiver whose key parameters, protocols and fundamental aspects of operation are defined in software, in the form of a waveform, and can be reconfigured by upgrading that software. In this way, a single radio platform is used to host several waveforms. The proposed physical layer algorithms of the CDMA/ATDMA based wideband networking waveform are implemented, tested and verified successfully on the SDR platform. The proposed timing synchronization algorithms (i.e. sampling clock recovery and burst detection) have been implemented on Field Programmable Gate Array (FPGA) and the remaining portions of the receiver like Carrier Frequency Offset (CFO) estimation, channel estimation, RAKE reception and M-PSK demodulation have been implemented in software on a Digital Signal Processor (DSP).

This chapter firstly presents the throughput analysis of the proposed wideband networking waveform. A brief description of the design partitioning for the effective implementation of the physical layer is presented, followed by the FPGA and DSP implementation results. Real-time experimental results are given and compared to the simulation results to demonstrate the effectiveness of the proposed technology.

7.1 Throughput Calculation

The mathematical framework for the calculation of achieved throughput of the proposed wideband waveform is now presented. The available RF bandwidth for the wideband waveform is 8 MHz. Using this available bandwidth B_{RF}, the maximum allowed sampling rate (f_s) (chips/sec) is calculated. Note that f_s is the rate at which the spreader block

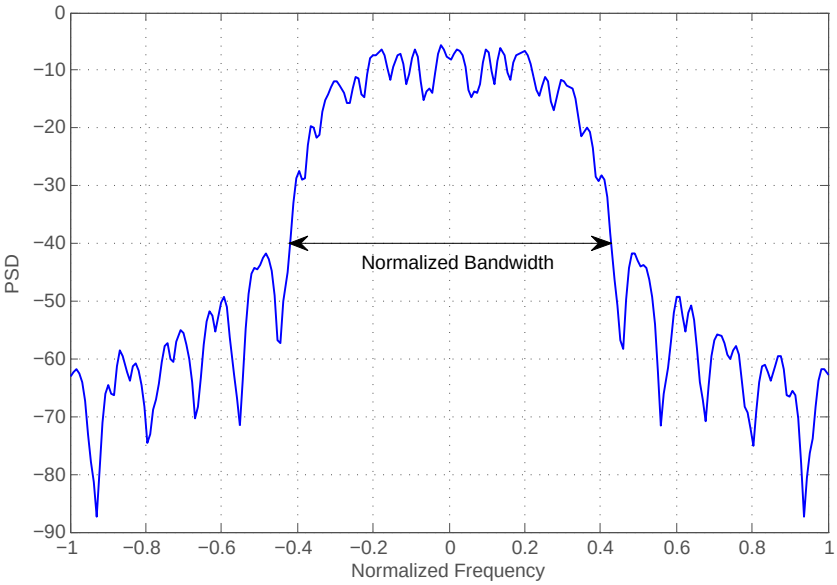

Figure 7.1: Method of finding the normalized bandwidth

generates the data. The burst detection block also takes the input data at the same rate. The sampling rate (f_s) is given as

$$f_s = \frac{2B_{RF}}{B_{norm}N_s} \tag{7.1}$$

where B_{RF} is the RF bandwidth, N_s is the upsampling factor and B_{norm} is the normalized bandwidth calculated from the normalized two-sided Power Spectral Density (PSD) of the transmitted data. Figure 7.1 shows the method of finding the normalized bandwidth (B_{norm}). Once f_s is found, the overall throughput for k^{th} user is given as

$$R_k = \frac{2B_{RF}I_{M,k}\log_2(M_k)r_{FEC}}{B_{norm}N_sG}.\frac{N_d}{N_0+N_d} \tag{7.2}$$

where M_k is the modulation index, $I_{M,k}$ is the multicode index, N_d is the number of data symbols/burst, N_0 is the number of symbols in training sequence r_{FEC} is the code rate of FEC and R_k is the throughput of k^{th} user.

As an example consider, $B_{RF} = 8$ MHz, $I_{M,k} = 1, M_k = 4, G = 8, r_{FEC} = 1, N_s = 4, N_d = 288, N_0 = 32$, and $B_{norm} = 0.4167$ (Figure 7.1). The throughput for k^{th} user using (7.2) comes out to be 1.08 Mbps.

7.2 Design Partitioning

The architectures of most SDRs consist of Field Programmable Gate Array (FPGA), General Purpose Processor (GPP), and Digital Signal Processor (DSP). Before waveform implementation, the design needs to be effectively partitioned so that the computationally extensive part normally uses FPGA and intelligent part of systems goes on processors (GPP or DSP). There are two types of design partitioning; (1) Coarse partitioning, in which the complete design is partitioned on block level, i.e. some blocks are implemented in hardware (HW) on FPGA and the others in software (SW) on DSP, and (2) Fine partitioning, in which HW/SW partitioning is applied within one block, so that a part of the block is implemented in HW on FPGA and the other part in SW on DSP. The fine partitioning is more beneficial than the coarse partitioning and results in efficient waveform implementation but it requires more development time and communication/interface overheads.

The proposed physical layer design of the wideband networking waveform is partitioned according to Figure 7.2. The FPGA device available for implementation is XC3SD3400A which belongs to the Spartan-3A DSP family of FPGAs. The DSP core available on the SDR platform is the high performance TMS320C64x+ core. This DSP core is incorporated on the TMS320DM6446 System-on-Chip (SoC) architecture. The FPGA and DSP are interfaced through External Memory Interface (EMIF). We have used coarse partitioning method, in which the blocks requiring high speed and computationally extensive processing e.g. synchronization, up/down conversion and high speed filtering are implemented on FPGA. On the other hand, the blocks requiring low speed and less extensive processing, e.g. modulation/demodulation, packet construction and narrowband channel estimation are implemented in software on DSP.

Keeping in view the coarse partitioning requirements, at the transmitter side, FEC encoding, low speed modulation and burst formation are implemented in software on DSP. The data spreading and digital up conversion, which include high speed filtering, are implemented on FPGA. At the receiver side, the data at high sampling rate is down converted

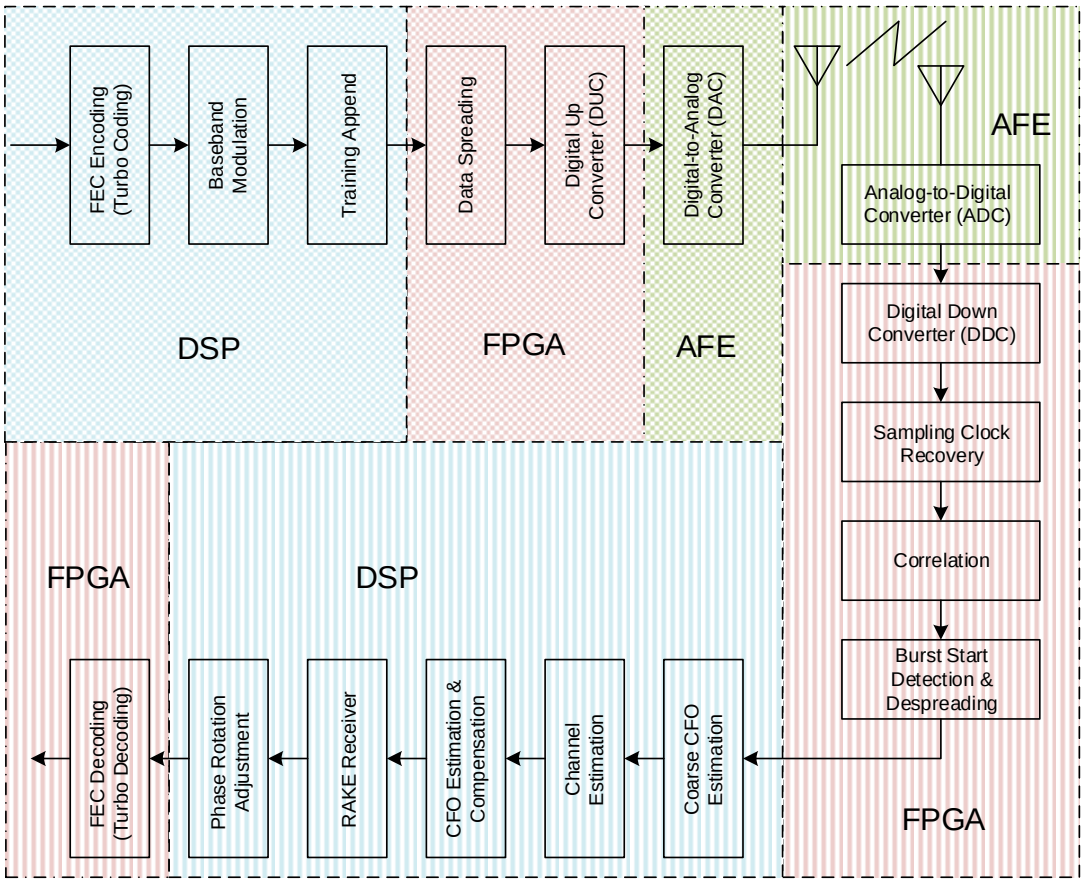

Figure 7.2: Design partitioning of the proposed physical layer design

using digital down converter which is implemented on FPGA. It is followed by sampling clock recovery and burst detection operations implemented on FPGA because of high speed and complex processing required in these stages. The despread data, which is at a relatively lower speed, goes to DSP. The subsequent stages including CFO estimation and compensation, channel estimation, RAKE receiver and demodulation are implemented on DSP. Since FEC decoding is computationally extensive operation, it is again implemented on FPGA.

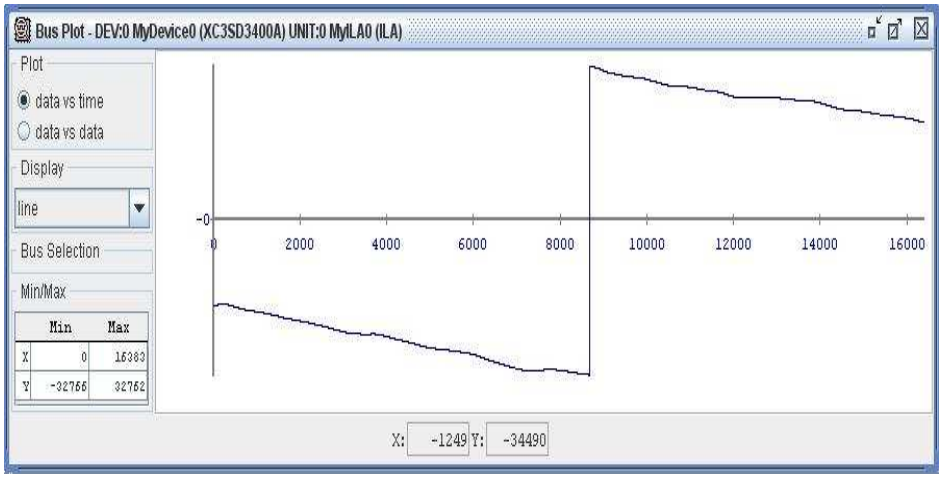

Figure 7.3: Performance of implemented SCO estimator on FPGA (captured from ChipScope)

7.3 Implementation Results

In this section, we firstly present the implementation results of the sampling clock recovery and burst detection stages which are implemented on FPGA and compare those results to that of the simulation.

Tracking performance of the proposed SCO estimator (for negative time varying offset) captured from ChipScope after implementation on FPGA is shown in Figure 7.3. The input data is taken at an $E_b/N_0 = -2$. It is obvious that the estimate has very low variance. The transition occurs from -32766 to 32762 (i.e. from -1.9999 to 1.996 for Q2.14 format), which is almost equal to that of simulated result (see chapter 3). This is further elaborated in Figure 7.4 which shows the comparison of SCO estimate obtained from MATLAB simulation and FPGA hardware. It can be seen that both the estimates are identical since they are overlapping each other. The bottom sub-figure shows the magnified SCO estimate of the last few samples from the first figure to have a clear visualization.

The detection performance of the proposed burst detection algorithm with precoding

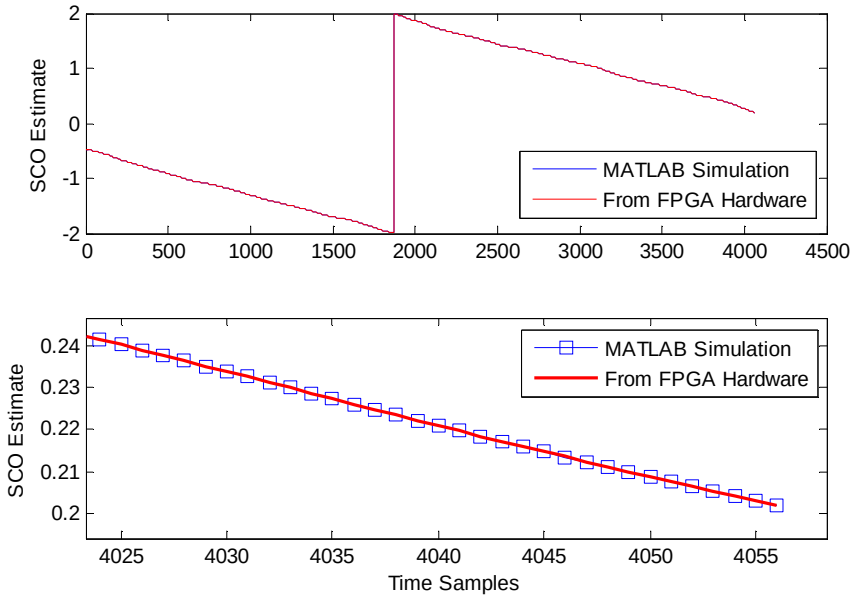

Figure 7.4: Comparison of MATLAB simulation and FPGA hardware results of the proposed SCO estimator

on FPGA hardware is investigated. For comparison of simulated proposed burst detection algorithm with the hardware implementation, the data from MATLAB at different SNRs has been dumped into FPGA and the probability of correct burst detection on hardware has been computed. The result is shown in Figure 7.5, which clearly indicates that the hardware results are identical to the simulation results.

Now, we present stage-by-stage analysis of the receiver by taking the results from the SDR platform. Figure 7.6 shows the method of extracting the outputs of specific stages which are implemented on FPGA or DSP. First, the output data from Digital Down Converter (DDC) is dumped into MATLAB for the receiver simulation. The data set is selected so that it includes the complete timing metric for burst detection. At the same time, the output of sampling clock recovery stage and burst detection stage are also dumped into MATLAB for comparison. The output data from burst detection stage is fed to the DSP through FIFOs. The SDR platform used for implementation contains high performance

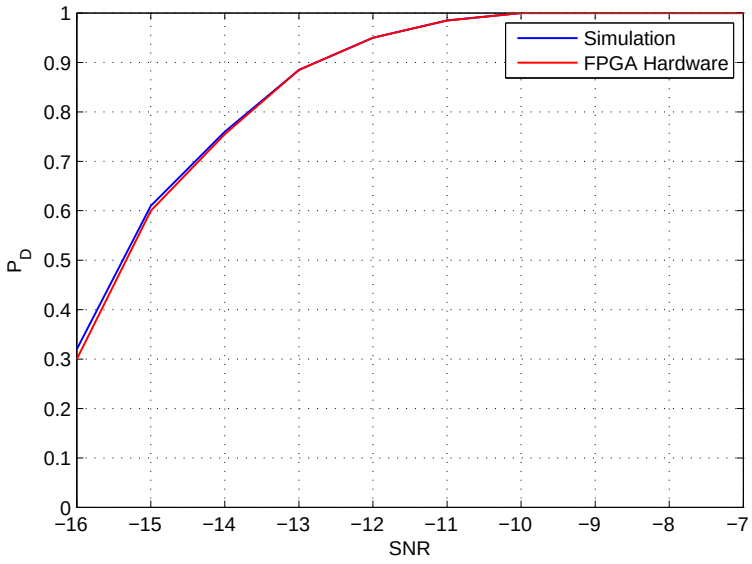

Figure 7.5: Comparison of correct detection probability for simulation and FPGA hardware results

TMS320C64x+ DSP core. This DSP core is incorporated on the TMS320DM6446 System-on-Chip (SoC) architecture. The same data is also dumped into MATLAB. The outputs of coarse frequency compensation, fine frequency compensation and RAKE receiver stages are dumped into MATLAB for comparison with the simulation results.

Figure 7.7 shows the comparison of simulation and FPGA result of the burst detection stage. It is shown through the timing metric and Threshold×Energy plots that the results from hardware are identical to the simulation results. Figures 7.8 to 7.12 show the error between the results of MATLAB simulation and SDR implementation for the output data taken from sampling clock recovery, burst detection, coarse frequency compensation, fine frequency compensation and RAKE receiver, respectively. For better visualization, the second half all the error data sets are shown in a zoomed view. It is clear that error in all the cases is within 10^{-3} range, which is normal for 16-bit fixed point implementation. Figure 7.13 show the constellation diagram of the received QPSK data prior to symbol

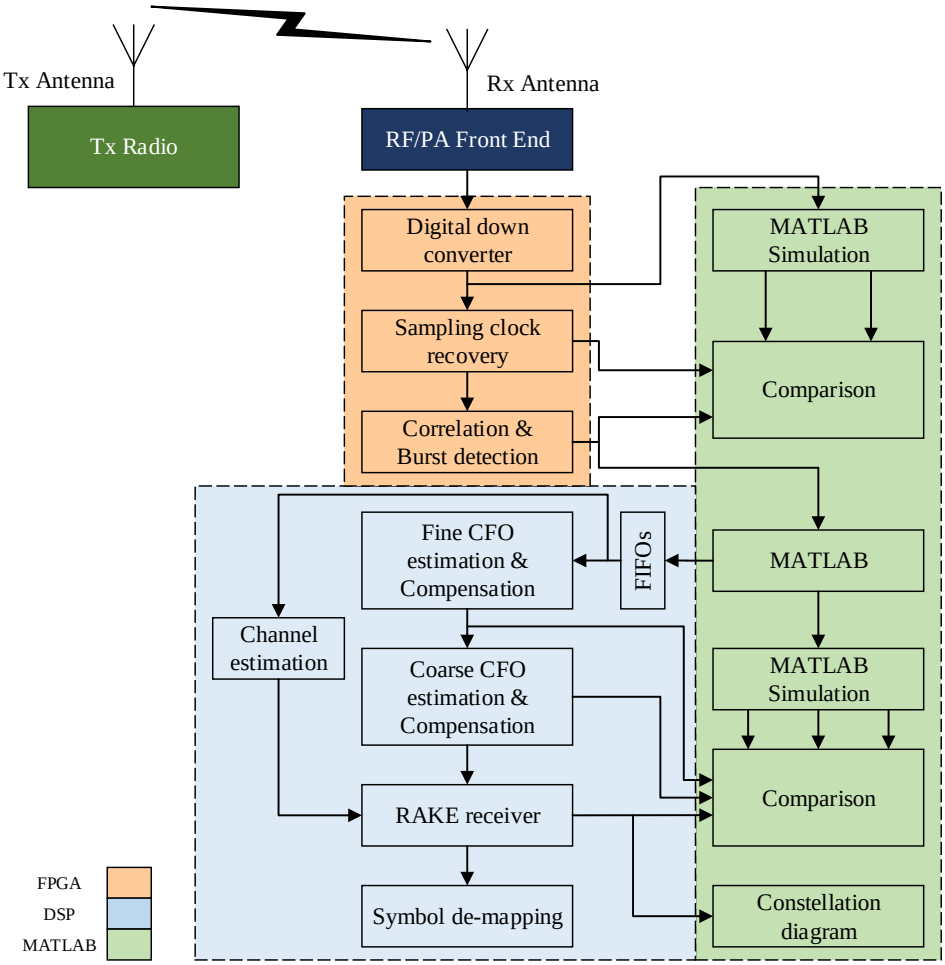

Figure 7.6: Method of extracting the outputs of receiver stages implemented on SDR platform

de-mapping.

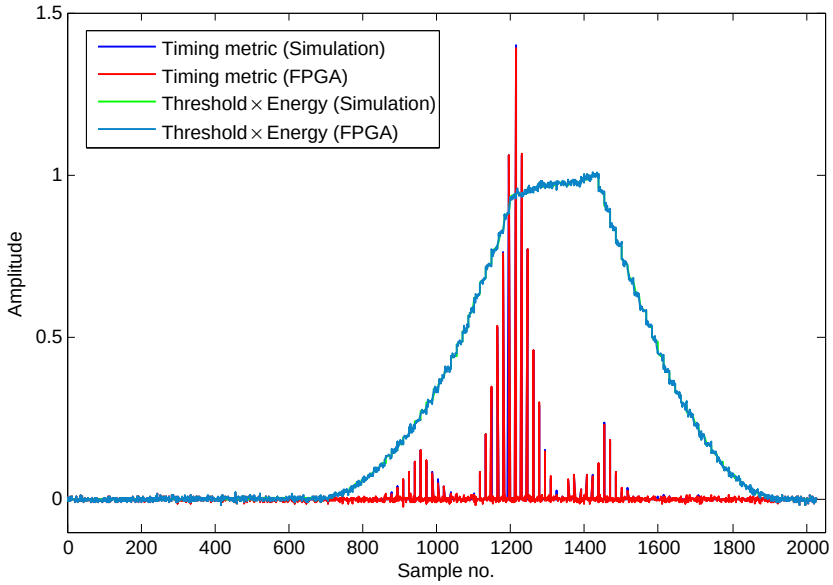

Figure 7.7: Comparison of the MATLAB simulation and SDR implementation results: Timing metric

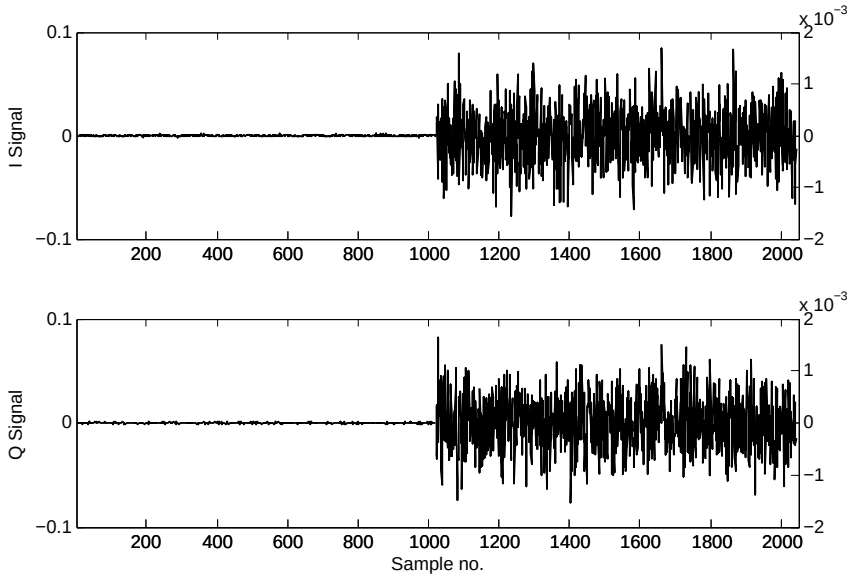

Figure 7.8: Error between MATLAB simulation and SDR implementation results: Output of SCR stage

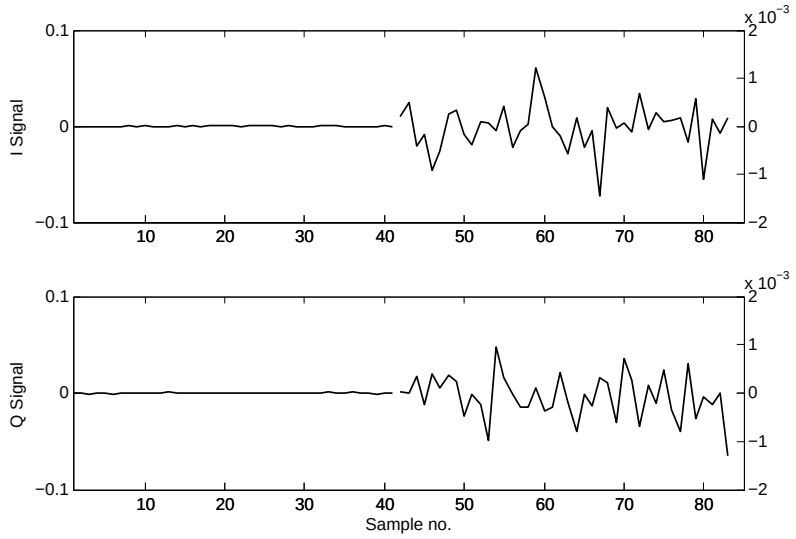

Figure 7.9: Error between MATLAB simulation and SDR implementation results: Output of burst detection stage

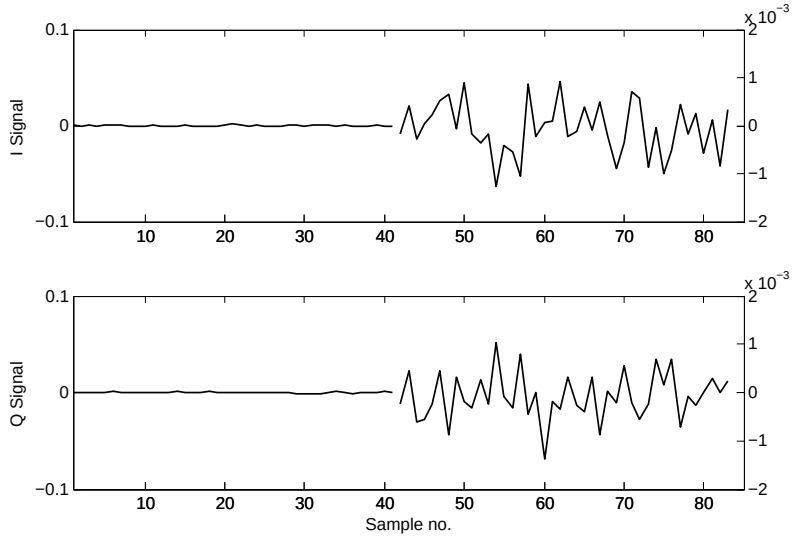

Figure 7.10: Error between MATLAB simulation and SDR implementation results: Output of coarse CFO compensation stage

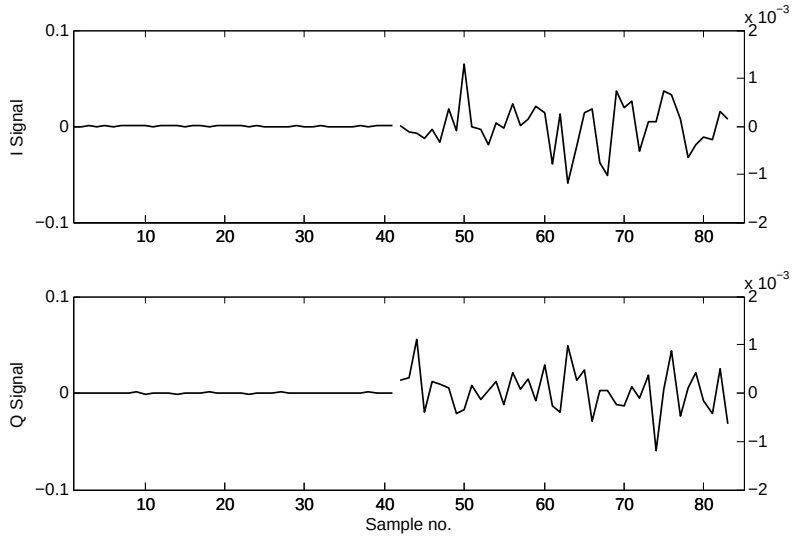

Figure 7.11: Error between MATLAB simulation and SDR implementation results: Output of fine CFO compensation stage

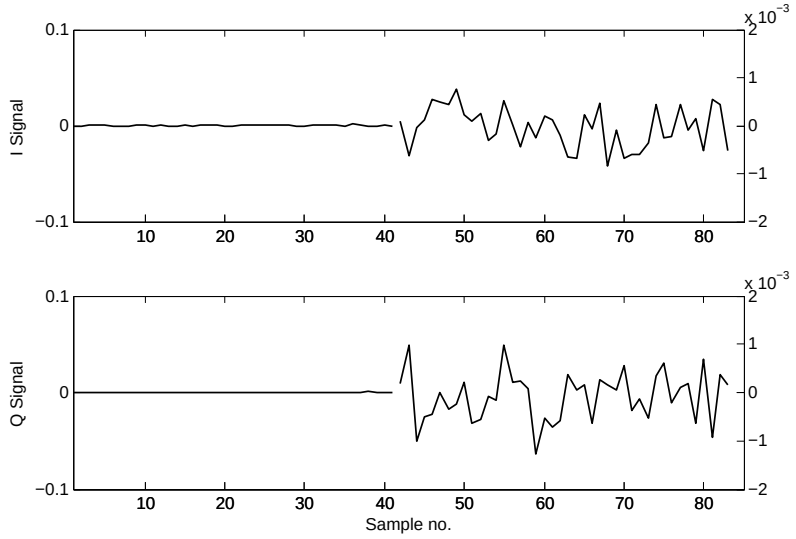

Figure 7.12: Error between MATLAB simulation and SDR implementation results: Output of RAKE receiver stage

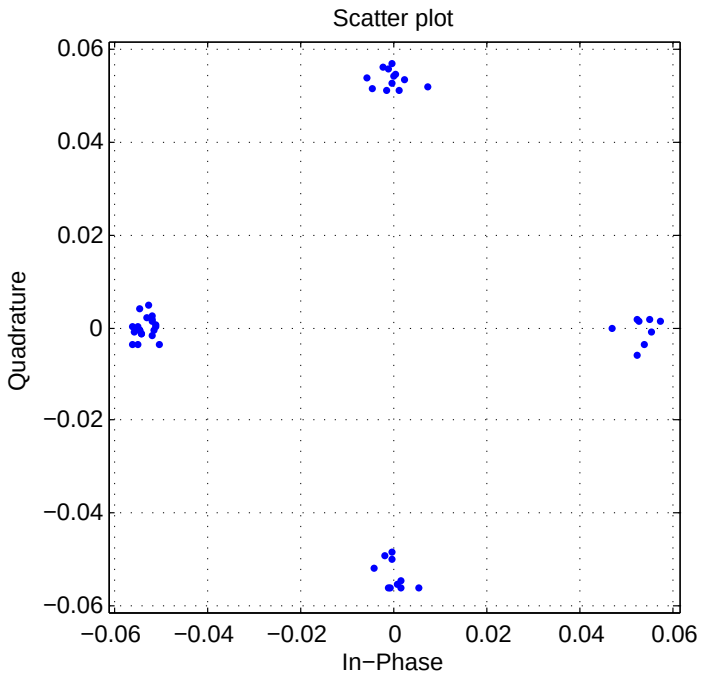

Figure 7.13: Constellation diagram of received QPSK data prior to symbol de-mapping

Chapter 8

Conclusion and Future Work

8.1 Conclusion

The major requirement of the future strategic and tactical systems is network based seamless communication. Such networks demand precise, accurate and reliable information to be delivered at the other end.

In this thesis, we have proposed a multi-mode high throughput wideband networking waveform for software defined radio. The proposed waveform has several different modes of operation and can achieve a maximum throughput of 17.2 Mbps. We have used Time Division Multiple Access (TDMA) and Code Division Multiple Access (CDMA) as multiple access schemes. Novel algorithms for the transmitter and receiver operations of the physical layer of the wideband waveform are proposed. They include training sequence design, sampling clock offset estimation and compensation, burst detection, and carrier frequency offset estimation and compensation. We have considered both the single and multiuser scenarios.

For Sampling clock recovery, we have proposed Modified Square Timing Recovery (MSTR) algorithm consisting of three stages including SCO estimation, S4RLSWAM-based post-filtering and cubic interpolation for SCO compensation. For burst detection, two algorithms have been proposed. The first algorithm is based on Time Domain Repetitive (TDR) training sequence and exploits the repetitive training sequence structure in the calculation of decision metric. The second algorithm is based on Differentially Modulated (DM) training sequence and exploits the precoding sequence in the calculation of decision metric. Both the operations (SCR and burst detection) are important as they directly

affect the adaptive time slot allocation algorithm. For CFO estimation, we have proposed two novel algorithms. In the first algorithm, modified FFT and quadratic interpolation are used to estimate CFO efficiently. The second algorithm consists of two stages namely Maximum Likelihood Data Aided (MLDA) estimation and Sample-by-Sample Residual Offset (S2RO) estimation.

To reduce the packet re-transmissions overhead and achieving better throughput, a novel link adaptation technique based on fuzzy inference system by considering Quality of Service and throughput requirement of user/application has been proposed. The constrained optimization problem is solved by changing the modulation technique and the number of multicodes assigned to each user. The performance of the proposed algorithms is evaluated by using Stanford University Interim (SUI) channel models. The performance improvement of our proposed algorithms is demonstrated by comparing them with set of known existing methods. Simulation results showed that the proposed algorithms are superior in terms of performance, throughput and ease of implementation. To demonstrate the implementation affinity of the proposed technology, the proposed algorithms are implemented using Field Programmable Gate Array (FPGA) and Digital Signal Processor (DSP) on SDR platform. Actual results from hardware are compared and verified with the simulation results.

8.2 Contributions

The major contributions of this thesis are

1. It proposed a complete physical layer design for adaptive high data rate CDMA-based wideband waveform for SDR tactical networks, considering almost all the synchronization problems and channel impairments.

2. The proposed waveform design supports several modes of operation and can achieve a maximum throughput of 17.2 Mbps.

3. As the first part of timing synchronization, a new sampling clock recovery algorithm

namely modified square timing recovery (MSTR) is proposed. A novel usage of S4RLSWAM filter for the post-filtering of estimates is also proposed. The algorithm is further modified to be successfully applied to the multiuser CDMA environment.

4. For the second part of timing synchrnization, two new data-aided burst detection techniques based on Time Domain Repetitive (TDR) and Differentially Modulated (DM) training sequences are proposed.

5. For frequency synchronization, two novel algorithms are proposed. The first algorithm is based on modified FFT and biquadratic Lagrange interpolation. The second algorithm consists of two stages; coarse estimation stage based on Maximum Likelihood Data Aided (MLDA) estimation, and fine estimation stage based on sample-by-sample residual offset estimation.

6. A dynamic link adaptation algorithm using fuzzy rule based system is proposed. The proposed technique changes the waveform parameters at the physical layer based on varying channel conditions to avoid packet re-transmissions overhead.

7. Performance of all the proposed algorithms is compared with a set of known algorithms. It is found that the proposed algorithms are superior as compared to the existing algorithms. The design is effectively partitioned for FPGA and DSP implementation on SDR platform. The actual results are compared and verified against the simulation values.

8.3 Future Recommendations

This thesis presented the complete design of the physical layer of CDMA based wideband networking waveform by proposing efficient algorithms for the time/frequency synchronization and link adaptation. The proposed algorithms are implemented on SDR platform that includes FPGA, DSP and GPP. Efficient implementation of the proposed algorithms require

in-depth analysis of design partitioning which can be very interesting area for researchers in the field of embedded systems.

To achieve high throughput in a given bandwidth, source coding is used for data compression in wireless communication systems. Efficient source coding schemes need to be investigated which are computationally less extensive and can provide a significant throughput enhancement for voice, data and video communications.

The use of both the CDMA and TDMA in a wideband waveform is proposed in this thesis. This concept can further be extended by using other multiple access schemes at the physical layer of the wideband waveform. The following schemes are recommended for future.

Multicarrier CDMA

Multicarrier code division multiple access (MC-CDMA) has been evolved as an emerging multiple access scheme since the last decade. It is a combination of DS-CDMA and OFDM. Due to this reason it sometimes referred to as OFDM-CDMA. It is one of the emerging candidates for the next generation communication technologies [108]. In this scheme, data symbol of each user is transmitted simultaneously on narrowband sub-channels which are then multiplied by the user specific spreading sequence.

MC-CDMA, like CDMA, provides multiuser support, high throughput and anti-jamming ability. Additionally, it provides immunity towards Intersymbol Interference (ISI) by reducing the symbol rate. In very high chip rate systems, this ISI reduction is very significant. Though MC-CDMA is robust against the interference caused by the multipath fading channels, it is sensitive to the factors that destroy the orthogonality between the carriers. In this regard, CFO appears very destructive and needs to be estimated with very high precision.

Hybrid Direct Sequence-Time Hopped-CDMA

The hybrid Direct Sequence-Time Hopped-CDMA (DS-TH-CDMA) is a novel idea to be used in the wideband waveform design of SDR. This technique combines the advantages

of both DS- and TH-CDMA systems. The transmission is in the form of frames which consist of time slots. The user transmits its data in one of the total N_T time slots per frame determined by the code assigned to that user. In this way, instead of using parts of spectrum all the time, TH-CDMA uses whole wideband spectrum for short time periods. In multiple user scenarios, each of the N_T time slots is occupied by different user. Each user has its different code which decides the slot number in which that corresponding user transmits its data.

Since hybrid DS-TH CDMA is completely a new idea, so it has never been used in the wideband waveform design in SDRs. In this technique, the user transmits the spread data (at chip rate) in its time slot after direct sequence spreading instead of transmitting the actual data. In this way, anti-jamming capability of the resulting system is doubly increased. Furthermore, the Multiple Access Interference (MAI), which is the most severe problem in conventional CDMA, is mitigated to a large extent.

References

[1] A. C. Tribble, "The software defined radio: Fact and fiction," in *Proceedings of IEEE Radio and Wireless Symposium*, 2008, pp. 5–8.

[2] P. B. Kenington, *RF and baseband technologies for software defined radio.* Artech House, London, 2005.

[3] D. Scaparoth, "Cognitive software defined radio," Tech. Rep., 2005.

[4] D. Lau, J. Blackburn, and J. A. Seely, "The use of hardware acceleration in SDR waveforms."

[5] J. Rohde and T. S. Toftegaard, "Adaptive cognitive radio technology for low power wireless personal area network devices," *Wireless Personal Communications*, vol. 58, no. 1, pp. 111–123, 2011.

[6] S. Han, J.-H. Park, H.-H. Shin, and B.-S. Kim, "Performance enhancements in TDMA-based tactical wireless networks," in *Proceedings of Vehicular Technology Conference*, 2012, pp. 1–5.

[7] M. Nakagawa, "Consumer communications based on spread spectrum technologies," in *Proceedings of IEEE 3rd International Symposium on Spread Spectrum Techniques and Applications*, 1994, pp. 138–145.

[8] "Link adaptation," http://en.wikipedia.org/wiki/Link_adaptation, accessed: 2015-01-25.

[9] "Software defined radio (SDR)," http://www.ti.com/solution/software-defined-radio-sdr-diagram, accessed: 2015-01-27.

[10] J. E. Kleider, S. Gifford, K. Nolan, D. Hughes, and S. Chuprun, "Demonstrating robust high data rate capability on a software defined radio using anti-jam wideband OFDM waveform," in *Proceedings of IEEE Military Communications Conference*, 2005, pp. 1648–1653.

[11] J. E. Kleider, S. Gifford, G. Maalouli, S. Chuprun, and B. Sadler, "Synchronization for RF carrier frequency hopped OFDM: Analysis and simulation," in *Proceedings of IEEE Military Communications Conference*, vol. 2, 2003, pp. 1237–1242.

[12] J. E. Kleider and S. Gifford, "Synchronization for broadband OFDM mobile ad hoc networking: simulation and implementation," in *Proceedings of International Conference on Acoustics, Speech and Signal Processing*, vol. 4, 2002, pp. 3756–3759.

[13] J. E. Kleider, S. Gifford, G. Maalouli, and S. Chuprun, "Preamble and embedded synchronization for RF carrier frequency hopped OFDM," *IEEE Journal on Selected Areas in Communications*, vol. 23, no. 5, pp. 920–931, 2005.

[14] "Software defined networking radio," www.aselsan.com.tr, ASELSAN, Tech. Rep.

[15] "PRC-9661 Radio," http://defenceproducts.ssm.gov.tr/Pages/ProductDetails.aspx?pId=69, accessed: 2012-05-28.

[16] "Multiband networking radio," http://rf.harris.com, Harris Corporation, Tech. Rep.

[17] C. G. Martin, "Progress in tactical wideband waveform development," http://www.battle-technology.com/this_issue09.asp, accessed: 2015-01-28.

[18] "Thales wideband networking radio (WNR)," http://www.thalescomminc.com, Thales Communications, Inc., Tech. Rep.

[19] "Wideband networking waveform OFDM PHY," http://www.spectrumsignal.com, Spectrum signal processing, Tech. Rep.

[20] M. Zeeshan and S. A. Khan, "Robust sampling clock recovery algorithm for wideband networking waveform of SDR," *International Journal of Communication Networks and Information Security*, vol. 5, no. 1, pp. 10–18, 2013.

[21] E. Grass, K. Tittelbach-Helmrich, U. Jagdhold, A. Troya, and e. a. G. Lippert, "On the Single-Chip implementation of a hiperlan/2 and IEEE 802.11a capable modem," *IEEE Personal Communications*, vol. 8, no. 6, pp. 48–57, 2001.

[22] M. Zeeshan and S. A. Khan, "A robust carrier frequency offset estimation algorithm in burst mode multicarrier CDMA based ad hoc networks," *International Journal of Communication Networks and Information Security*, vol. 4, no. 3, pp. 174–181, 2012.

[23] M. Zeeshan, S. A. Khan, and I. Haq, "A two stage algorithm for carrier frequency offset recovery with DSP implementation on SDR platform," *IEICE Transactions on Communications*, vol. E97-B, no. 11, pp. 2449–2458, 2014.

[24] C. Lin, G. P. Pollini, L. Ozarow, and R. D. Gitlin, "Performance of multicode CDMA wireless personal communication networks," in *Proceedings of IEEE 45th Vehicular Technology Conference*, vol. 2, 1995, pp. 907–911.

[25] B. Ai, Y. Shen, Z. D. Zhong, and B. H. Zhang, "Enhanced sampling clock offset correction based on time domain estimation scheme," *IEEE Transactions on Consumer Electronics*, vol. 57, no. 2, pp. 696–704, 2011.

[26] A. Montazeri and K. Kiasaleh, "Design and performance analysis of a low complexity digital clock recovery algorithm for software dened radio applications," *IEEE Transactions on Consumer Electronics*, vol. 56, no. 3, pp. 1258–1263, 2010.

[27] M. Oerder and H. Meyr, "Digital lter and square timing recovery," *IEEE Transactions on Communications*, vol. 36, no. 5, pp. 605–612, 1988.

[28] W.-P. Zhu, Y. Yan, M. O. Ahmed, , and M. N. S. Swamy, "Feedforward symbol timing recovery technique using two samples per symbol," *IEEE Transactions on Circuits and Systems-I*, vol. 52, no. 11, pp. 2490–2500, 2005.

[29] C.-F. Li, Y.-S. Chu, J.-S. Ho, and W.-H. Sheen, "Cell search in WCDMA under large-frequency and clock errors: Algorithm to hardware implementation," *IEEE Transactions on Circuits and Systems-I*, vol. 55, no. 2, pp. 659–671, 2008.

[30] D. Wang and A. Q. Hu, "A combined residual frequency and sampling clock offset estimation for OFDM systems," in *Proceedings of IEEE Asia Pacific Conference on Circuits and Systems*, 2006, pp. 1184–1187.

[31] W. D. Xiang and T. Pratt, "A simple cascade carrier frequency and sampling clock offsets estimation method for OFDM systems," in *Proceedings of 1st IEEE Consumer Communications and Networking Conference*, 2004, pp. 718–720.

[32] S. Y. Liu and J. W. Chong, "A study of joint tracking algorithms of carrier frequency offset and sampling clock offset for OFDM-based WLANs," in *Proceedings of IEEE International Conference on Communications, Circuits and Systems and West Sino Expositions*, vol. 1, 2002, pp. 109–113.

[33] I. Trigui, S. Affes, A. Stephenne, , and M. Siala, "Ml-based joint estimation of frequency and sampling clock offsets for OFDM systems," in *Proceedings of IEEE 9th Workshop on Signal Processing Advances in Wireless Communications*, 2008, pp. 346–350.

[34] L. Mailaender, "Detection statistics for a packet-based cdma system," in *Proceedings of IEEE 49th Vehicular Technology Conference*, 1999, pp. 526–530.

[35] D. Yan and P. Ho, "On-off keying assisted acquisition scheme for burst mode ds/ss packet radio," in *Proceedings of IEEE 44th Vehicular Technology Conference*, 1994, pp. 582–586.

[36] ——, "Acquisition using differentially encoded barker sequence in ds/ss packet radio," in *Proceedings of IEEE International Conference on Communications*, 1995, pp. 1647–1651.

[37] G. J. R. Povey, "Spread spectrum pn code acquisition using hybrid correlator architectures," *Wireless Personal Communications*, vol. 8, no. 2, pp. 151–164, 1998.

[38] Z. Zhao, Z. Sun, and F. Mei, "A threshold detection method of DSSS signal based on stft," in *Proceedings of IEEE International Symposium on Microwave, Antenna, Propagation and EMC Technologies for Wireless Communications*, vol. 2, 2005, pp. 879–882.

[39] L. Chang, F. Wang, and Z. Wang, "Detection of DSSS signal in non-cooperative communications," in *Proceedings of International Conference on Communication Technology*, 2006, pp. 1–4.

[40] Z. Deng, L. Shen, N. Bao, B. Su, J. Lin, and D. Wang, "Autocorrelation based detection of DSSS signal for cognitive radio system," in *Proceedings of International Conference on Wireless Communications and Signal Processing*, 2011, pp. 1–5.

[41] S. Nagaraj, S. Khan, C. Schlegel, and M. Burnashev, "On preamble detection in packet-based wireless networks," in *Proceedings of IEEE Ninth International Symposium on Spread Spectrum Techniques and Applications*, 2006, pp. 476–480.

[42] H.-S. Oh, D.-S. Han, and K.-H. Park, "Adaptive double-dwell PN code acquisition in direct-sequence spread-spectrum systems," in *Proceedings of the 21st Century Military Communications Conference*, 2000, pp. 139–143.

[43] S. Yeom, Y. Jung, and S. Lee, "An adaptive threshold technique for fast PN code acquisition in DSSS systems," *IEEE Transactions on Vehicular Technology*, vol. 60, no. 6, pp. 2870–2875, 2011.

[44] K. Li and H. Liu, "Joint channel and carrier offset estimation in CDMA communications," *IEEE Transactions on Signal Processing*, vol. 47, no. 7, pp. 1811–1822, 1999.

[45] H. Fu and K. Abed-Meraim, "Joint channel and frequency offset estimation in CDMA systems," in *Proceedings of the 11th IEEE International Symposium on Personal, Indoor and Mobile Radio Communications*, vol. 2, 2000, pp. 1126–1130.

[46] S. Attallah and H. Fu, "Joint channel and carrier offset estimation in multiuser CDMA systems," *IEEE Communication Letters*, vol. 6, no. 10, pp. 428–430, 2002.

[47] A. D'Amico and M. Morelli, "Frequency estimation and timing acquisition in the uplink of a DS-CDMA system," *IEEE Transactions on Communications*, vol. 52, no. 10, pp. 1809–1819, 2004.

[48] L. Thiagarajan, S. Attallah, and H. Fu, "Non-data-aided synchronization and channel estimation for asynchronous CDMA uplink," in *Proceedings of the IEEE International Conference on Communications*, 2007, pp. 2906–2911.

[49] S. Tao, L. Xu-Wen, and C. Xiao-Ting, "Decision-directed estimation of carrier frequency and phase for burst PSK transmission," in *Proceedings of the 5th International*

Conference on Wireless Communications, Networking and Mobile Computing, 2009, pp. 1–4.

[50] H. Poveda, E. Grivel, and G. Ferre, "Kalman vs H∞ filter in terms of convergence and accuracy, application to CFO estimation," in *Proceedings of the 20th European Signal Processing Conference*, 2012, pp. 121–125.

[51] L. Thiagarajan, S. Attallah, and Y. Liang, "Two stage frequency synchronization of uplink MC-CDMA system," in *Proceedings of the Wireless Communications and Networking Conference*, 2007, pp. 2443–2447.

[52] M. Moh, A. F. Gamal, and I. I. Ibrahim, "A two-stage frequency-offset estimation scheme for OFDMA system," in *Proceedings of the 3rd International Conference on New Technologies, Mobility and Security*, 2009, pp. 1–6.

[53] H. Qingwen, Z. Peng, and Z. Youfang, "A large frequency offset estimation algorithm for IEEE 802.11a system," in *Proceedings of the International Conference on Communications and Mobile Computing*, 2009, pp. 316–320.

[54] E. Casini, R. D. Gaudenzi, and A. Ginesi, "DVB-S2 modem algorithms design and performance over typical satellite channels," *International Journal of Satellite Communications and Networking*, vol. 22, no. 1, pp. 281–318, 2004.

[55] U. Mengali and A. N. D'Andrea, *Synchronization Techniques for Digital Receivers (Applications of Communications Theory)*. Plenum Press, New York, 1997.

[56] M. Luise and R. Reggiannini, "Carrier frequency recovery in all-digital modems for burst-mode transmissions," *IEEE Transactions on Communications*, vol. 43, no. 2/3/4, pp. 1169–1178, 1995.

[57] L. G. Oh and J. T. Kim, "A simple and robust carrier frequency recovery scheme for DVB-S2 systems," in *Proceedings of the 14th International Symposium on Consumer Electronics*, 2010, pp. 1–4.

[58] T. M. Schmidl and D. C. Cox, "Robust timing and frequency synchronization for OFDM," *IEEE Transactions on Communications*, vol. 45, no. 12, pp. 1613–1621, 1997.

[59] U. Mengali and M. Morelli, "An improved frequency offset estimator for OFDM applications," *IEEE Communications Letters*, vol. 3, no. 3, pp. 75–77, 1999.

[60] J. G. Oh, S. H. Son, and J. T. Kim, "Efficient carrier frequency offset estimation algorithm for DVB-RCS systems," in *Proceedings of the 13th International Symposium on Consumer Electronics*, 2009, pp. 342–345.

[61] A. Barbieri and G. Colavolpe, "On pilot-symbol-assisted carrier synchronization for DVB-S2 systems," *IEEE Transactions on Broadcasting*, vol. 53, no. 3, pp. 685–692, 2007.

[62] D. Zhang, L. Yu, P. Zhou, Q. Huang, and W. Chen, "A high performance frequency offset estimation method for OFDM," in *Proceedings of the 3rd International Conference on Intelligent System Design and Engineering Applications*, 2013, pp. 73–76.

[63] "Physical layer aspects of UTRA high speed downlink packet access," 3rd Generation Partnership Project, Technical Report 3G TR25.858, Tech. Rep., 2002.

[64] K. L. Baum, T. A. Kostas, P. J. Sartori, and B. K. Classon, "Performance characteristics of cellular systems with different link adaptation strategies," *IEEE Transactions on Vehicular Technology*, vol. 52, no. 6, pp. 1497–1507, 2003.

[65] B. Lakshmi and B. S. K. Reddy, "Adaptive modulation and coding for mobile-wimax using SDR in GNU radio," in *Proceedings of International Conference on Circuits, Systems, Communication and Information Technology Applications (CSCITA)*, 2014, pp. 173–178.

[66] M. Miyashita, M. Mikami, and H. Yoshino, "An MMI based adaptive modulation and coding for cooperative MIMO-OFDM in frequency selective channels," in *Proceedings of International Symposium on Antennas and Propagation (ISAP)*, 2012, pp. 738–741.

[67] C. Sunu and E. Aktas, "Adaptive modulation and coding (AMC) in cooperative communication channels," in *Proceedings of 22nd Signal Processing and Communications Applications Conference (SIU)*, 2014, pp. 1571–1574.

[68] M. Taki, M. Rezaee, and M. Guillaud, "Adaptive modulation and coding for interference alignment with imperfect CSIT," *IEEE Transactions on Wireless Communications*, vol. 13, no. 9, pp. 5264–5273, 2014.

[69] H. Chen, H. C. B. Chan, C.-K. Chan, and V. C. M. Leung, "Qos-based cross-layer scheduling for wireless multimedia transmissions with adaptive modulation and coding," *IEEE Transactions on Communications*, vol. 61, no. 11, pp. 4526–4538, 2013.

[70] J. Meng and E.-H. Yang, "Constellation and rate selection in adaptive modulation and coding based on finite blocklength analysis," in *Proceedings of IEEE Wireless Communications and Networking Conference (WCNC)*, 2013, pp. 4064–4070.

[71] S. Abedi, "Efficient radio resource management for wireless multimedia communications: A multidimensional QoS-based packet scheduler," *IEEE Transactions on Wireless Communications*, vol. 4, no. 6, pp. 2811–2822, 2005.

[72] H. Holma and A. Toskala, *WCDMA for UMTS Radio Access for Third Generation Mobile Communications*. John Wiley and Sons, 2002.

[73] H. D. Schotten, H. Elders-Boll, and A. Busboom, "Adaptive multi-rate multi-code CDMA systems," in *Proceedings of 48th IEEE Vehicular Technology Conference*, 1998, pp. 782–785.

[74] R. Kwan, P. Chong, and M. Rinne, "Analysis of the adaptive modulation and coding algorithm with the multicode transmission," in *Proceedings of 56th IEEE Vehicular Technology Conference*, 2002, pp. 2007–2011.

[75] G. Garg, A. Nakajima, and F. Adachi, "Throughput comparison of MC-CDMA and DS-CDMA with frequency-domain equalization and adaptive modulation and coding," in *Proceedings of 61st IEEE Vehicular Technology Conference*, 2005, pp. 1575–1579.

[76] R. Kwan and C. Leung, "Adaptive modulation and coding with multicodes over nakagami fading channels," in *Proceedings of IEEE Wireless Communications and Networking Conference*, 2005, pp. 927–932.

[77] S. Ulukus, E. Biglieri, and M. Z. Win, "Optimum modulation and multicode formats in CDMA systems with multiuser receivers," in *Proceedings of IEEE 20th Annual Joint Conference of the IEEE Computer and Communications Societies*, 2001, pp. 395–402.

[78] R. Kwan and C. Leung, "Downlink scheduling schemes for CDMA networks with adaptive modulation and coding and multicodes," *IEEE Transactions on Wireless Communications*, vol. 6, no. 10, pp. 3668–3677, 2007.

[79] K. Fazel and S. Kaiser, *Multicarrier and Spread Spectrum Systems.* John Wiley and Sons, 2003.

[80] T. Rappaport, *Wireless Communications: Principles and Practice.* Englewood Cliffs, NJ: Prentice-Hall, 1996.

[81] M. B. Malik, "State-space recursive least squares with adaptive memory," *Signal Processing Journal*, vol. 86, pp. 1365–1374, 2006.

[82] D. S. Baum, "Channel models for fixed wireless applications," IEEE 802.16 Broadband Wireless Access Working Group, Tech. Rep., 2001.

[83] U. Mengali and M. Morelli, "Data-aided frequency estimation for burst digital transmission," *IEEE Transactions on Communications*, vol. 45, no. 1, pp. 23–25, 1997.

[84] A. Goldsmith, *Wireless Communications.* Cambridge University Press, UK, 2005.

[85] M. Zeeshan, S. A. Khan, and Z. Mehtab, "Data aided algorithm for burst detection in wideband networking waveform with FPGA implementation on SDR platform," in *Proceedings of 11th Annual High-capacity Optical Networks and Emerging/Enabling Technologies*, vol. 1, 2014, pp. 154–158.

[86] M. Zeeshan and S. A. Khan, "A novel algorithm for burst detection in wideband networking waveform of software defined radio," *IEICE Transactions on Fundamentals of Electronics, Communications and Computer Sciences*, vol. E98-A, no. 6, pp. 1225–1233, 2015.

[87] U. Lambrette, M. Speth, and H. Meyr, "OFDM burst frequency synchronization by single carrier training data," *IEEE Communications Letters*, vol. 1, no. 1, pp. 46–48, 1997.

[88] M. J. E. Golay, "Complementary series," *IRE Transactions on Information Theory*, vol. IT-7, pp. 82–87, 1961.

[89] M. B. Mollah and M. R. Islam, "Comparative analysis of gold codes with PN codes using correlation property in CDMA technology," in *Proceedings of International Conference on Computer Communication and Informatics*, 2012, pp. 1–6.

[90] J. Lindholm, "An analysis of the pseudo-randomness properties of subsequences of long m-sequences," *IEEE Transactions on Information Theory*, vol. 14, no. 4, pp. 569–576, 1968.

[91] H. Minn, V. K. Bhargava, and K. B. Letaief, "A robust timing and frequency synchronization for OFDM systems," *IEEE Transactions on Wireless Communications*, vol. 2, no. 4, pp. 822–839, 2003.

[92] S. M. Kay, *Fundamentals of Statistical Signal Processing: Detection Theory*. Prentice hall, 1998.

[93] Y. J. Guo, *Advances in Mobile Radio Access Networks*. Artech House Mobile Communication Series, 2004.

[94] P. Ciblat and L. Vandenorpe, "Blind carrier frequency offset estimation for noncircular constellation-based transmissions," *IEEE Transactions on Signal Processing*, vol. 51, no. 5, pp. 1378–1389, 2003.

[95] R. L. Burden and J. D. Faires, *Numerical Analysis*. Brooks/cole, Cengage learning, 2010.

[96] F. J. Harris, "On the use of windows for harmonic analysis with the discrete fourier transform," *Proceedings of the IEEE*, vol. 66, no. 1, pp. 51–83, 1978.

[97] Ramirez and W. Robert, *The FFT, Fundamentals and concepts*. Prentice-hall, New Jersey, 1985.

[98] R. W. S. A. V. Oppenheim, *Discrete-time Signal Processing*. Pearson Education, 2010.

[99] F. Classen, H. Meyr, and P. Sehier, "Maximum likelihood open loop carrier synchronizer for digital radio," in *Proceedings of the IEEE International Conference on Communications*, 1993, pp. 493–497.

[100] F. Gardner, "Frequency detectors for digital demodulators via maximum likelihood derivation," ESA-ESTEC Final Report: Part 2, Tech. Rep., 1990.

[101] Y. Li, "Single frequency estimation based on modified window scaling constant with maximum deviation criterion," in *Proceedings of the IEEE Region 10 Conference*, 2010, pp. 712–715.

[102] A. J. Viterbi and A. M. Viterbi, "Nonlinear estimation of PSK modulated carrier phase with application to burst digital transmission," *IEEE Transactions on Information Theory*, vol. 29, no. 4, pp. 543–551, 1983.

[103] M. Zeeshan and S. A. Khan, "A novel algorithm for link adaptation using fuzzy rule based system for wideband networking waveform of SDR," *AEU - International Journal of Electronics and Communications*, vol. 69, no. 9, pp. 1366–1373, 2015.

[104] H. Xu and H. Zheng, "The simple SNR estimation algorithms for MPSK signals," in *Proc. of 7th International Conference on Signal Processing*, 2004, pp. 1781–1785.

[105] L. Jatunov and V. K. Madisetti, "Computationally-efficient SNR estimation for bandlimited wideband CDMA systems," *IEEE Transactions on Wireless Communications*, vol. 5, no. 12, pp. 3480–3491, 2006.

[106] M. Alvarez-Diaz, R. Lopez-Valcarce, and C. Mosquera, "SNR estimation for multi-level constellations using higher-order moments," *IEEE Transactions on Signal Processing*, vol. 58, no. 3, pp. 1515–1526, 2010.

[107] C. C. Lee, "Fuzzy logic in control systems: Fuzzy logic controller - part I," *IEEE Transactions on Systems, Man and Cybernetics*, vol. 20, no. 2, pp. 404–418, 1990.

[108] P. Fan, "Multiple access technologies for next generation mobile communications," in *Proc. of 6th International Conference on ITS Telecommunications*, 2006, pp. 10–11.

Appendix A

Stanford University Interim Channel Models

Stanford University Interim (SUI) channels are modelled to represent three different terrain types and various values of delay spreadl, Doppler spread, and LOS/NLOS conditions. The summary of these six channel models is given in Table A.1. The detailed specifications of all SUI channel models is given in tables Tables A.2 to A.7. In these specifications, K-factor is the ratio of LOS component to NLOS components. For NLOS case, K-factor is zero.

Table A.1: Summary of SUI channel terrain types

	SUI-1	**SUI-2**	**SUI-3**	**SUI-4**	**SUI-5**	**SUI-6**
Terrain category	C	C	B	B	A	A
Terrain type	Flat	Flat	Hilly	Flat	Hilly	Hilly
Tree density	Light	Light	Light	Moderate to heavy	Moderate to heavy	Moderate to heavy
Line of sight	Strong	Strong	Weak	Weak	Weak	Weak
Delay spread	Low	Low	Low	Moderate	High	High
Path loss	Low	Low	Intermediate	Intermediate	High	High
Doppler spread	Low	Low	Low	High	Low	High

Table A.2: SUI-1 channel model specifications

	Tap 1	**Tap 2**	**Tap 3**
Delay (μs)	0.0	0.4	0.9
Power (dB)	0	-15	-20
K-factor	4	0	0
Doppler (Hz)	0.40	0.30	0.50

Table A.3: SUI-2 channel model specifications

	Tap 1	**Tap 2**	**Tap 3**
Delay (μs)	0.0	0.4	1.1
Power (dB)	0	-12	-15
K-factor	2	0	0
Doppler (Hz)	0.20	0.15	0.25

Table A.4: SUI-3 channel model specifications

	Tap 1	**Tap 2**	**Tap 3**
Delay (μs)	0.0	0.4	0.9
Power (dB)	0	-5	-10
K-factor	1	0	0
Doppler (Hz)	0.40	0.30	0.50

Table A.5: SUI-4 channel model specifications

	Tap 1	**Tap 2**	**Tap 3**
Delay (μs)	0.0	1.5	4.0
Power (dB)	0	-4	-8
K-factor	0	0	0
Doppler (Hz)	0.20	0.15	0.25

Table A.6: SUI-5 channel model specifications

	Tap 1	**Tap 2**	**Tap 3**
Delay (μs)	0.0	4.0	10.0
Power (dB)	0	-5	-10
K-factor	0	0	0
Doppler (Hz)	2.00	1.50	2.50

Table A.7: SUI-6 channel model specifications

	Tap 1	**Tap 2**	**Tap 3**
Delay (μs)	0.0	14.0	20.0
Power (dB)	0	-10	-14
K-factor	0	0	0
Doppler (Hz)	0.40	0.30	0.50

Appendix B

Publications

B.1 Journal Papers

1. **Muhammad Zeeshan** and Shoab A. Khan, "A novel algorithm for link adaptation using fuzzy rule based system for wideband networking waveform of SDR", *AEU - International Journal of Electronics and Communications*, Vol. 69, No. 9, pp. 1366-1373, 2015. [**Impact factor: 0.601**]

2. **Muhammad Zeeshan** and Shoab A. Khan, "A Novel Algorithm for Burst Detection in Wideband Networking Waveform of Software Defined Radio", *IEICE Transactions on Fundamentals of Electronics, Communications and Computer Sciences*, Vol. E98-A, No. 6, pp. 1225-1233, 2015. [**Impact factor: 0.231**]

3. Muhammad Waqas Khan, Mohammad Ahmad Choudhry, **Muhammad Zeeshan** and Ahsan Ali, "Adaptive Fuzzy Multivariable Controller Design based on Genetic Algorithm for an Air Handling Unit", *Energy (Elsevier)*, Vol. 81, pp. 477-488, March 2015. [**Impact factor: 4.159**]

4. **Muhammad Zeeshan**, Shoab A. Khan and Ibtsam Haq, "A Two Stage Algorithm for Carrier Frequency Offset Recovery with DSP Implementation on SDR Platform", *IEICE Transactions on Communications*, Vol. E97-B, No. 11, pp. 2449-2458, 2014. [**Impact factor: 0.326**]

5. **Muhammad Zeeshan** and Ihsan Ullah, "Comparative Analysis of SSRLS and SS-RLS with Adaptive Memory for Wireless Channel Equalization", *International Jour-*

nal of Future Computer and Communication, Vol. 2, No. 6, pp. 604-607, Dec. 2013.

6. **Muhammad Zeeshan** and Shoab A. Khan, "Robust Sampling Clock Recovery Algorithm for Wideband Networking Waveform of SDR", *International Journal of Communication Networks and Information Security (IJCNIS)*, Vol. 5, No. 1, pp. 10-18, Apr. 2012. [**HEC Recognized Journal in X Category**]

7. **Muhammad Zeeshan** and Shoab A. Khan, "A Robust Carrier Frequency Offset Estimation Algorithm in Burst Mode Multicarrier CDMA based Ad Hoc Networks", *International Journal of Communication Networks and Information Security (IJCNIS)*, Vol. 4, No. 3, pp. 174-181, Dec. 2012. [**HEC Recognized Journal in X Category**]

B.2 Book

1. **Muhammad Zeeshan**, Shoab A. Khan, *Power Optimization of CDMA based Tactical Networks; A Multiuser Detection Approach*, LAP Lambert Academic Publishing, Saarbrcken, Germany, 2012, ISBN: 978-3-659-19912-7.

B.3 International Conference Papers

1. **Muhammad Zeeshan** and Shoab A. Khan, "Data Aided Algorithm for Burst Detection in Wideband Networking Waveform with FPGA Implementation on SDR Platform", *11th HONET Photons for Electronics (PfE) Conference*, Charlotte, North Carolina, USA, 2014.

2. **Muhammad Zeeshan** and Shoab A. Khan, "An Efficient Burst Detection Algorithm for CDMA/Adaptive TDMA based Wideband Networking SDR Waveform", *33rd IEEE International Performance Computing and Communications Conference (IPCCC)*, Austin, Texas, USA, 2014.

3. Muhammad Waqas Khan, M. A. Choudhry and **Muhammad Zeeshan**, "Multivariable Adaptive Fuzzy Logic Controller Design based on Genetic Algorithm applied to HVAC Systems", *3rd International Conference on Computer, Control and Communication (IC4)*, Karachi, Pakistan, Sep 2013.

4. Muhammad Waqas Khan, M. A. Choudhry and **Muhammad Zeeshan**, "An Efficient Design of Genetic Algorithm based Adaptive Fuzzy Logic Controller for Multivariable Control of HVAC Systems ", *5th Computer Science and Electronic Engineering Conference (CEEC)*, Colchester, UK, 2013.

5. **Muhammad Zeeshan**, Shoab A. Khan, M. Waqas Khan and Sabahat A. Malik, "An Efficient Capacity Improvement Technique for Multiuser DS-CDMA based Fixed Wireless Applications", *International Conference on Open Source Systems and Technologies (ICOSST)*, Lahore, Pakistan, Dec. 2012.

6. **Muhammad Zeeshan**, Shoab A. Khan and M. Yasir Malik, "A Secure DS-CDMA based Technique with Capacity Enhancement for Ad Hoc Wireless Networks", *2nd International Conference on IT Convergence and Security (ICITCS)*, South Korea, 2012.

7. **Muhammad Zeeshan** and Shoab A. Khan, "A Modified FFT and Biquadratic Interpolation based Algorithm for Carrier Frequency Offset Estimation in MC-CDMA based Ad Hoc Networks", *8th International Conference on Emerging Technologies (ICET)*, Islamabad, Pakistan, 2012.

8. M. Shahzad Anwar, **Muhammad Zeeshan**, Saira Aslam, M. Asim Ajaz and M. Salman, "Comparative Performance Evaluation of LDPC coded and Turbo Coded OFDM systems in SUI Multipath Channel Models", *International Conference on Computer Applications & Industrial Electronics (ICCAIE)*, Malaysia, 2010.

9. **Muhammad Zeeshan** and Ihsan Ullah, "Comparative analysis of SSRLS and SS-

RLS with Adaptive Memory for Wireless Channel Equalization", *International Conference on Intelligence and Information Technology (ICIIT)*, Lahore, Pakistan, 2010.

10. Nauman A. Baig, M. B. Malik and **Muhammad Zeeshan**, "Analysis of Various Configurations of Jammer and Transmitter", *International Colloquium on Computing, Communications, Control and Management (CCCM)*, China, Aug. 2010.

11. **Muhammad Zeeshan** and Shoab A. Khan, "Power Optimization of Multiuser CDMA based Mobile Ad Hoc Network in tactical Setting", *International Colloquium on Computing, Communications, Control and Management (CCCM)*, China, Aug. 2010.